Synthesis and modelling of Tungsten catalysts for alkene metathesis

Morena Samuel Xaba

B.Sc Hons. (NWU)

Dissertation submitted in partial fulfilment of the requirements for the degree

Master of Science in Chemistry

At the North-West University (Potchefstroom Campus)

Supervisor: Dr. AM Viljoen

Co-Supervisor: Dr. CGCE van Sittert

Potchefstroom

2011

Acknowledgements

First and foremost I am eternally grateful to my Heavenly Father for His grace, mercy and the strength He gave me to persevere until the end of this work.

I would like to express my sincerest appreciation and gratitude to the following people who assisted me in their own special ways:

- My study leader, Dr. A. M. Viljoen for her assistance, support and countless suggestions throughout my studies.
- Dr. Cornie van Sittert for her motivation, trust in my abilities and endless contributions towards my study.
- Prof Manie Vosloo, for giving me the opportunity to do a masters degree in his research group.
- Mr. Andre Joubert for NMR spectra.
- Dr. Charles Williams, Mr. Andrew Fouche and Mrs. Lynette van der Walt for the chemicals and apparatus.
- Professor Frans Martins for his help with NMR spectra elucidation.
- My colleagues within the Catalysis and Synthesis Research group for providing a good working environment.
- My siblings; Elvis and Moleboheng for their patience, constant support and for always believing in me.
- All my friends who encouraged and supported me throughout the duration of my study.
- C*change for financial grant.

Summary

The aim of this study was to investigate, theoretically and experimentally, the $W(O\text{-}2,6\text{-}C_6H_3Cl_2)_2Cl_4$ catalyst and to synthesise 'cage' alicyclic ligands that will help retain the catalyst during the membrane separation process. Furthermore, molecular modelling was used in order to explain the metal-ligand coordination, the active sites in carbosilane dendritic catalysts and to investigate the mechanistic steps of the $W(O\text{-}2,6\text{-}C_6H_3Cl_2)_2Cl_4$ catalyst in the metathesis of 1-octene.

The $W(O\text{-}2,6\text{-}C_6H_3X_2)_2X_4$ (X = Cl, Br and Ph) catalytic system has been reported in literature, and the complex with X = Cl substituent was found to have higher activity than the complex with Br and Ph substituents. However, the complex with Br and Ph substituents were found to have high selectivity but lower activity. The metathesis of 1-octene by the $W(O\text{-}2,6\text{-}C_6H_3Cl_2)_2Cl_4$ system was investigated and the results matched well with literature. A theoretical study was done on the metathesis mechanism of 1-octene in the presence of carbosilane dendritic catalysts and the $W(O\text{-}2,6\text{-}C_6H_3Cl_2)_2Cl_4$ catalytic system. The electronic energy profiles were plotted by using a Potential Energy Surface (PES) scan. The preferred routes in the activation steps and in the catalytic cycles were predicted. The activation steps of the two carbosilane dendritic catalysts are different from the activation step of the $W(O\text{-}2,6\text{-}C_6H_3Cl_2)_2Cl_4$ catalyst, but the catalytic cycle is in agreement with that of $W(O\text{-}2,6\text{-}C_6H_3Cl_2)_2Cl_4$. Electronic energy gaps, orbital symmetry and the orientation of ligands or 1-octene with metal complexes were calculated and analysed. A striking observation is that in the coordination of the metal complex with either the ligand or 1-octene the smallest energy gap of the frontier orbitals is always between the lowest unoccupied molecular orbitals (LUMO) of the metal complex and the highest occupied molecular orbitals (HOMO) of the ligand/alkene. It was also observed on the energy profiles that the heptylidene species is more stable than the methylidene species.

Two 'cage' alicyclic compounds which differ in their periphery, the "cage divinyl ether" and "cage diallyl ether" were synthesised and obtained in good yields. Attempts to synthesise dendritic catalysts/complexes with these ligands as cores of the dendritic catalysts were undertaken. An electrophilic addition reaction of HCl and Cl_2 on the double bonds was observed. An energy gap analysis of these ligands with the $W(O\text{-}2,6\text{-}C_6H_3Cl_2)_2Cl_4$ system was undertaken. It was found that the LUMO of $W(O\text{-}2,6\text{-}C_6H_3Cl_2)_2Cl_4$ and the HOMO of the "cage alicyclic compounds" showed a good possibility of coordination. However, the orbital symmetry and orientation of the metal and ligand does not permit the coordination of the ligands with the metal complex. *In-situ* metathesis of "cage alicyclic compounds" as ligands with $W(O\text{-}2,6\text{-}C_6H_3Cl_2)_2Cl_4$ as catalyst did not give any metathesis products.

Samevatting

Die doel van die studie was om die W(O-2,6-$C_6H_3Cl_2)_2Cl_4$ katalisator teoreties en eksperimenteel te ondersoek en om 'hok' alisikliese ligande te sintetiseer wat kan help om die katalisator terug te hou gedurende 'n membraanskeidingsproses. Verder is molekuulmodellering gebruik om die metal-ligandinteraksie en die aktiewe posisies in die karbosilaan dendritiese katalisatore te verduidelik, sowel as die meganistiese stappe van die W(O-2,6-$C_6H_3Cl_2)_2Cl_4$ katalisator in die metatese van 1-okteen te ondersoek.

Die W(O-2,6-$C_6H_3X_2)_2X_4$ (X = Cl, Br en Ph) katalitiese sisteem is in die literatuur geraporteer, en daar is gevind dat die kompleks met X = Cl substituent 'n hoër aktiwiteit het as dié met Br en Ph substituente. Daar is egter gevind dat die met Br en Ph substituente hoër selektiwiteit het maar laer aktiwiteit. Die metatese van 1-okteen met die W(O-2,6-$C_6H_3Cl_2)_2Cl_4$ sisteem is ondersoek en die resultate stem goed ooreen met dié in literatuur. 'n Teoretiese studie is op die metatese-meganisme van 1-okteen in die teenwoordigheid van karbosilaan dendritiese katalisatore en die W(O-2,6-$C_6H_3Cl_2)_2Cl_4$ katalitiese sisteem uitgevoer. Die elektroniese energieprofiele is gestip deur van 'n Potensiële Energie Oppervlak (Potenial Energy Surface, PES) skandering gebruik te maak. Die voorkeurroetes in die aktiveringstappe en katalitiese siklusse is voorspel. Die aktiveringstap van die twee karbosilaan dendritiese katalisatore verskil van die aktiveringstap van die W(O-2,6-$C_6H_3Cl_2)_2Cl_4$ katalisator, maar hul katalitiese siklusse stem ooreen met die van W(O-2,6-$C_6H_3Cl_2)_2Cl_4$. Elektroniese energie gapings, orbitaalsimmetrie en die orientasie van ligande of 1-okteen met metaalkomplekse is bereken en geanaliseer. 'n Opvallende waarneming is dat in die koördinasie van die metaalkompleks met of die ligand of 1-okteen die kleinste energie gaping van die grensorbitale altyd tussen die laagste ongevulde molekuulorbitaal (LUMO) van die metaalkompleks en die hoogste gevulde molekuulorbitaal (HOMO) van die ligand/alkeen is. Daar is ook op die energieprofiele waargeneem dat die heptilideen spesies meer stabile is as die metilideen spesies.

Twee 'hok' alisikliese verbindings wat in die periferie verskil, die "hokdivinieleter" en "hokdiallieleter" is gesintetiseer en in goeie opbrengs verkry. Pogings om dendritiese katalisatore/komplekse met hierdie ligande as kerne te berei is onderneem. 'n Elektrofiele addisie van HCl of Cl_2 oor die dubbelbindings is waargeneem. 'n Energiegaping-analise van hierdie ligande met die W(O-2,6-$C_6H_3Cl_2)_2Cl_4$ sisteem is onderneem. Daar is gevind dat die LUMO van W(O-2,6-$C_6H_3Cl_2)_2Cl_4$ en die HOMO van die "hokalisikliese verbindings" 'n groot moontlikheid van koördinasie vertoon. Maar die orbitaalsimmetrie en oriëntasie van die metal en ligand verhoed koördinasie van die ligand met die metaalkompleks. *In-situ* metatese van "hokalisikliese

verbindings” as ligande met $W(O\text{-}2,6\text{-}C_6H_3Cl_2)_2Cl_4$ as katalisator het egter geen metatese produkte gegee nie.

Table of contents

List of abbreviations

ADMET	:	Acyclic diene metathesis polymerization
CM	:	Cross metathesis
DFT	:	Density functional theory
DNP	:	Double numeric polarization
GC	:	Gas chromatography
GC-MS	:	Gas chromatography mass spectrometry
HOMO	:	Highest occupied molecular orbital
^{1}H NMR	:	Hydrogen-1 nuclear magnetic resonance spectroscopy
IP	:	Isomerisation products
LUMO	:	Lowest unoccupied molecular orbital
NBE	:	Norbornene
NHC	:	N-heterocyclic carbene
PMP	:	Primary metathesis products
PES	:	Potential energy surface
PCU	:	Pentacyclo undecane
PCy_3	:	Tricyclohexylphosphine
RCM	:	Ring closing metathesis
ROM	:	Ring-opening metathesis
ROMP	:	Ring-opening metathesis polymerization
R_f	:	Response factor
SCF	:	Self consistent field
SRNF	:	Solvent Resistant Nanofiltration
SMP	:	Secondary metathesis products
SM	:	Self metathesis
TLC	:	Thin-layer chromatography
TS	:	Transition state

Chapter 1. Introduction and Aims of Study

1.1 Introduction

The term metathesis is derived from the Greek words *meta* (change) and *tithemi* (place). In chemistry it refers to a reaction in which the carbon-carbon double bonds in alkenes are broken and rearranged in a statistical fashion to form new alkenes.[1]

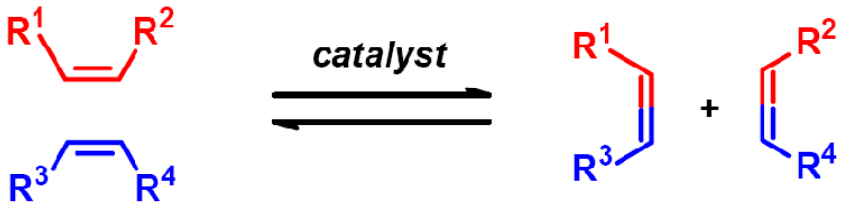

Metal-catalysed alkene metathesis have a huge impact on organic synthesis, and is one of the most often used chemical transformation processes.[2] In 1966 Natta (Nobel Prize in Chemistry, 1963) and co-workers showed that combinations of tungsten hexachloride with either triethylaluminium or diethylaluminium chloride polymerize cycloheptene, cyclooctene and cyclododecene.[3] The following year Calderon and co-workers reported their extension of these findings to other cycloalkenes using a mixture of tungsten hexachloride and ethylaluminium chloride as an initiator.[4,5] Calderon suggested that the polymerization of cyclic alkenes to polyalkenes and the disproportionation of acyclic alkenes are the same type of reaction and named the reaction alkene metathesis.[6] The contribution of metathesis reaction in the 21st century is still evident. Yves Chauvin, Robert H. Grubbs and Richard R. Schrock were awarded the Nobel Prize in Chemistry in 2005 for their outstanding work in the field of alkene metathesis.[7]

There are however three kinds of catalytic systems namely, homogeneous, heterogeneous and biological catalysts. Homogeneous catalysts offer high catalytic activity and selectivity. In homogeneous catalysis the metal complex is available to the substrate when the catalyst is completely soluble in the reaction media, however recovery is generally more difficult.[8-10] In this study we will focus on homogeneous catalysis.

The most important homogeneous catalyst systems for metathesis are derived from compounds of the non-italised nine transition metals shown in **Table 1.1**; those shown in bold are generally the most effective.[1]

Table 1.1 Transition metals used for metathesis catalysts.

IVb	Vb	VIb	VIIb	VIII	
Ti	*V*	*Cr*			*Co*
Zr	Nb	**Mo**	*Tc*	Ru	*Rh*
	Ta	**W**	**Re**	Os	Ir

Traditional tungsten pre-catalyst for metathesis is $WCl_6/EtAlCl_2$[11-13]. Basset *et al*. introduced tungsten catalytic systems $W(O\text{-}2,6\text{-}C_6H_3X_2)_2X_4$ (X = Cl, Br and Ph) which are active, stable and can be handled in air.[16,17] High activities are obtained in the presence of co-catalysts like R_nAlCl_{3-n}, R_4M (R = methyl or butyl, M = Sn or Pb) alkyltinhydrides.[12,13,16,17]

The cost and problematic separation of homogeneous catalysts from reaction products in solution has hampered the commercialisation of many excellent homogeneous catalysts. This leads to an increasing need for recycling. One possibility is the use of dendritic catalysts or catalytic dendrimers such as **1** and **2** below.[18-20] Catalytic dendrimers show kinetic behaviour, activity and selectivity of a homogeneous catalyst, with the advantage of the heterogeneous catalyst, that they can be removed from the reaction mixture by solvent resistant nanofiltration (SRNF) membrane techniques (**Figure 1.1**) and therefore can be recycled.[19, 21-24]

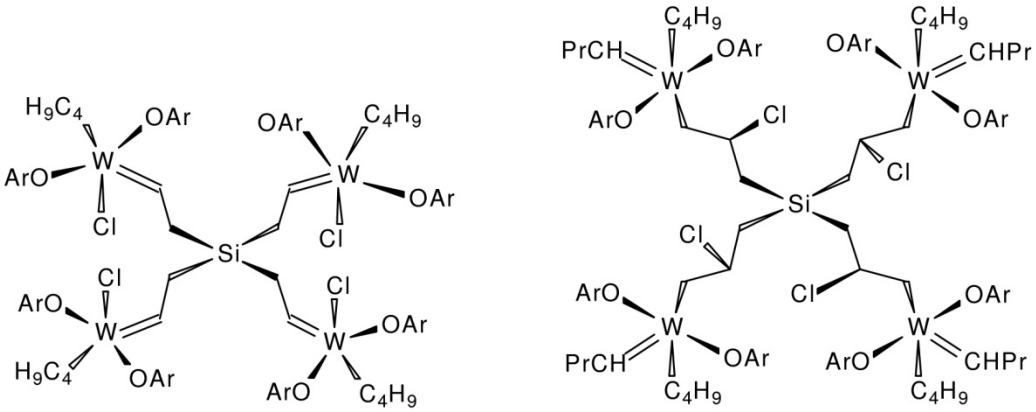

1 **2**

(OAr = O-2,6-$C_6H_3Cl_2$)

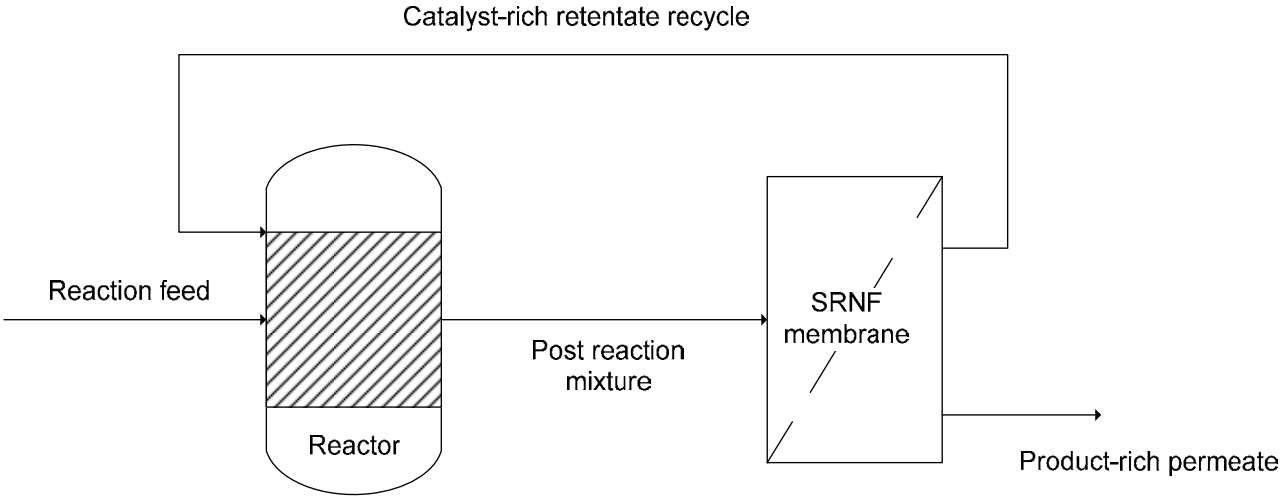

Figure 1.1 A schematic representation of a homogeneous catalyst recycling system.

One disadvantage of dendritic catalysts is that they have a flexible skeleton. This means that they change in size and shape in solution and this may cause the dendritic catalysts to escape through the pores of the nanofiltration membrane. This drawback can be overcome by the incorporation of aromatic[25] or alicyclic[26] molecules as ligands, which will help maintain the dendrimer shape in solution.[25,26] Alicyclic hydrocarbons, especially the carbocyclic 'cage' compounds, for example, **3**[27,28] could be used to prepare derivatives with the diallyl ether functionality that can serve as three dimensional cores and also as ligands for the catalysts.[29] These compounds can be used to synthesise novel alicyclic diene derivatives with stable and rigid polycyclic carbon skeletons.[28-32] These ligands would have a less flexible skeleton, addressing the problem stated above.

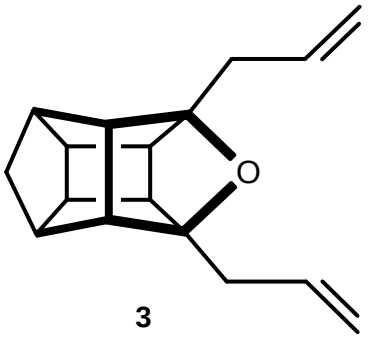

3

1.2 Aims and objectives

The aim of this study is to synthesise a $W(O\text{-}2,6\text{-}C_6H_3Cl_2)_2Cl_4$ catalyst with cage alicyclic hydrocarbons as ligands, test its metathesis behaviour and investigate the reaction mechanism theoretically.

To achieve this, the following objectives are set:

- An extensive literature study on large and bulky compounds, and especially their use as ligands in homogeneous catalysis must be conducted;
- the 'cage' alicyclic compounds must be synthesised;
- the $W(O\text{-}2,6\text{-}C_6H_3Cl_2)_2Cl_4$ catalysts with cage alicyclic hydrocarbons as ligands must be synthesised;
- the above mentioned catalysts must be tested for metathesis activity of 1-octene; and
- the nature of the active species of the Basset's, Beerens's[33] (**1**), Mbhele's[34] (**2**) and the above mentioned catalysts, and their mode of formation must be elucidated by means of computational methods.

1.3 References

1. Ivin KJ and Mol JC, *Olefin Metathesis and Metathesis Polymerization*, Academic Press, San Diego, 1997
2. Fürstner A, *Topics in Organometallic Chemistry*., 1998, **1**, 37
3. Natta G, Dall'Asta G, Bassi IW and Garella G, *Makromol. Chem*., 1966, **91**, 87
4. Calderon N, Chen HY and Scott KW, *Tetrahedron Lett*., 1967, 3327
5. Calderon N, Ofstead EA, Ward JP, Judy WA and Scott KW, *J. Am. Chem. Soc*., 1968, **90**, 4133
6. Calderon N, *Acc. Chem. Res*., 1972, **5**, 127
7. http://nobelprize.org/chemistry/laureates/2005/ [Date of access: 15 January 2010]
8. Van Heerbeek R, Kamer PCJ, Van Leeuwen PWNM and Reek JNH, *Chem. Rev*., 2002, **102**, 3717
9. Van Klink GPM, Dijkstra HP and Van Koten G, *Comptes. Rendus. Chimie*., 2003, **6**, 1079
10. Nair D, Luthra SS, Scarpello JT, White LS, Dos Santos LMF and Livingston AG, *Desalination*, 2002, **147**, 301
11. Kawai T, Shida Y, Yoshida H, Abe J and Iyoda T, *J. Mol. Catal. A: Chem*, 2002, **190**, 33
12. Van Schalkwyk C, *Ondersoek van 'n Homogene Metatesekatalisatorsisteem vir Gebruik in 'n Skeidingsproses*, MSc dissertation, PU vir CHO, 1997
13. Van Schalkwyk C, *Die Katalitiese Sintese van Lineêre Alkene via 'n Metatesereaksie*, PhD thesis, PU vir CHO. 2001
14. Wu Z. Nguyen ST, Grubbs RH and Ziller JW, *J. Am. Chem. Soc.*, 1995, **117**, 5503
15. Faulkner J, Edlin CD. Fengas D, Preece I, Quayle P and Richard SN, *Tetrahedron Lett*., 2005, **46**, 2381

16. Quignard F, Leconte M, Basset JM, Hsu LY, Alexander JJ and Shore SG, *Inorg. Chem*., 1987, **26**, 4272
17. Quignard F, Leconte M and Basset JM, *J. Mol. Catal.*, 1987, **36**, 13
18. Van Schalkwyk C, Vosloo HCM and Du Plessis JAK, *Adv. Synth. Catal*., 2002, **344**, 781
19. Dasgupta M, Peori MB and Kakkar AK, *Coord. Chem. Rev*., 2002, 233-234, 223
20. King ASH and Twyman LJ, *J. Chem. Soc*. , 2002, **1**, 2209
21. Lindhorst TK and Diekmann S, *Rev. Mol. Biotechnol.*, 2002, **90**, 157
22. Reek JNH, de Groot U, Oosterom GE, Kamer PCJ and van Leeuwen PWNM, *Rev. Mol. Biotechnol*., 2002, **90,** 159
23. Van Koten G and Jastrzebski JTBH, *J. Mol. Catal. A: Chem*., 1999, **146**, 317
24. Van der Gryp P, *Separation of Grubbs-based catalysts with nanofiltration*, PhD Thesis, North-West University, 2009
25. Kleij AW, Gebbink RJMK, Lutz M, Spek AL and Van Koten G, *J. Organomet. Chem.*, 2001, **621**, 190
26. Marx FTI, *Modellering en sintese van alisikliese fosfienverbindings as ligande*, MSc Dissertation, North-West University, 2007
27. Osawa E and Yonemitsu O, *Carbocyclic Cage Compounds*, VCH (New York), 1992
28. Marchand AP, Huang Z, Chen Z, Hariprakasha HK, Namboothiri INN, Brodbelt JS, and Reyzer ML, *J. Heterocyclic. Chem.*, 2001, **38**, 1361-1368
29. Röscher P, *Modellering en sintese van Grubbs-tipe komplekse met imienligande*, MSc Dissertation, NWU, 2010
30. Jordaan JHL, *Die Sintese van Geselekteerde C_{11}-tetrasikliese aminosuurderivate*, PhD Thesis, PU vir CHO, 2003
31. Read CE, *Die Sintese van Tioonderivate van Pentasiklo[5.4.0.0^{2,6}.0^{3,10}.0^{5,9}]undekaan,* PhD Thesis, PU vir CHO, 2003
32. Röscher J, *Die Sintese en Chemie van Tetrasiklo[6.3.0.0^{4,11}.0^{5,9}]undek-2-een-6-oon*, MSc Dissertation, PU vir CHO, 1998
33. Beerens H, Verpoort F, and Verdonck L, *J. Mol. Catal*., 2000, **159**, 197
34. Mbhele ZH, *Experimental Investigation of Dendritic Catalysts for Alkene Metathesis*, MSc Dissertation, North-West University, 2006

Chapter 2. Literature Review

2.1 Introduction

The term alkene metathesis was first introduced by Calderon in 1967 to describe the skeletal transformations of unsaturated hydrocarbons.[1] Alkene metathesis can be described as the interchange of carbon atoms between a pair of double bonds.[2] Alkene metathesis has developed to become an interdisciplinary field, comprising aspects of organic and inorganic chemistry, coordination and organometallic chemistry, homogeneous and heterogeneous catalysis, reaction kinetics, thermodynamics, chemical engineering and materials science.[3]

In 1931, Schneider and Frohlich[8] observed the pyrolytic combination of propene molecules to form ethene and butene, which was a non-catalytic metathesis reaction. Although it is generally thought that Banks and Bailey[9] discovered the metathesis reaction in 1964, Eleuterio[10,11] had already patented it in 1957. He observed the formation of a propene-ethene copolymer from propene in the presence of a $MoO_3/Al_2O_3/LiAlH_4$ catalytic system.[11] The first open publication on alkene metathesis was a report by Truett *et al*.[15] in 1960 on the ring opening metathesis polymerisation (ROMP) of norbornene. Banks and Bailey applied the process of Evering and Peters[12,13] for the transformation of propene into ethene and 2-butene on supported molybdenum oxide in 1964 in the Phillips Triolefin Process.[14] The reaction was initially known as alkene disproportionation until the term 'alkene metathesis' was used in 1967 with the discovery of the first homogeneous $WCl_6/EtOH/EtAlCl_2$ catalytic system, which produced both metathesis and polymerisation products.[1] It was not until the discovery of heterogeneous and homogeneous catalysts, which could promote the reaction at lower temperatures and minimise side-reactions, that the potential of the metathesis reaction was realised.[16] It is with transition metals that metathesis has become a very useful organic reaction.

In the presence of transition metal complexes, the metal carbene is generated and can be controlled to facilitate the metathesis reaction into subdivisions of metathesis (**Figure 2.1**).[2,4,5] The switching of groups between two acyclic alkenes, i.e. homo- or self-metathesis (SM) and cross metathesis (CM); formation of dienes from cyclic and acyclic alkenes, i.e. ring-opening metathesis polymerization (ROMP); closure of large rings, i.e. ring-closing metathesis (RCM); polymerization of cyclic alkenes, i.e. acyclic diene metathesis polymerization (ADMET).

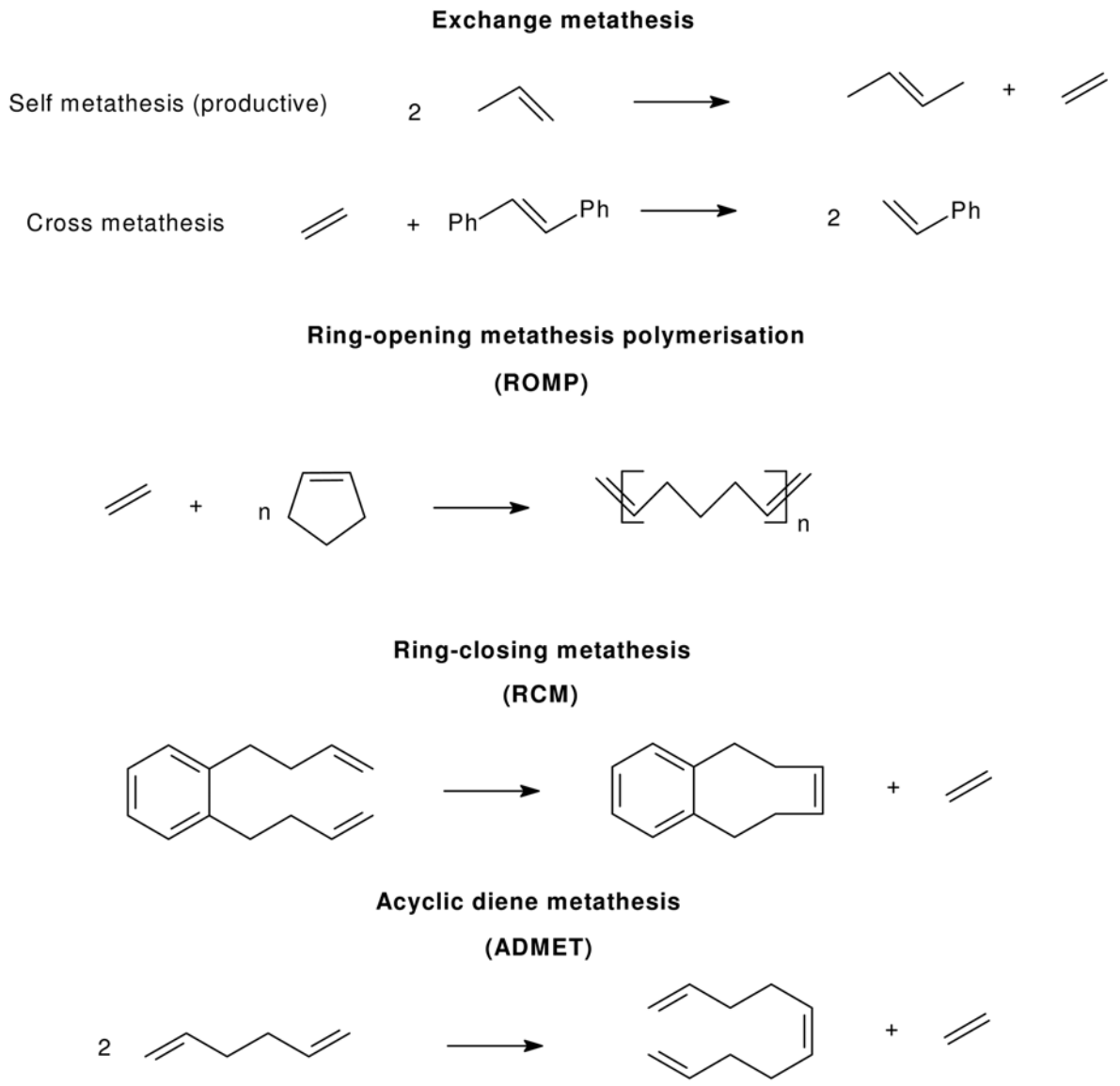

Figure 2.1 Types of alkene metathesis reaction.

One of the most impressive features of the reaction is the fact that metathesis can be catalysed homogeneously and heterogeneously by catalysts containing the same elements.[6] These reactions are generally reversible and thermoneutral, and equilibrium can be obtained in a matter of seconds.[7]

The most important homogeneous catalyst systems are derived from transition metal complexes. Transition metal complexes have a central metal atom, with either ions or groups of atoms called ligands bonded to it. The ligands surround the metal atom and form a polyhedron with the metal in the centre. The most frequently observed geometries are octahedral, tetragonal pyramidal, trigonal pyramidal, tetrahedral and s/quare planar.[17] The range of effective transition metal compounds is continually being extended by the manipulation of ligands.[2]

2.2 The development of alkene metathesis catalysts

Early developments in alkene metathesis involved the generation of active catalysts from MoO_3, WCl_6, $W(O)Cl_4$ and Re_2O_7 in the presence of alkylating agents (such as AlR_3, LiR, or SnR_4) or alumina in ethanol or chlorobenzene.[6,9,18,19] Despite tremendous advances in the area of alkene metathesis, there is still a need to develop more efficient catalysts, *i.e*. highly active, stable, stereoselective and compatible with functional groups.[20,21] This study will focus on obtaining a catalyst that could be separated from products by filtration without losing activity of the catalyst.

2.2.1 Tungsten(VI) aryloxide complexes

The use of ethanol as an activator for metathesis in the $WCl_6/EtAlCl_2$ catalyst system is well known.[22] A number of phenoxides of tungsten have been documented[23-25] and were believed to show metathesis activity similar to that of the ethanol-activated $WCl_6/EtAlCl_2$ system.[23-25] The presence of the aromatic ring in the phenoxides also affords the possibility of making systematic changes in the steric and electronic properties of the ligands on the tungsten by incorporation of different substituents on the phenol.[26]

The stereoselectivity of alkene metathesis have been investigated using *cis* and *trans* substrates since, in principle, they could elucidate the contribution of steric factors in the mechanism of metathesis.[22,27-29] Dodd and Rutt[30] found that by using acyclic alkenes, the consistency of the *cis/trans* ratios obtained for the products at zero conversion with a wide variety of catalysts, was an unexpected result. However, several explanations for that were given,[31-33] for example, metathesis of internal and terminal alkenes, as well as olefinic esters, can be achieved with the complexes $W(OAr)_2Cl_4$ (OAr = O-2,6-$C_6H_3Me_2$, O-2,6-$C_6H_3(C_6H_5)_2$, O-2,6-$C_6H_3Br_2$, O-2,6-$C_6H_3Cl_2$ and O-2,6-$C_6H_3F_2$) (**Figure 2.2**) associated with MR_4 (M = Sn, Pb; R = Me, n-Bu).[34]

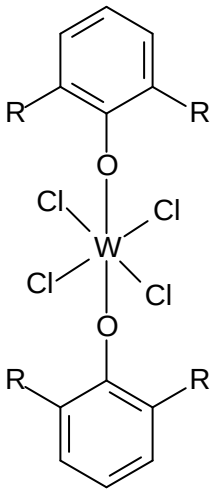

R = CH_3, C_6H_5, Cl, Br and F

4 when R = Cl

Figure 2.2 Tungsten(VI) aryloxide pre-catalyst with different substituents.[34]

For *cis*-2-pentene metathesis, many parameters play a role in the activity: the electron withdrawing property of the aryloxide ligand, the nature of the cocatalyst and the time of interaction between the precursor and the cocatalyst.[34] For a given cocatalyst and a given time of interaction, the activity varies with the nature of the substituent in o,o'-position on the aryloxide (X = CH_3 < C_6H_5 < F < Cl < Br). For a given precursor complex and a given time of interaction, the activity increases with the nature of the cocatalyst in the following order: $SnMe_4$ < $Sn(n\text{-}Bu)_4$ < $Pb(n\text{-}Bu)_4$. For a given catalyst and cocatalyst, there is an optimum time of interaction before introducing the alkene. The stereochemical results obtained with $W(OAr)_2Cl_4$ and $Pb(n\text{-}Bu)_4$ show an increase of the stereoselectivity with the nature of the aryloxide substituents in the following order F ≈ Cl < Br ≈ Me < Ph.[34]

In the late 90's Vosloo et al.[35,36] reported the tungsten compounds with the aryloxide ligands, i.e., $W(O\text{-}2,6\text{-}C_6H_3X_2)_2Cl_4$ (X = Cl, Ph) and Bu_4Sn, as catalytic systems for the metathesis of 1-alkenes of varying carbon lengths. They found that the catalytic system was activated at 85˚C for 20 minutes prior to use and that the optimum metathesis activity with 1-alkenes was observed at 85°C and a Sn/W molar ratio = 3. They further summarized that the $W(O\text{-}2,6\text{-}C_6H_3X_2)_2Cl_4/Bu_4Sn$ catalytic system is very active for the metathesis of 1-alkenes with a carbon chain length of about six to eight and it favours a more polar solvent such as chlorobenzene. Alkylation of $W(OAr)_2Cl_4$ by MR_4 (M = Sn, Pb; R = Me, n-Bu) has been investigated for the determination of the coordination sphere of the catalyst.[34,35] The results obtained with M = Sn and OAr = $O\text{-}2,6\text{-}C_6H_3Br_2$ or $O\text{-}2,6\text{-}C_6H_3Cl_2$ suggest a process of double alkylation, α-H elimination and reductive elimination of alkene leading to SnR_3Cl and $W(OAr)_2Cl_2(CHR')$ + RH (**Scheme 2.1**). Side reactions of β-H elimination which would give a tungsten species and an alkene were also observed.[35]

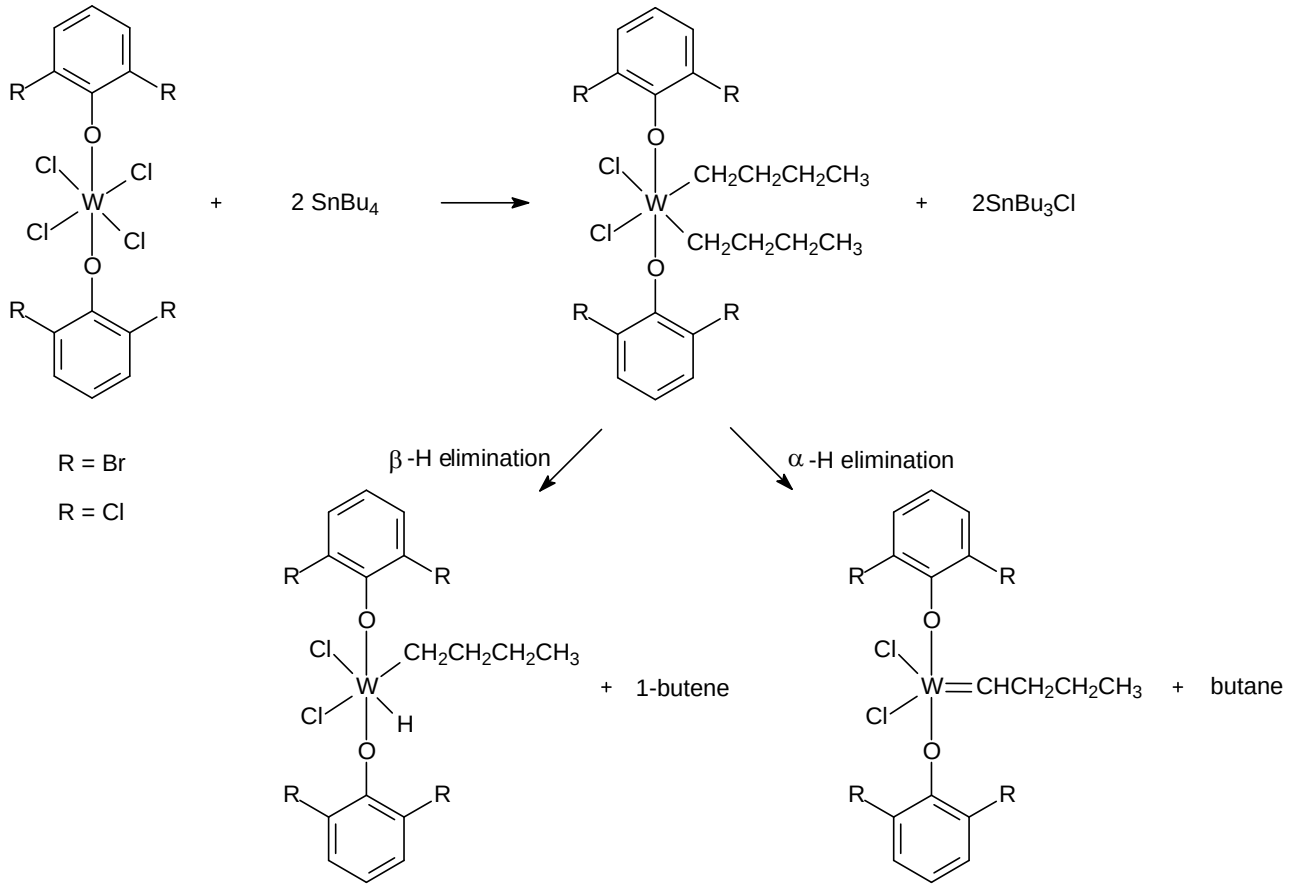

Scheme 2.1 Alkylation of $W(OAr)_2Cl_4$ by tetrabutyl tin.[35]

Tungsten(VI) aryloxide complexes of the type $W(O\text{-}2,6\text{-}C_6H_3X_2)_2Cl_4$ (X = Cl, Br, Ph), are known to be very active metathesis catalysts in the presence of cocatalysts like $EtAlCl_2$, $Et_3Al_2Cl_3$ or R_4M (R = methyl or butyl, M = Sn or Pb). The problem with these catalysts is their separation from products after the catalytic reaction. Addition of dendrimers or large ligands to these catalysts can address this challenge.

2.2.2 Ligands

The key to successful development of homogeneous catalysts has been the exploitation of the effects that ligands exert on the properties of metal complexes. By adjusting the electronic and steric properties of a catalyst, selectivities and rates can be changed.[39] If the Cl-ligands of the WCl_6-catalyst are substituted with oxyaryl or alkoxy groups the activity of the metathesis catalyst can be drastically influenced. The presence of the aromatic ring in the aryloxide ligand enhances the possibility to change the substituents on the ring, and thus to influence the electronic as well as the steric properties of the ligands on the tungsten core.[21,35,36]

Ligands such as NH_3 and H_2O, which have a lone pair for interaction with the metal, form classical coordination complexes with metal atoms. They are formed only by interaction of the ligand electrons with empty *d* orbitals of the metal. Ligands including Cl^-, Br^-, I^-, and OH^- have two or more filled orbitals which can interact with two empty *d* metal orbitals (**Figure 2.3**).[17] One of the ligand orbitals (p_x) forms a σ bond, but the second (p_y), which must be oriented perpendicular to the metal-ligand axis, can only form a bond having no rotational symmetry; it is therefore called a π bond.[17]

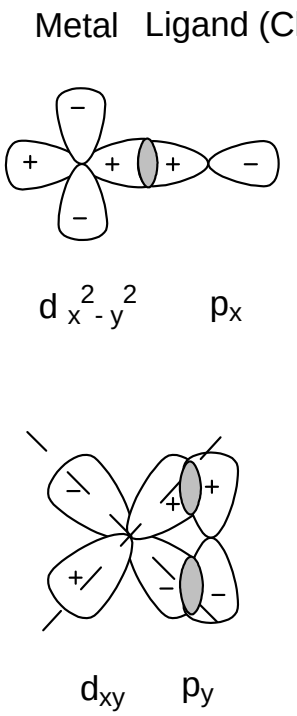

Figure 2.3 Back-bonding involving two filled ligand orbitals and two empty metal *d* orbitals.[17]

The electronic structure of metal carbene alkene complexes can be described as a combination of donor–acceptor interactions between the HOMO (Highest Occupied Molecular Orbitals) of the ligand and the LUMO (Lowest Unoccupied Molecular Orbitals) of metal carbene located at the carbene carbon.[54] The HOMO are the electron rich and interacts as nucleophiles, while the LUMO are electron deficient and interacts as electrophiles. The difference in energy between these orbitals and the overlap between them will largely determine the probability of the reaction from occurring.[55] Recently HOMO/LUMO energies of ligands have been reported for different properties such as ionisation potentials, electron affinities and HOMO-LUMO energy gaps.[56] In this study, the HOMO-LUMO energy gaps between tungsten complexes and different ligands will be investigated.

2.2.3 Dendritic catalysts

The term dendrimer is derived from the Greek word *dendra*, meaning a tree. Ideally, dendrimers are perfect monodisperse macromolecules with a regular and highly branched three-dimensional architecture.[37] Dendrimers are produced in an iterative sequence of reaction steps, in which each additional iteration leads to a higher generation material. The first example of an iterative synthetic procedure toward well-defined branched structures has been reported by Vögtle,[37] who named this procedure a '*cascade synthesis*'. These molecules are chemically inert, compatible with most organometallic reagents[38,39] and easy to prepare.

Dendrimers have nanoscopic dimensions and can be molecularly dissolved. In other words, dendrimers will combine the advantages of homo- and heterogeneous catalysts, when soluble dendrimers with defined catalytical sites are developed that can be removed from homogeneous reaction mixtures by simple separation techniques (i.e., ultrafiltration or dialysis).[40] There are two ways in which the active species or the metal can be placed within the dendrimer, first is within the core of the dendrimer and second is at the periphery of the dendrimer. In this study, we investigate the latter case. In periphery functionalised dendrimers, the transition metal is directly available for the substrate, in contrast to core-functionalised systems in which the substrate has to penetrate the dendrimer before it is converted.

Steric crowding was reported in organometallic dendrimers with high catalytic loading.[41,42] An investigation of the catalytic activity of the organometallic dendrimers by several groups has generally led to a conclusion that the performance of these systems decreases with an increase in surface congestion due to extensive branching of dendritic structure.[41,42] The interactions between neighbouring metal centres in these congested scaffolds contribute significantly to the lower rates of catalysis with an increasing number of generations.[41,43] For example, Van Koten *et al.*[44] in their study with periphery functionalised silicon dendrimers with aryl nickel(II) centres capable of catalysing the Kharasch addition of perhaloalkanes to alkenes, reported that the local concentration of nickel centres resulted in an interaction between neighbouring Ni(II) and Ni(III) sites formed during the catalytic reaction.

In one of the studies on W-carbosilane dendrimers[45] it was found that by increasing the reaction time, W-alkylidenes present on the carbosilane periphery react mutually by an intermolecular metathesis reaction (**Scheme 2.2**). Two metal complexes are deactivated due to a dismutation, resulting in a coupling between two dendrimer units. As a result, two metal complexes (one of each dendrimer branch) are eliminated from the dendrimer surfaces and an unidentified tungsten species is formed.

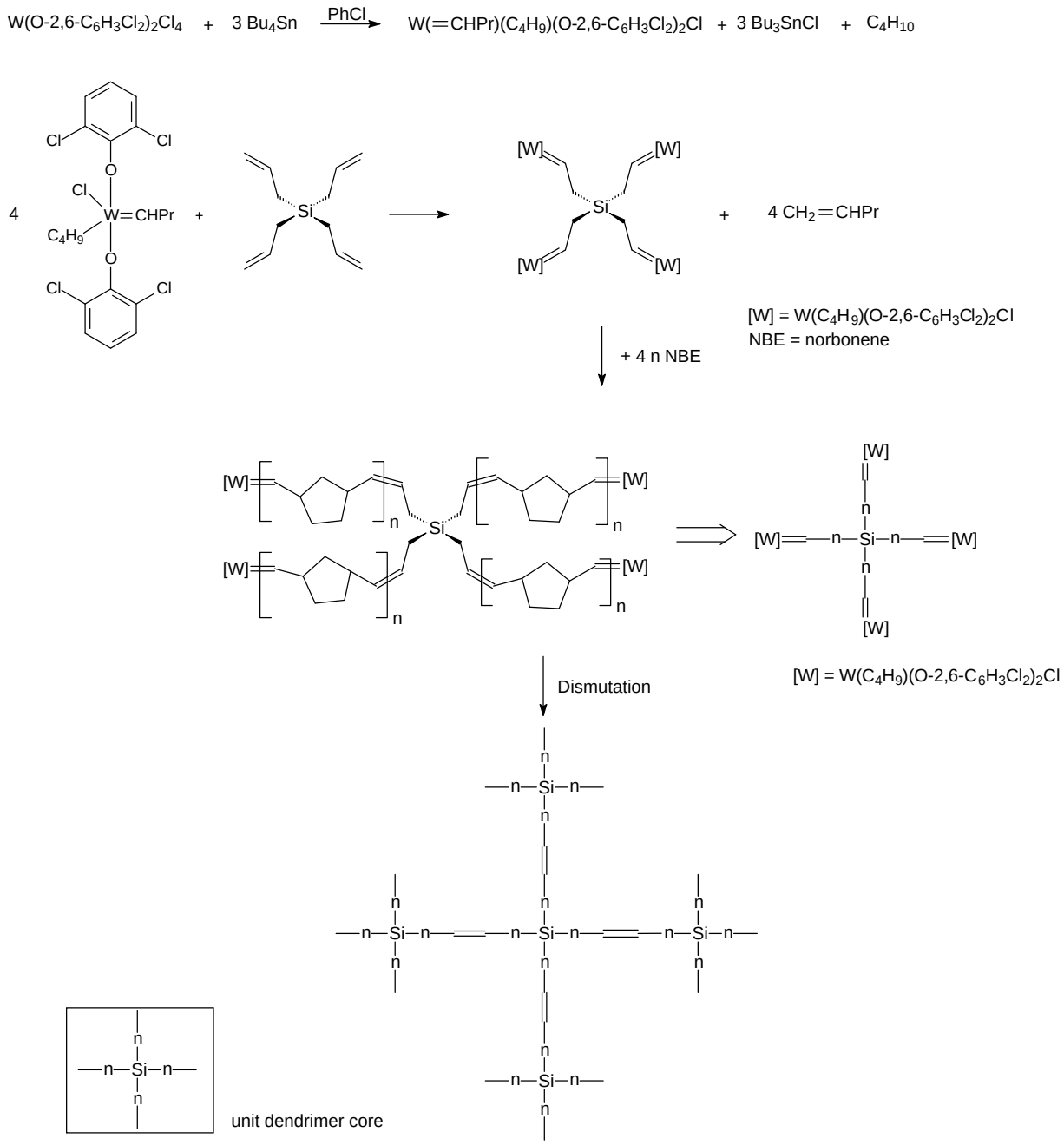

Scheme 2.2 Synthesis of starpolymers by dismutation.[45]

One disadvantage of the metallic dendrimers is that they have a flexible skeleton.[43] This means that they change size and shape in solution, and this may cause the first and second generation dendrimers to leak through the nanofiltration membrane. Even higher generation dendrimers are still not fully retained by nanofiltration membranes.[43,44] This drawback can be overcome by incorporation of alicyclic molecules in the skeleton of the dendrimer, which will help maintain the dendrimer shape in solution.[46]

2.2.4 Carbocyclic ‘cage’ compounds

An alicyclic compound is an organic compound that is both aliphatic and cyclic. These compounds contain one or more all-carbon rings which may be either saturated or unsaturated, but do not have aromatic character. These compounds have been the subject of various interesting investigations over the past few decades.[47] With the exception of adamantane, most saturated alicyclic cage molecules contain considerable strain energy as evidenced by the fact that they [48]

i. contain unusually long framework carbon-carbon σ-bonds,
ii. contain unusually C-C-C bond angles that deviate significantly from 109.5°,
iii. possess unusually negative heats of combustion, and
iv. possess unusually positive heats of formation when compared with nonstrained systems.

These properties contribute to the unusual chemical reactivity and exceptional thermal stability of these so-called “cage” or “bird-cage” compounds.[49] In this study we focus on the pentacyclo[5.4.0.$0^{2,6}$.$0^{3,10}$.$0^{5,9}$]undecane-8,11-dione (**8**) derivative as a starting material of ligands for the W(O-2,6-$C_6H_3Cl_2)_2Cl_4$ precatalyst. This compound is synthesised by photocyclisation of the endo-conformer of the Diels-Alder adduct **7** (**Scheme 2.3**).[50]

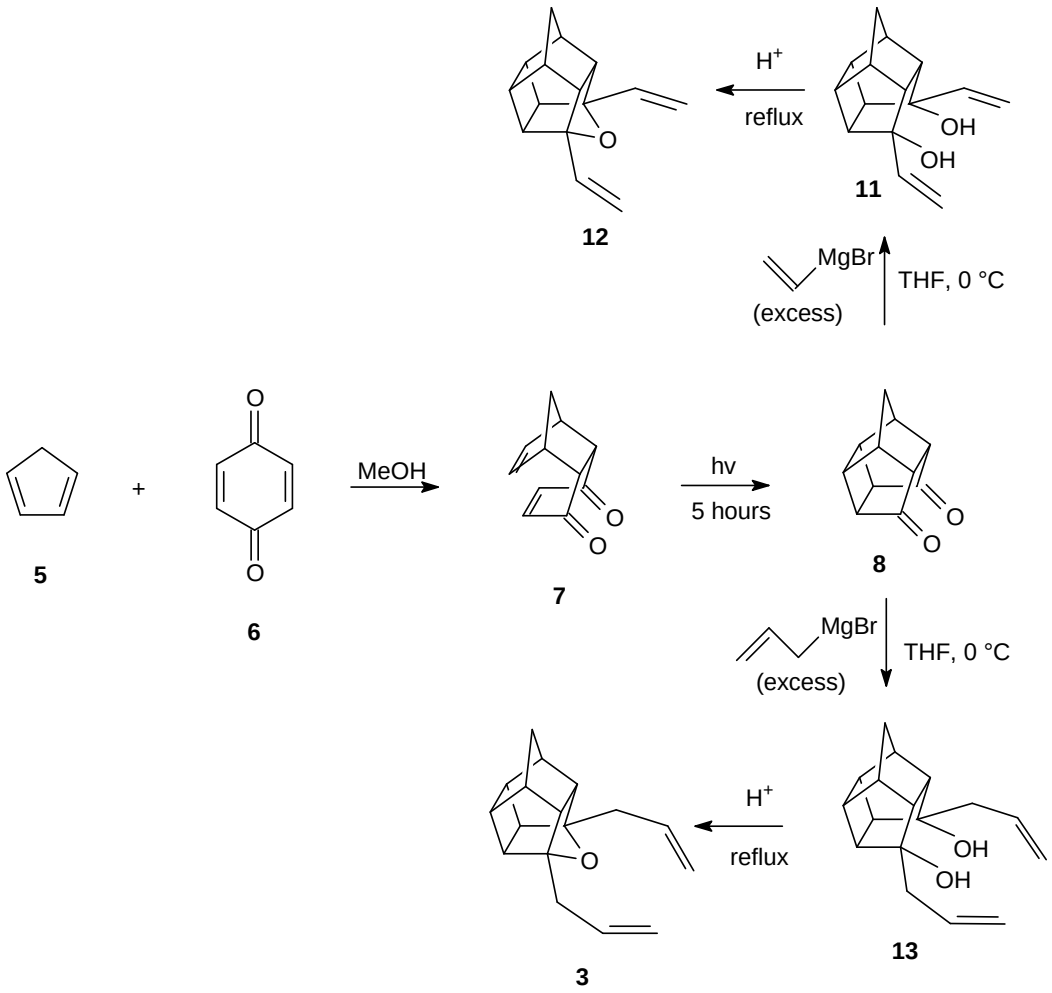

Scheme 2.3 Synthesis route of the cage compounds.

This study will focus on the alicyclic tungsten-type pre-catalyst with **8** as a starting material. Although there are several molybdenum[51] and platinum[52] based alicyclic ligands **9** and **10** (**Figure 2.4**) reported in literature, there is no alicyclic tungsten based pre-catalyst reported in literature.

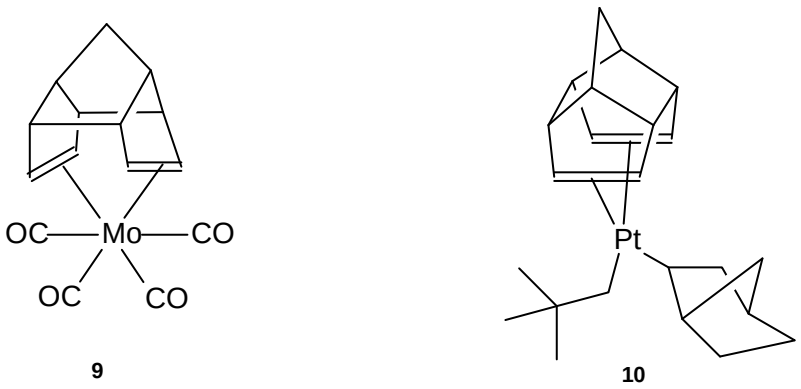

Figure 2.4 Literature catalysts containing alicyclic ligands.[51,52]

Recently, Kotha *et al*.[53] showed that highly functionalised cage compounds can be prepared *via* cross-metathesis using a ruthenium catalyst. Some of these polycyclic compounds are highly symmetrical in nature, and possess inherent ring strain. Due to the lack of conformational mobility, their molecular architecture has generated considerable attention.[53] The synthesis of 'cage' molecules can thus take part in catalytic metathesis reactions such as photo-thermal metathesis reactions.

2.3 Reaction mechanism of alkene metathesis

A variety of mechanisms were suggested during the seventies for the olefin metathesis reaction based on experimental and theoretical studies.[2] The different mechanisms can be divided into two groups which are the pair-wise and non-pairwise mechanisms.

2.3.1 Pairwise mechanism

The 'pairwise' exchange between two alkenes in the coordination sphere of a metal via a weakly held cyclobutane-type complex mechanism was initially considered as the metathesis mechanism.[2,22] A number of different mechanisms have been studied and the proposed intermediates (**Figure 2.5**) were suggested to be the quasi-cyclobutane,[57] the tetramethylene metal-complex,[58] or the tetra-methylene ring complex.[59,60]

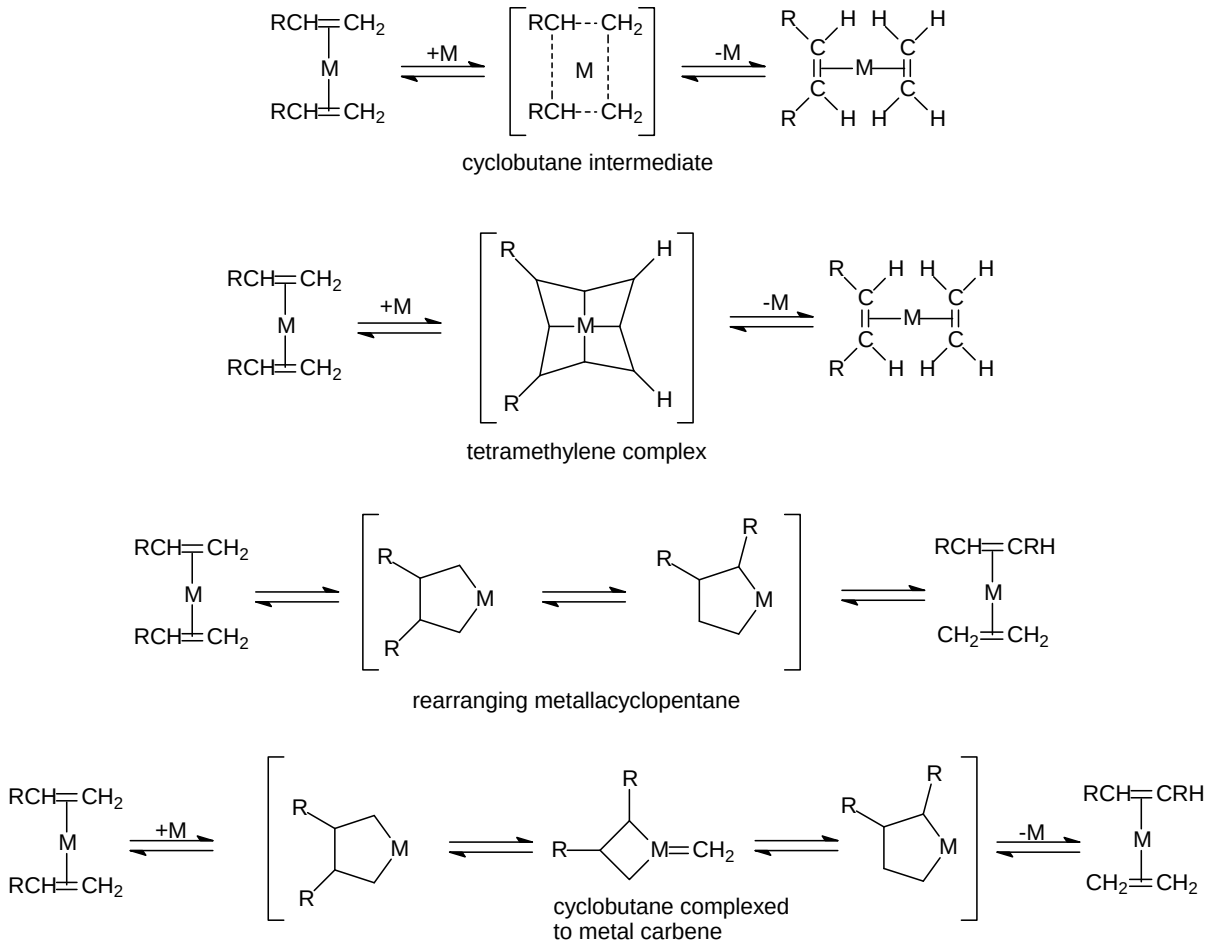

Figure 2.5 Intermediates proposed for the alkene metathesis mechanism.

Although the quasi-cyclobutane mechanism indicated that the reaction involved the cleavage of the C-C double bonds and not the transfer of groups attached to the double bond,[22] minimal experimental support was obtained. Therefore Pettit *et al*.[58] proposed a tetramethylene complex in which four methylene units are bonded to a central metal atom. In a further attempt to explain alkene metathesis, Grubbs *et al*.[59] proposed that the redistribution of groups around the double bonds was due to a rearranging metallacyclopentane intermediate and not a tetramethylene complex. Later, he suggested that one mode of rearrangement could lead to formation of a cyclobutane complexed to a metal carbene as illustrated in **Figure 2.5**.[60] Grubbs's reaction mechanism received support from studies of the metal catalysed [2+2] cycloaddition reaction e.g. valence isomerisation of cubane of syn-tricyclooctadiene,[61] cycloaddition reactions of norbornadiene[62] and rearrangements of exo-tricyclo[3.2.1.0.^{2,4}]octene,[63] but was eventually discarded in favour of the non-pairwise metal carbene chain mechanism (abbreviated to carbene mechanism), in which the propagating species is a metal carbene complex formed from the catalyst/substrate system.

2.3.2 Non-pairwise mechanism

In 1971, Herrison and Chauvin[64] suggested that the olefin metathesis is initiated by a metal carbene. The metal carbene mechanism is the generally accepted mechanism for the alkene metathesis reaction (**Scheme 2.4**). The mechanism consists of successive [2+2]-cycloadditions followed by cycloreversions. This involves the coordination of the alkene to the metal centre to form a π-complex followed by the formation of a metallacyclobutane intermediate, which in turn can revert to a new π-complex to yield the products after dissociation.

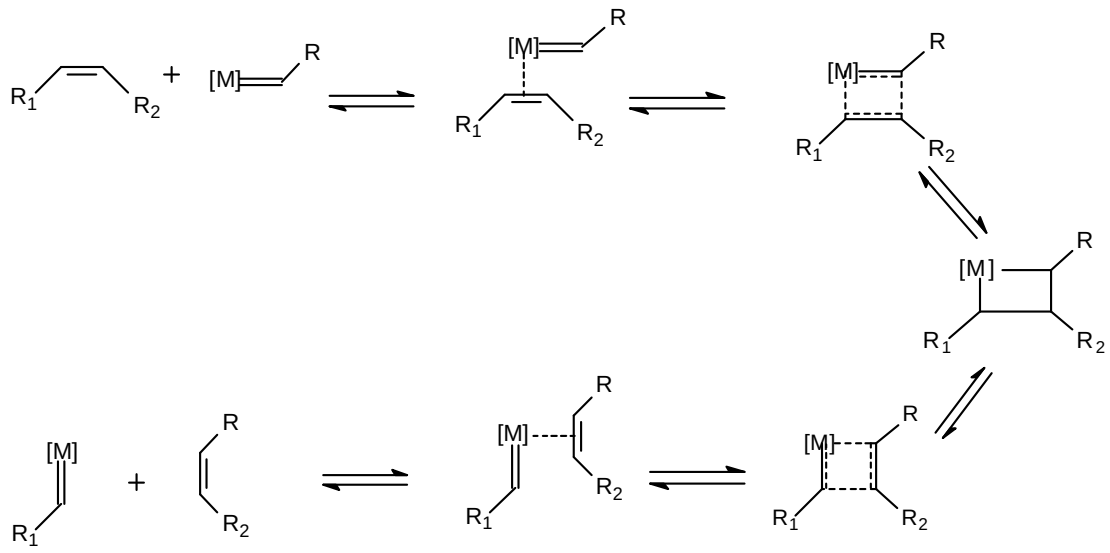

Scheme 2.4 Chauvin's metallacyclobutane mechanism.[64]

Initially this proposal received little support, but by 1975 the evidence in its favour became so compelling that the pairwise mechanism was discarded.[22] For example, labelling experiments (**Scheme 2.5**) revealed that the kinetic product of the metathesis of 1,7-octadiene derivatives is a statistical distribution (1:2:1) of d_0-, d_2- and d_4-labelled ethene and not a non-statistical distribution (1:1.6:1) as predicted by the pairwise mechanism.[65-67]

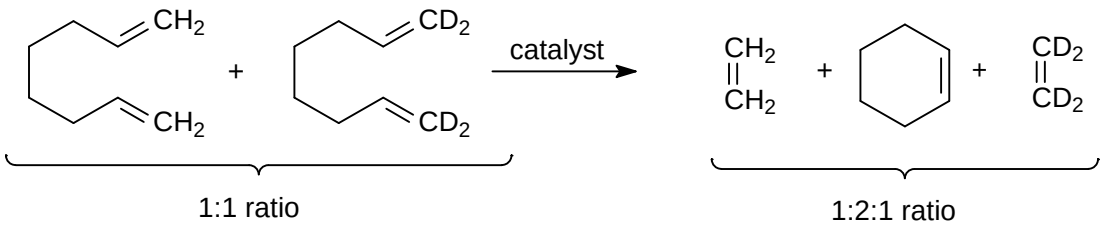

Scheme 2.5 Labelling experiment to confirm the Chauvin mechanism for the alkene metathesis reaction.

With the discovery of well-defined carbene complexes of Ta, Mo, W, Re and Ru which would act as initiators without the need for activation by heat, light or cocatalyst, spectroscopic techniques could be used to detect the propagating metal-carbene and intermediate metallacyclobutane complexes in some of these systems.[22] This provided additional support for the Chauvin mechanism.

2.4 Molecular modelling in alkene metathesis reactions

One of the main questions or aims of a computational study has to be the exploration of the mechanism of a given reaction, and in our case that of the alkene metathesis reaction. Molecular modelling can be used to investigate reactions in which the active species either has a very short lifetime, or is present in very low concentrations, so that it cannot be easily isolated. Through the construction of a potential energy surface (PES), *viz.* a plot of energy vs. reaction coordinate, a number of quantities which are of interest in molecular modelling, *inter alia* equilibrium and transition state (TS) geometries and energies, can be directly obtained.[68] An example of a PES is given in **Figure 2.6.**[69] Although it is possible to derive TS energies experimentally from the kinetic data relative to reactants and/or products, only a qualitative idea of the TS structure can be obtained. This is mainly due to the fact that the techniques available for structure elucidation are either too slow or not sensitive enough.[70] Molecular modelling or theoretical methods can therefore be used to describe TS structures, conformer analysis, frontier orbitals and can also be applied to the design of new catalytic systems.[71]

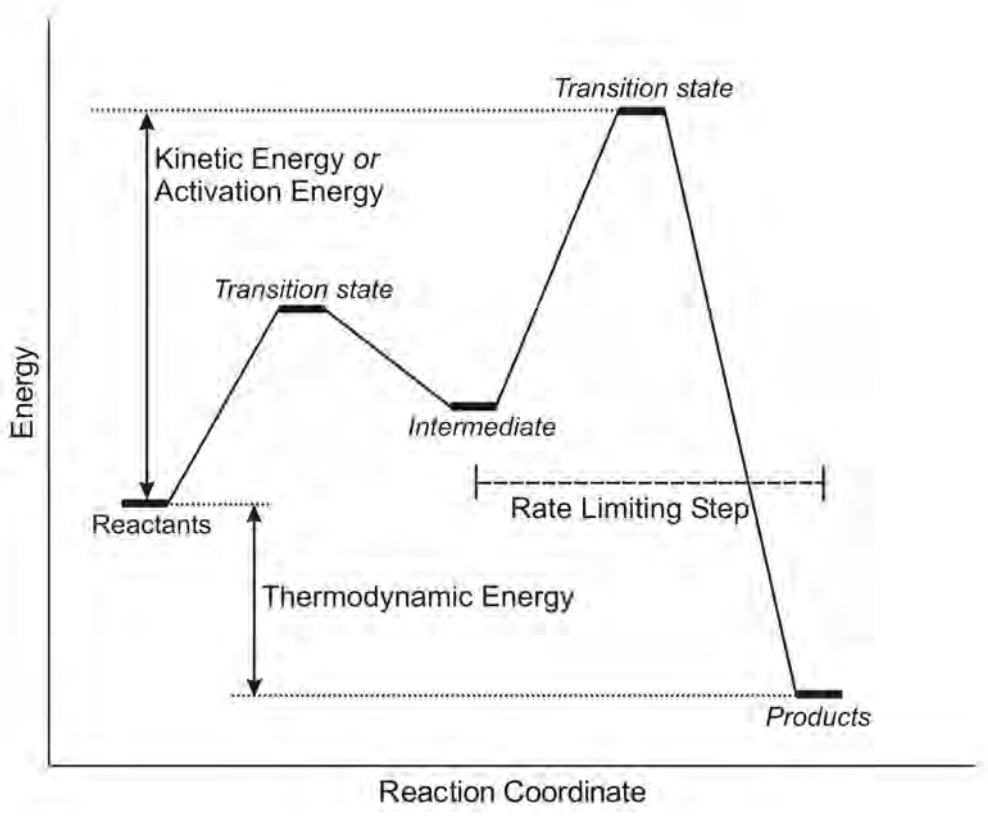

Figure 2.6 Illustration of a PES diagram.

The energy minima and maxima points on the PES are usually referred to as stationary points. The energy minima, also referred to as local minima, correspond to stable molecules (reactants and products), and while energy maxima correspond to transition states. An intermediate on the PES refers to species that may be too reactive during a reaction to allow easy isolation and characterisation.

The energy minima along the PES given in **Figure 2.6** correspond to equilibrium geometries with relative energies relating to thermochemical stabilities. Therefore, the overall process in **Figure 2.6** is thermodynamically favoured and therefore exothermic.[68] The position of TS's along the reaction coordinate usually corresponds to TS geometries and their energies to kinetic or activation energies, relative to the local minima. The reaction step that involves the highest energy TS is referred to as the rate limiting step of the reaction.[71] In this study, activation energies, transition states and intermediates will be investigated by employing the PES scans obtained from molecular mechanics and quantum mechanical calculations methods.

Although the alkene metathesis reaction is one of the most studied reaction in organometallic chemistry, there have been few reports dealing with modelling of this metal-catalysed reaction using quantum chemistry tools. Thus, Rappe[72] reported the modelling of a metathesis reaction

catalysed by high-valent group VI metals and recently, a DFT study showed that the formation of imidotungsten(VI) complexes with similar ligands can give different products through the disproportionation of the intermediates.[73] Experimental results of ^{1}H NMR were explained in a 1-octene conversion reaction from the energy profile of the catalytic cycle by a ruthenium catalyst.[74]

2.5 References

1. Calderon N, Chen HY and Scott KW, *Tetrahedron Lett.*, 1967, **8**, 3327
2. Ivin KJ and Mol JC, *Olefin Metathesis and Metathesis Polymerization*. Academic Press, San Diego, 1997
3. Streck R, *J. Mol. Catal.*, 1988, **46**, 305
4. Mol, JC in *Applied Homogeneous Catalysis with Organometallic Compounds*, Cornils B. and Herrmann WA, Eds., Metathesis, Vol. 2, VCH (Weinheim), 1996, p. 318
5. Astruc D, *New J. Chem*., 2005, **29**, 42
6. Banks RL and Bailey GC, *Ind. Eng. Chem., Prod. Res. Dev*., 1964, **3**, 170
7. Mortreux A and Petit F, *Industrial Applications of Homogeneous Catalysis*, D. Riedel Publishing (Dordrecht), 1988, p. 229
8. Schneider V and Frolich PK, *Ind. Eng. Chem*., 1931, **23**, 1405
9. Banks RL and Bailey GC, *Ind. Eng. Chem*, *Prod. Res. Dev.*, 1964, **3**, 170
10. Eleuterio HS, *J. Mol. Catal*., 1991, **65**, 55
11. Eleuterio HS, 1963, *Polymerization of cyclic olefins*., Patent: US 3 074 918
12. Peters EF and Evering BL, 1960, *Olefin-polymerization catalysts*. Patent: US 2 936 291
13. Peters EF and Evering BL, 1960, *Catalysts and their preparation*. Patent: US 2 963 447
14. Wagner PH, *Chem. Ind*., 1992, 330
15. Truett WL, Johnson DR, Robinson IM and Montague BA, *J. Am. Chem. Soc*., 1960, **82**, 2337
16. Haines RJ and Leigh GJ, *Chem. Soc. Rev.*, 1975, **4**, 155
17. Gates BC, *Catalytic Chemistry*., Wiley (New York), 1992
18. Natta G, Dall'Asta G, Bassi IW and Carella G, *Makromol. Chem.* 1966, **91**, 87
19. Grubbs RH, *Handbook of Metathesis.*, Wiley-VCH: Weinheim, Germany, 2003, Vol 1
20. Coperet C, *Chemistry Today*, 2009, **27**, 6
21. Van Schalkwyk C**,** *Die Katalitiese sintese van Lineere Alkene via 'n Metatesereaksie*, PhD-thesis, PU vir CHO, 2001
22. Calderon N, Ofstead EA, Ward JP, Judy WA and Scott KW, *J. Am. Chem. Soc*., 1968, **90**, 4133
23. Funk H and Baumann W, *Z. Anorg. Chem*., 1937, **231**, 264
24. Prasad S and Krishnaiah KSR, *J. Ind. Chem*., 1960, **37**, 681

25. Moritmer PI and Strong MI, *Austr. J. Chem.*, 1965, **18**, 1579
26. Dodd HT and Rutt KJ, *J. Mol. Catal.*, 1982, **15**, 103
27. Taghizadeh N, Quignard F, Leconta M, Basset J-M, Larroche C, Laval JP and Lattes A, *J. Mol. Catal.*, 1982, **15**, 219
28. Leconte M and Basset J-M, *Ann. N. Y. Acad. Sci*., 1980, **333**, 165
29. Leconte M and Basset J-M, *J. Am. Chem. Soc*., 1979, **101**, 7296
30. Dodd HT and Rutt KJ, *J. Mol. Catal.*, 1985, **28**, 33
31. Bilhou JL, Basset J-M, Mutin R and Graydon WF, *J. Am. Chem. Soc*., 1977, **99**, 7376
32. Casey CP, Albin LD and Burkhardt T, *J. Am. Chem. Soc*., 1977, **99**, 2533
33. Katz TJ and Rutt KJ, *Tetrahedron Lett.*, 1977, 505
34. Quignard F, Leconte M and Basset J-M, *J. Mol. Catal*., 1986, **36**, 13
35. Vosloo HCM, Dickinson AJ and du Plessis JAK, *J. Mol. Catal.*, 1997, **115**, 199
36. van Schalkwyk C, Vosloo HCM and du Plessis JAK, *J. Mol. Catal.*, 1998, **133**, 167
37. Buhleier EW, Wehner W and Vögtle F, *Synthesis*, 1978, 155
38. Van Koten G and Jastrzeski JTBH, *J. Mol. Catal. A: Chem*., 1999, **146**, 317
39. Beerens H, Verpoort F and Verdonck L, *J. Mol. Catal.*, 2000, **151**, 279
40. Tomalia DA and Dvornic PR, *Nature*, 1994, 617
41. Dasgupta N, Peori MB and Kakkar AK, *Coord. Chem. Rev*., 2002, 223
42. Cuadrado I, Morán M, Moya A, Casado CM, Barranco M and Alonso B, *Inorganica. Chimica. Acta*., 1996, **251**, 5
43. Van Heerbeek R, Kamer PCJ, Van Leeuwen PWNM and Reek JNH, *Chem. Rev*., 2002, **102**, 3717
44. Van klink GPM, Dijkstra HP and Van Koten G, *Compt. Rend. Chim*., 2003, **6**, 1079
45. Beerens H, Verpoort F and Verdonck L, *J. Mol. Catal.*, 2000, **159**, 197
46. Van der Gryp P, *Separation of Grubbs-based catalysts with nanofiltration*, PhD Thesis, North-West University, 2009.
47. Griffin GW and Marchand AP, *Chem. Rev*., 1989, **89**, 997
48. Marchand AP, *Chem. Rev*., 1989, **89**, 1011
49. Mehta G, Singh V and Rao KS, *Tetrahedron Lett*., 1980, **21**, 1369
50. Cookson RC, Crundwell E, Hill RR and Hudec J, *J. Chem. Soc.*, **1964**, 3062
51. Chow TJ and Ding MF, *J. Organomet. Chem.*, 1987, **329**, 217
52. Lee TR and Whitesides GM, *J. Am. Chem. Soc.,* 1991, **113**, 368
53. Kotha S, Seema V, Singh K and Deodhar KD, *Tetrahedron. Lett*., 2010, **51**, 2301
54. Tlenkopatchev M and Fomine S, *J. Organomet. Chem*., 2001, **630**, 157
55. http://courses.chem.psu.edu/chem210/quantum/quantum3.html#Highest [Date of access: 06 June 2011]
56. Zhang G and Musgrave CB, *J. Phys. Chem. A*. 2007, **111**, 1554
57. Bradshaw P, Howman EJ and Tumer L, *J. Catal*., 1967, **7**, 269

58. Lewandos GS and Pettit R, *J. Am. Chem. Soc*., 1971, **93**, 7087
59. Grubbs RH and Brunck TK, *J. Am. Chem. Soc*., 1972, **94**, 2538
60. Biefeld CG, Eick HA and Grubbs RH, *Inorg. Chem*., 1973, **12**, 2166
61. Cassar L, Eaton PE and Halpern J, *J. Am. Chem. Soc*., 1970, **92**, 3515
62. Katz TJ and Acton N, *Tetrahedron. Lett*., 1967, **27**, 2601
63. Katz TJ and Cerefice S., *J. Am. Chem. Soc*., 1969, **91**, 2405
64. Hérisson JL and Chauvin Y., *Makromol. Chem*., 1971, **141**, 161
65. Grubbs RH, Burk PL and Carr DD, *J. Am. Chem. Soc*., 1975, **97**, 3265
66. Grubbs RH, Carr DD, Hoppin C and Burk PL, *J. Am. Chem. Soc*., 1976, **98**, 3478
67. Katz TJ and Rothchild R, *J. Am. Chem. Soc*., 1976, **98**, 2519
http://en.wikipedia.org/wiki/Molecular_modelling [Date of access: 06 May 2009]
68. Hehre WJ, Yu J, Klunzinger PE and Lou L, *A Brief Guide to Molecular Mechanics and Quantum Chemical Calculations*, Irvine Wavefunction, Inc., Carlifonia, 1998
69. Janse van Rensburg W, *Contrathermodynamic Isomerisation of Internal Olefins by Exploring the Migratory Aptitude of Various Substances. The Significance of Concurring Molecular Modelling*, PhD thesis, UOFS, 2001
70. Jordan RB, *Reaction Mechanisms of Inorganic and Organometallic Systems*, Oxford University Press, New York, 1998
71. Bray MR, Deeth RJ and Paget VJ, *Prog. Reaction Kinetics*, 1996, **21**, 169
72. Rappe AK and Goddard WA, *J. Am. Chem. Soc.*, 1982, **104**, 448
73. Hänninen MM, Sillanpää R, Kivelä H and Lehtonen A, *Dalton Trans.*, 2011, **40**, 2868
74. Vosloo HCM, van Sittert CGCE, van Helden P and Jordaan M, *J. Mol. Catal.*, 2006, **254**, 145

Chapter 3. Results and Discussions

3.1 Introduction

The alkene metathesis reactions catalysed by tungsten(VI) aryloxide catalyst have been reported in literature.[1-4] In this study, the 1-octene conversion by the W(O-2,6-$C_6H_3Cl_2)_2Cl_4$/Bu_4Sn catalytic system is reported and theoretical study of **1** and **2** is done.

In the metathesis of 1-octene by **4**, various metathesis products can be formed which are: primary metathesis products (PMP), secondary metathesis products (SMP) and isomerisation products (IP). These products are summarised in **Table 3.1**.

Table 3.1 Products formed in the W(O-2,6-$C_6H_3Cl_2)_2Cl_4$/Bu_4Sn catalysed reactions of 1-octene

	Reaction	**Substrate***	**Products***
1a	Primary metathesis	C_7=C	C_7=C + C=C
1b	Isomerisation	C_7=C	C_6=C_2
1c	Secondary metathesis		
	Cross metathesis	C_7=C + C_6=C_2	C_7=C_6 + C_2=C + C_7=C_2 + C_6=C
	Homometathesis	C_6=C_2	C_6=C_6 + C_2=C_2
1d	Dimerisation	C_7=C	C_8=C_8
2a	Isomerisation	C_6=C	C_5=C_2
2b	Secondary metathesis		
	Cross metathesis	C_6=C + C_5=C_2	C_2=C + C_6=C_5 + C_5=C + C_6=C_2
	Homometathesis	C_5=C_2	C_5=C_5 + C_2=C_2
3a	Isomerisation	C_5=C_2	C_4=C_2
3b	Secondary metathesis		
	Cross metathesis	C_5=C + C_4=C_2	C_5=C_4 + C_2=C + C_5=C_2 + C_4=C
	Homometathesis	C_4=C_2	C_4=C_4 + C_2=C_2

*Hydrogens omitted for clarity, i.e., C_7=C is $(CH_3)_6CH=CH_2$

Primary metathesis refers to the major metathesis reaction
Secondary metathesis refers to the metathesis side-reactions due to isomerisation
Scheme 2 refers to reactions due to C_6=C formed in 1c
Scheme 3 refers to reactions due to C_5=C formed in 2b
Cross-metathesis refers to the metathesis reaction between different alkenes
Homo-metathesis refers to the metathesis reaction between the same alkenes

3.2 Metathesis reactions with $W(O\text{-}2,6\text{-}C_6H_3Cl_2)_2Cl_4$ catalytic system

The conversion of 1-octene to products during the metathesis reaction with the $W(O\text{-}2,6\text{-}C_6H_3Cl_2)_2Cl_4$/ Bu_4Sn catalytic system was followed by GC. A typical gas chromatogram of the products, which were identified spectroscopically by GC-MS, is shown in **Figure 3.1**. The major product that was identified is 7-tetradecene which is one of the desired PMP. Apart from the primary and secondary metathesis products, Bu_3SnCl and Bu_4Sn were also identified.

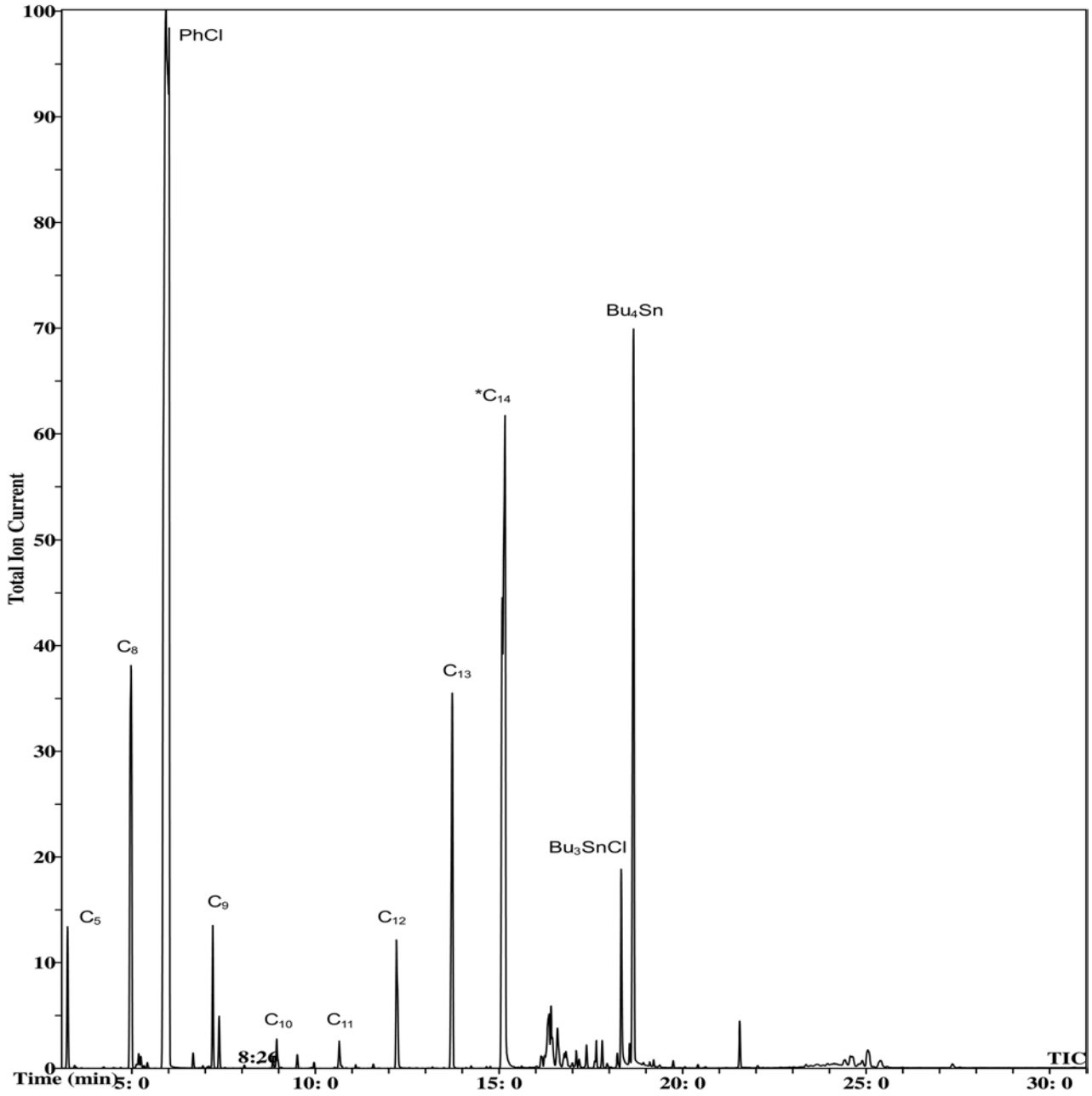

*alkenes abbreviation, eg; C_{14} is 7-tetradecene.

Figure 3.1 Typical gas chromatogram of the reaction products that formed during the metathesis of 1-octene in the presence of a $W(O\text{-}2,6\text{-}C_6H_3Cl_2)_2Cl_4/Bu_4Sn$ catalytic system.

Figure 3.2 shows the percentage yield of PMP's, SMP's and IP's and the conversion of 1-octene over a period of 210 minutes. The PMP's reach 63.6 %, SMP's and IP's reaches 2.5 % and 0.9 % respectively. 1-Octene is converted to 67 % of metathesis products in 30 minutes.

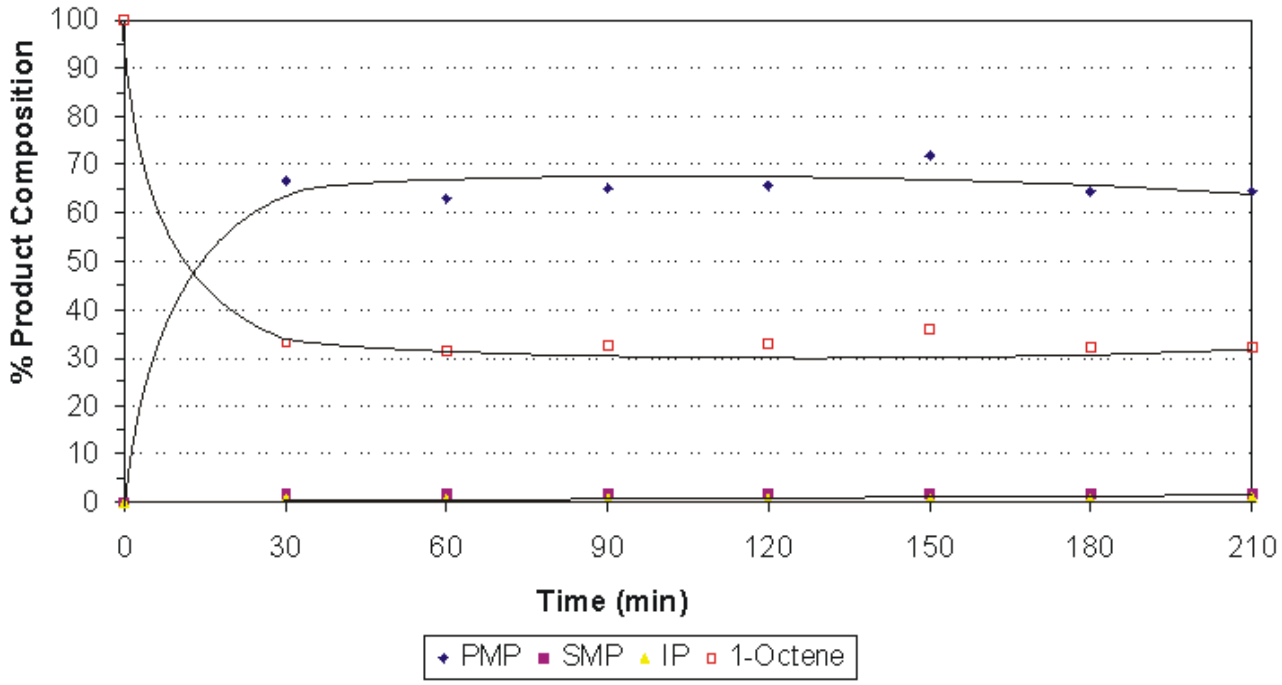

Figure 3.2 The conversion of 1-octene to PMPs, SMPs and IPs in the presence of the $W(O\text{-}2,6\text{-}C_6H_3Cl_2)_2Cl_4/Bu_4Sn$ catalytic system. (temperature = 85 ˚C; Sn/W molar ratio = 3/1; alkene/W molar ratio = 100/1; activation time = 20 min; solvent = PhCl)

3.3 Theoretical investigation of alkene metathesis

Mechanistic studies using calculated frontier orbitals and reaction energy profiles of the tungsten complexes are presented.

3.3.1 $W(O\text{-}2,6\text{-}C_6H_3Cl_2)_2Cl_4$ catalytic system

We proposed a mechanism for the metathesis of 1-octene into higher alkenes in the presence of the $W(O\text{-}2,6\text{-}C_6H_3Cl_2)_2Cl_4/Bu_4Sn$ catalytic system. This mechanism consists of three steps, namely; the formation of metal-carbene, activation step and the catalytic cycle.

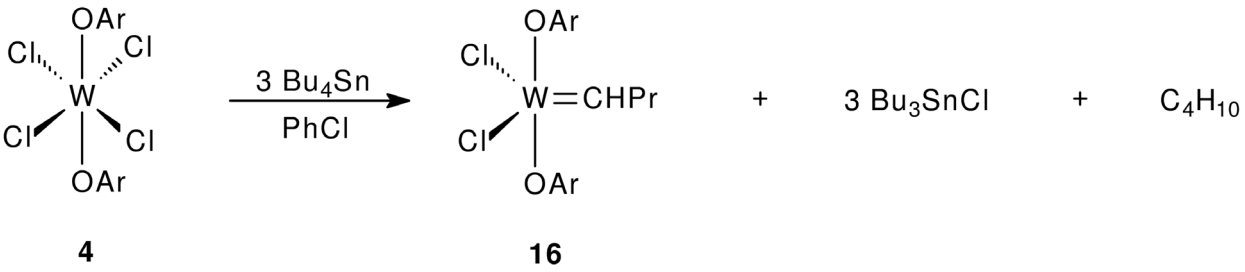

4 **16**

OAr = O-2,6-$C_6H_3Cl_2$

Scheme 3.1 The formation of a metal carbene by the W(O-2,6-$C_6H_3Cl_2$)$_2Cl_4$/Bu_4Sn catalytic system.

Scheme 3.1 shows the first step which is the formation of the metal carbene **16** which occurs by α-elimination reaction, three moles of tetrabutyltin reacts with one mole of tungsten pre-catalyst to form the metal-carbene **16**, tributyltin chloride and butane.[5] **Figure 3.3** shows the HOMO and LUMO pictures of the tungsten pre-catalyst (**4**) and their energies.

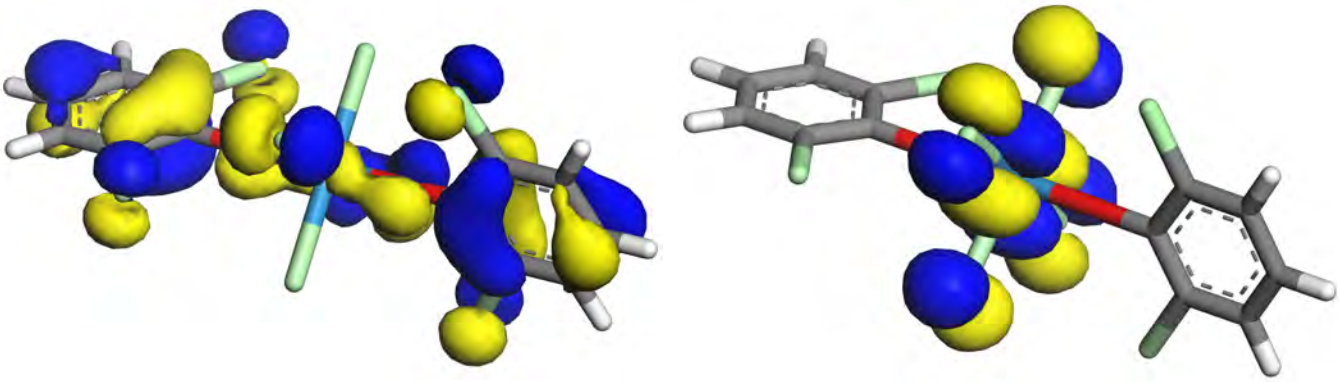

HOMO
E = -0.233568 eV

LUMO
E = -0.195718 eV

Figure 3.3 HOMO and LUMO of **4**.

For the metal-carbene **16** to be formed from **4**, a co-catalyst is required which in this case is the Bu_4Sn. **Figure 3.4** shows the pictures of the HOMO and LUMO of the Bu_4Sn and their energies.

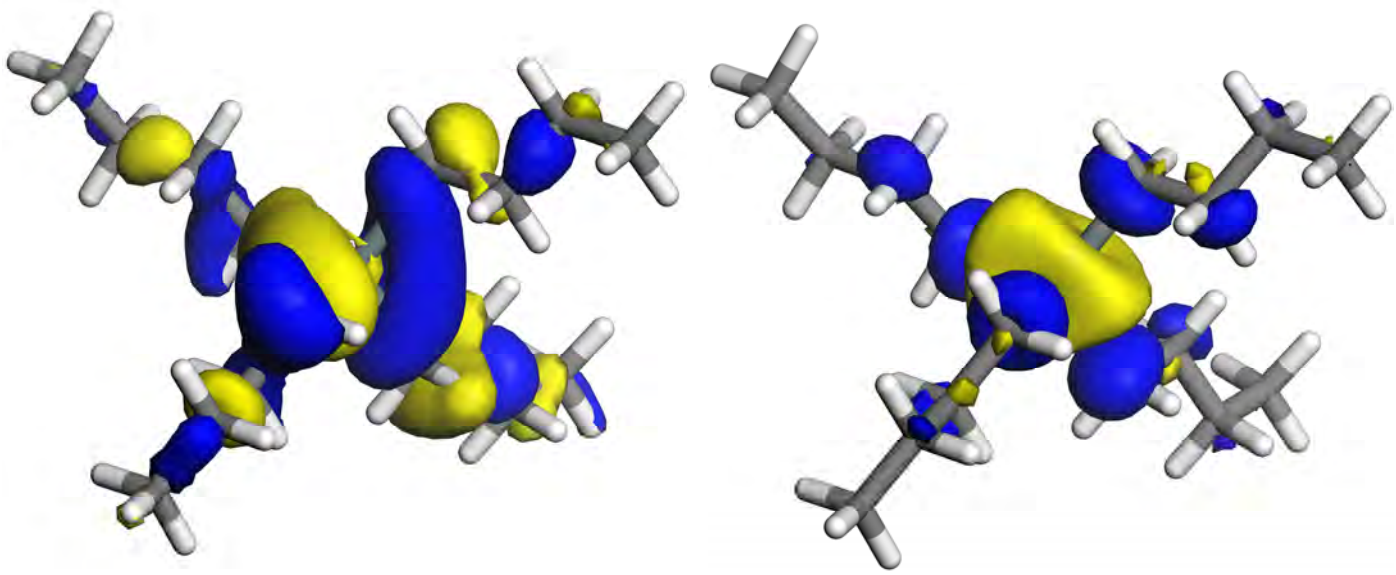

HOMO
E = -0.218114 eV

LUMO
E = 0.01173 eV

Figure 3.4 HOMO and LUMO of tetrabutyltin (Bu_4Sn).

Table 3.2 shows that the smallest HOMO/LUMO energy gap between the pre-catalyst **4** and the co-catalyst (Bu_4Sn) must be between the HOMO of Bu_4Sn and the LUMO of the W(O-2,6-$C_6H_3Cl_2)_2Cl_4$ pre-catalyst (**4**). The energy gap between these two interacting molecules is 0.022396 eV.

Table 3.2 Energies of the frontier orbitals of Bu_4Sn and W(O-2,6-$C_6H_3Cl_2)_2Cl_4$ pre-catalyst (**4**)

	4	**Bu_4Sn**
HOMO (eV)	-0.233568	-0.218114
LUMO (eV)	-0.195718	0.011730
	Bu_4Sn HOMO vs. 4 LUMO	**Bu_4Sn LUMO vs. 4 HOMO**
E (eV)	-0.218114	0.011730
E (eV)	-0.195718	-0.195718
Energy difference (eV)	-0.022396	0.207448
Absolute values	0.022396	0.207448

The next important aspects of orbital overlap are the symmetry and orientation of the orbitals. **Figure 3.5** shows how the LUMOs of **4** and HOMOs of Bu_4Sn overlaps, the symmetry of these orbitals are the same and that their orientation allows them to approach each other with minimal steric hindrance.

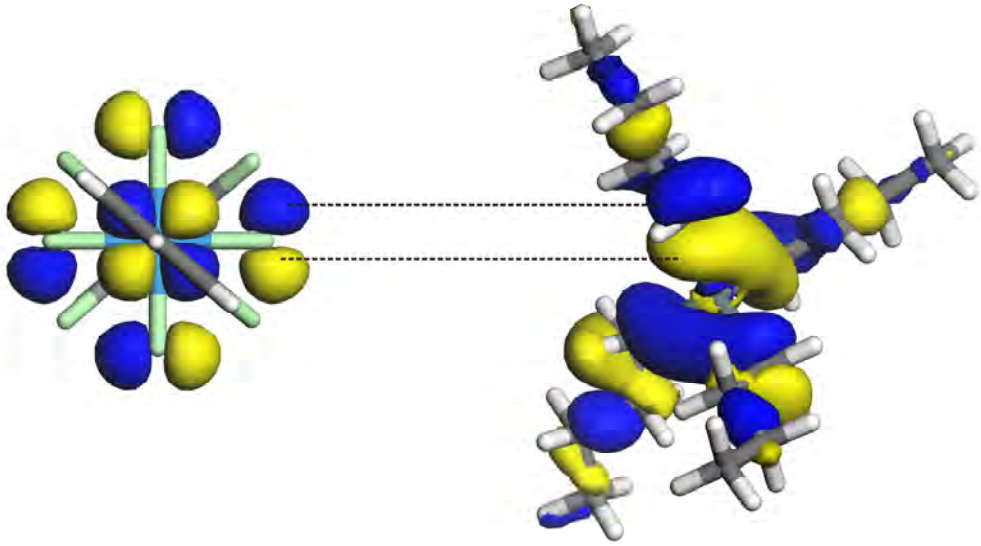

Figure 3.5 Symmetry and orientation of **4** and Bu_4Sn.

The second step is the activation step of the metathesis reaction. In this step, the interaction of the metal-carbene **16** and 1-octene occurs *via* a [2+2] cycloaddition followed by cycloreversion. In **Scheme 3.2** two possible activation steps are proposed, one route leading to the heptylidene species and the other leading to the methylidene species. These routes are determined by the orientation in which the 1-octene approaches the metal carbene to form the active species.

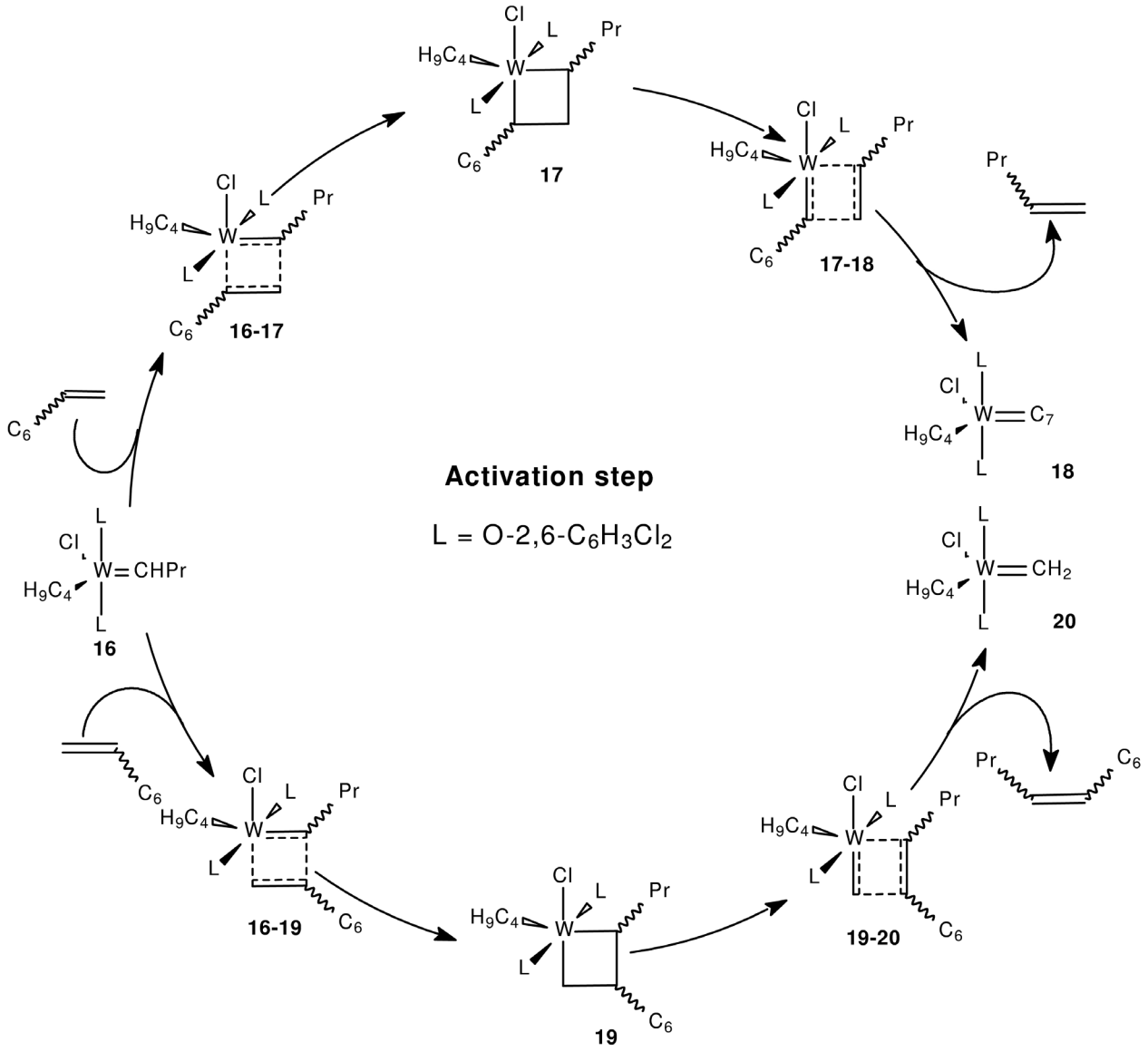

Scheme 3.2 Two activation routes of the metathesis of 1-octene with the $W(O\text{-}2,6\text{-}C_6H_3Cl_2)_2Cl_4$ catalytic system.

The frontier orbitals and the energies of the metal-carbene (**16**) (**Figure 3.5**) and 1-octene (**Figure 3.6**) shows the overlap to be in a geometry and size proportional for the formation of the active species i.e., the heptylidene and the methylidene, **18** and **20** respectively. There is the heptylidene route **16** to **18** and the methylidene route **16** to **20** can be distinguished, each route has two transition states **16-17** and **17-18** along the heptylidene route and **16-19** and **19-20** along the methylidene route. There exist one intermediate or the metallacyclobutane for each route, **17** for the heptylidene route and **19** for the methylidene route. The heptylidene route forms 1-pentene while the methylidene route forms 4-undecene which are the metathesis products observed in **Figure 3.1**.

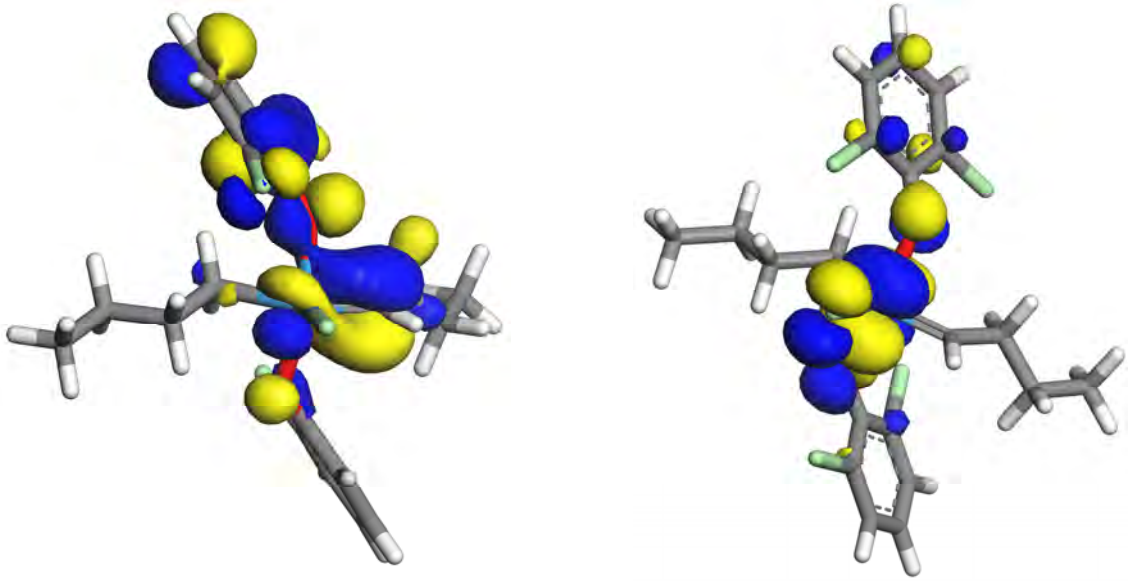

HOMO
E = -0.204498 eV

LUMO
E = -0.13904 eV

Figure 3.5 HOMO and LUMO of **16**.

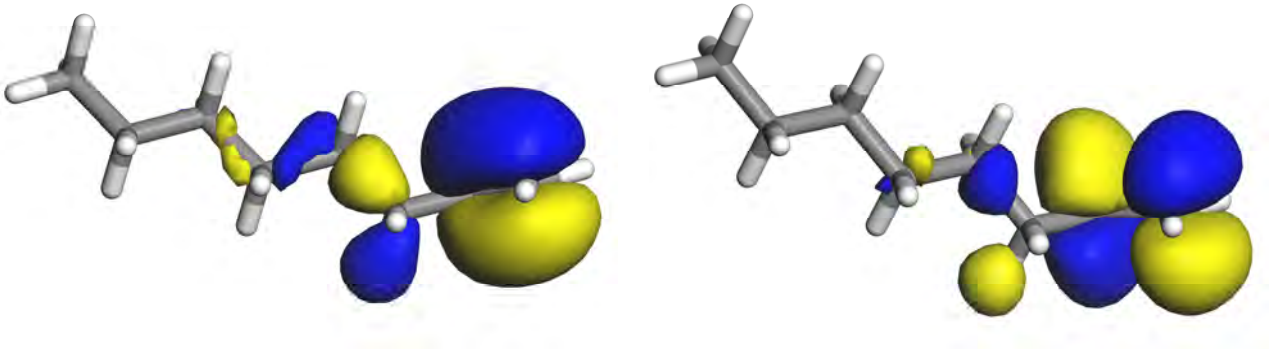

HOMO
E = -0.217262 eV

LUMO
E = -0.009538 eV

Figure 3.6 HOMO and LUMO of 1-octene.

Table 3.3 shows the energies of the frontier orbitals of the metal-carbene (**16**) and 1-octene, the most favourable overlap is between the metal-carbene (**16**) LUMO and the 1-octene HOMO which have an energy gap of 0.078222 eV. This overlap is consistent with the orbitals size, shape and geometry.

Table 3.3 Energies of the frontier orbitals of **16** and 1-octene

	16	**1-octene**
HOMO	-0.204498	-0.217262
LUMO	-0.13904	-0.009538
	16 HOMO vs. 1-octene LUMO	**16 LUMO vs. 1-octene HOMO**
E (eV)	-0.204498	-0.139040
E (eV)	-0.009538	-0.217262
Energy difference (eV)	-0.194960	0.078222
Absolute values	0.194960	0.078222

Scheme 3.2 shows the two activation steps of **16** leading to **18** and **20**, these two species are formed by the orientation in which 1-octene approaches **16**. If 1-octene approaches from the butyl face of **16** therefore **18** will be formed, but if 1-octene approaches away from the butyl face of **16** then **20** will be formed (**Figure 3.7**). In each approach, 1-octene is oriented accordingly such that there will be symmetry on the orbitals.

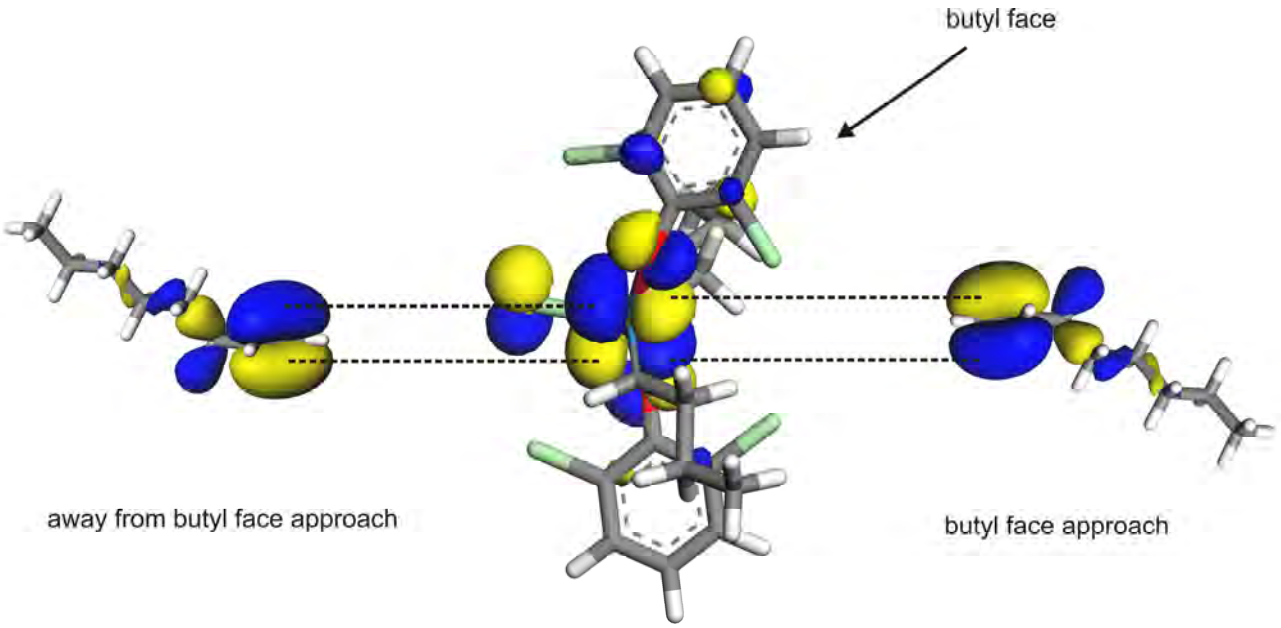

Figure 3.7 Symmetry and orientation of **16** and 1-octene.

Figure 3.8 shows the energy profile of the 1-octene activation of **16**. The energies of all the structures are normalised with respect to **16** and all the energy values in the profile are given in kcal/mol units. The mechanism of this reaction occurs in a manner that the bonds break and form

simultaneously suggesting an associative mechanism. The metal-carbene (**16**), heptylidene (**18**) and methylidene (**20**) are all 14-electron species. The electronic energy which is required to convert **16** to the metallacyclobutane **17**, is the activation energy of 32.55 kcal/mol. Once **17** is formed an energy barrier of 49.12 kcal/mol is required to form **18**, which has a lower energy (-8.89 kcal/mol) than its starting material **16**. The methylidene species (**20**) is formed *via* a metallacyclobutane (**19**) when **16** goes through an activation energy of 20.39 kcal/mol. This metallacyclobutane must overcome an energy barrier of 41.23 kcal/mol to form **20**, which has an energy of 1.57 kcal/mol higher than its starting material **16**.

The heptylidene route is thermodynamically favoured or is exothermic and **18** is more stable than **20**. The step **16→(16-17)→17** is the rate limiting step of the heptylidene route, because **16-17** is at 32.56 kcal/mol compared to **17-18** which lies at 30.18 kcal/mol. The rate limiting step of the methylidene route is **16→(16-19)→19** which has **16-19** at 20.39 kcal/mol while **19-20** lies at 11.50 kcal/mol. Therefore the methylidene route will be most favoured because of its lower activation energy.

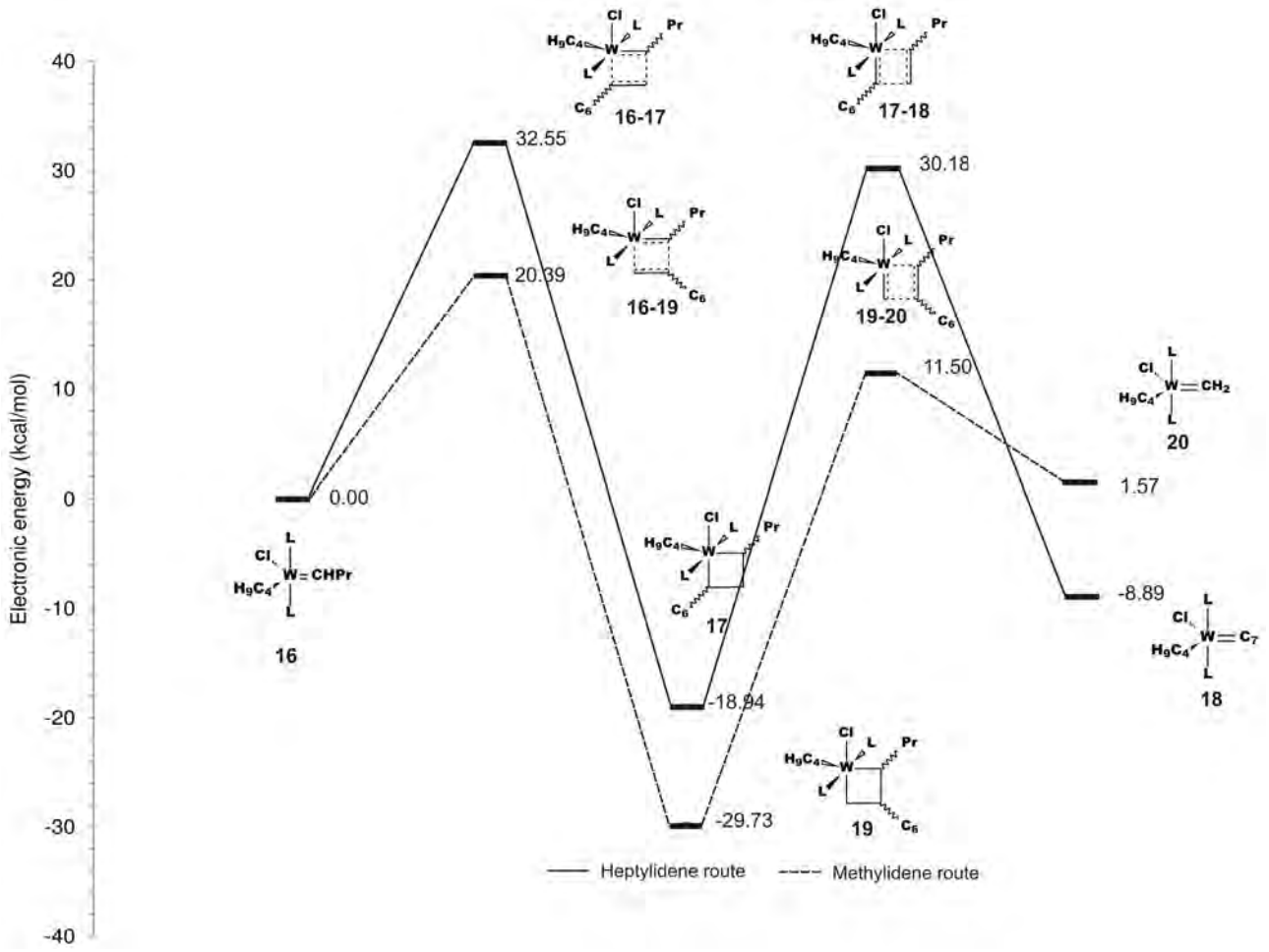

Figure 3.8 Electronic energy profile for the activation steps of the tungsten pre-catalyst by the metathesis of 1-octene.

The third step; which is the productive catalytic cycle of the conversion of 1-octene by the metal-carbenes **18** and **20** is shown in **Scheme 3.3**, and it is the last step in the reaction mechanism. The products of this cycle are the 7-tetradecene and ethene from two moles of 1-octene. The cycle has four transition states (**18-21**), (**21-20**), (**20-22**) and (**22-18**) and two intermediates **21** and **22**. The size, shape and geometry of the orbitals are, by observation and by calculations determined for the most probable overlap, which will lead to both the heptylidene and the methylidene species.

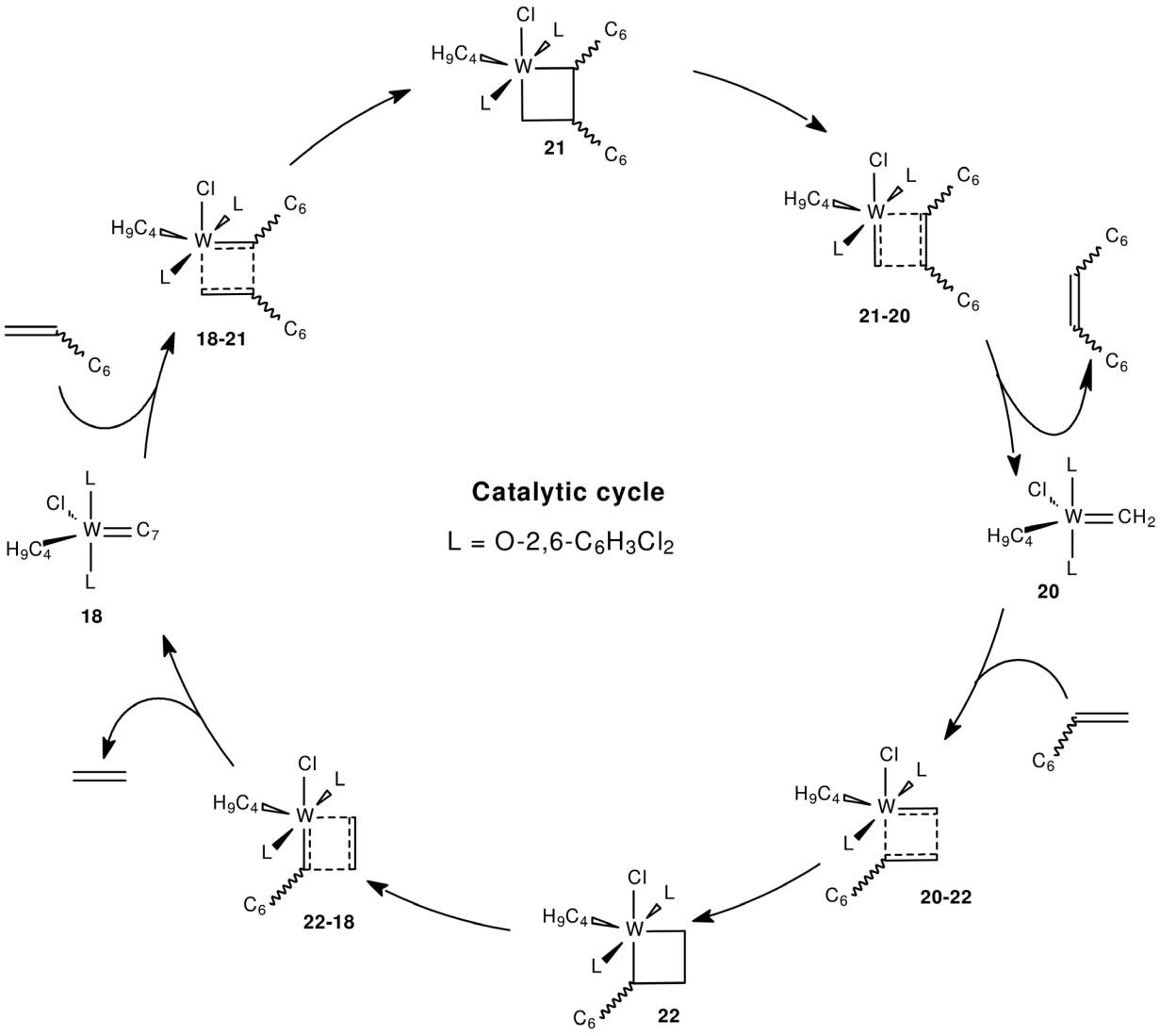

Scheme 3.3 The productive catalytic cycle of **18** and **20** with 1-octene.

The geometry, size and shape of the frontier orbitals of the heptylidene (**18**) are illustrated in **Figure 3.9**. **Table 3.4** shows that the frontier orbitals of the heptylidene **18** and 1-octene will overlap by the heptylidene LUMO and 1-octene HOMO, which is a combination that gives the lowest energy gap of 0.073425 eV.

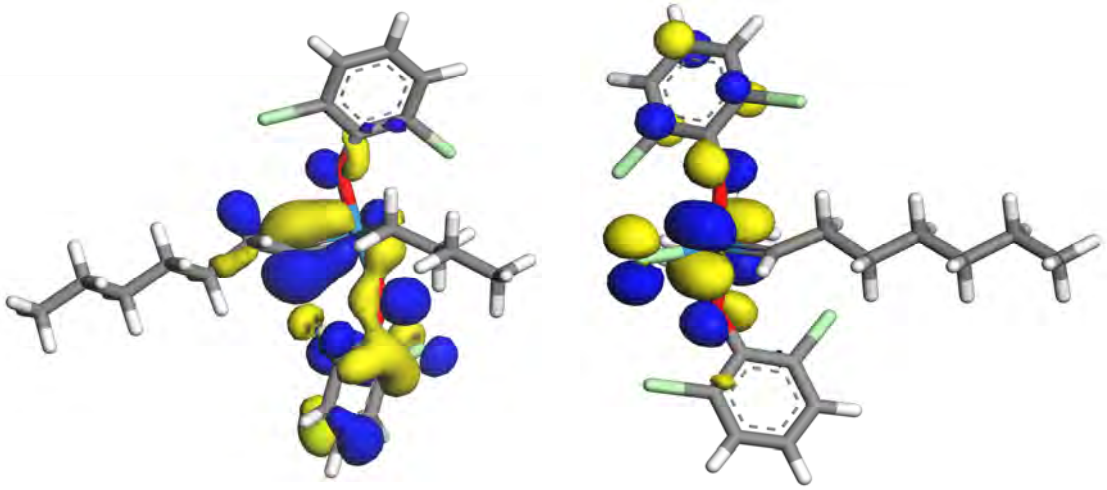

HOMO
E = -0.203923 eV

LUMO
E = -0.143837 eV

Figure 3.9 HOMO and LUMO of **18**.

Table 3.4 Energies of the frontier orbitals of the heptylidene(**18**) and 1-octene

	18	**1-octene**
HOMO **LUMO**	-0.203923 -0.143837	-0.217262 -0.009538
	18 HOMO vs. 1-octene LUMO	**18 LUMO vs. 1-octene HOMO**
E (eV) **E (eV)** **Energy difference (eV)** **Absolute values**	-0.203923 -0.009538 -0.194385 0.194385	-0.143837 -0.217262 0.073425 0.073425

Figure 3.10 shows how the LUMOs of **18** and HOMOs of 1-octene overlaps, the symmetry of these orbitals are the same and that their orientation allows them to approach each other without any hindrance. This interaction will lead to the methylidene (**20**) and 7-tetradecene as shown in **Scheme 3.3**.

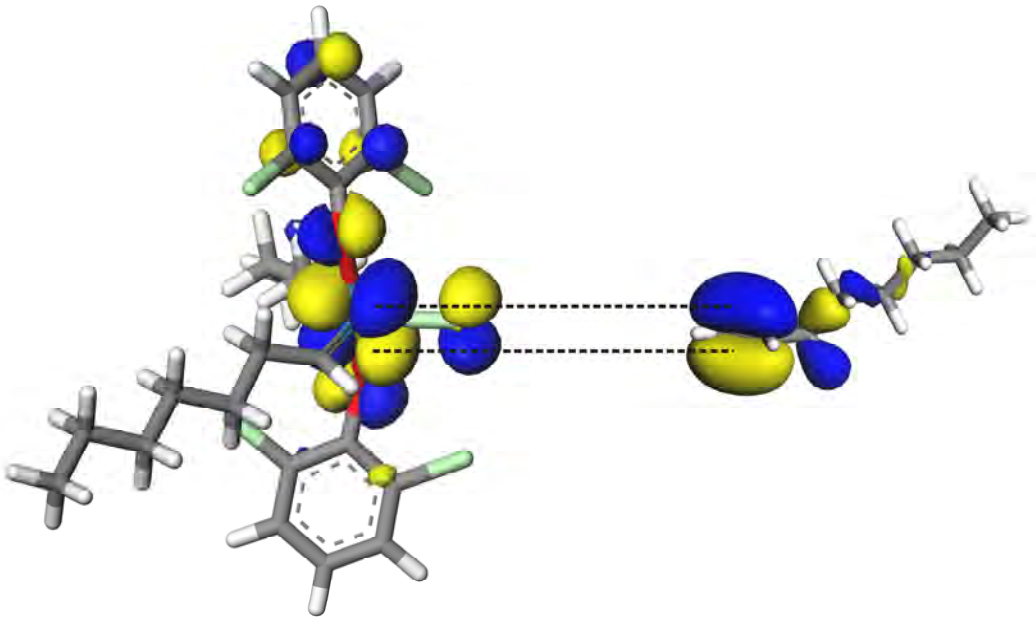

Figure 3.10 Symmetry and orientation of **18** and 1-octene.

The second half of the catalytic cycle is the interaction of the methylidene (**20**) and 1-octene, leading back to **18** and thus completing the cycle. The frontier orbitals energies are presented in **Table 3.5** for determining the probable overlap. The HOMO and LUMO structures of **20** are shown in **Figure 3.11**.

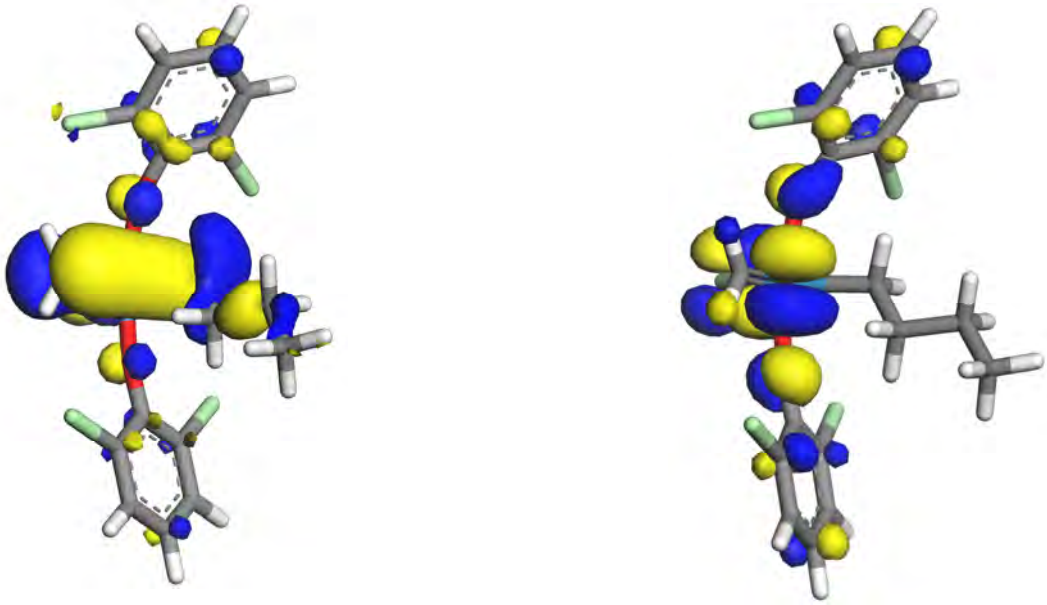

HOMO
E = -0.209115 eV

LUMO
E = -0.148448 eV

Figure 3.11 HOMO and LUMO of **20**.

Table 3.5 Energies of the frontier orbitals of **20** and 1-octene

	20	**1-octene**
HOMO (eV)	-0.209115	-0.217262
LUMO (eV)	-0.148448	-0.009538
	20 HOMO vs. 1-octene LUMO	**20 LUMO vs. 1-octene HOMO**
E (eV)	-0.209115	-0.148448
E (eV)	-0.009538	-0.217262
Energy difference (eV)	-0.199577	0.068814
Absolute values	0.199577	0.068814

Table 3.5 shows that the frontier orbitals will overlap by the methylidene (**20**) LUMO and 1-octene HOMO, which is a combination that gives the lowest energy gap of 0.068814 eV. **Figure 3.12** shows how the LUMO of **20** and HOMO of 1-octene overlaps, the symmetry of these orbitals are also the same and that their orientation allows them to approach each other, therefore there will be minimal steric hindrance for these two molecules to overlap. This interaction will lead back to **18** and forms ethene as shown in **Scheme 3.3** and thus completing the cycle.

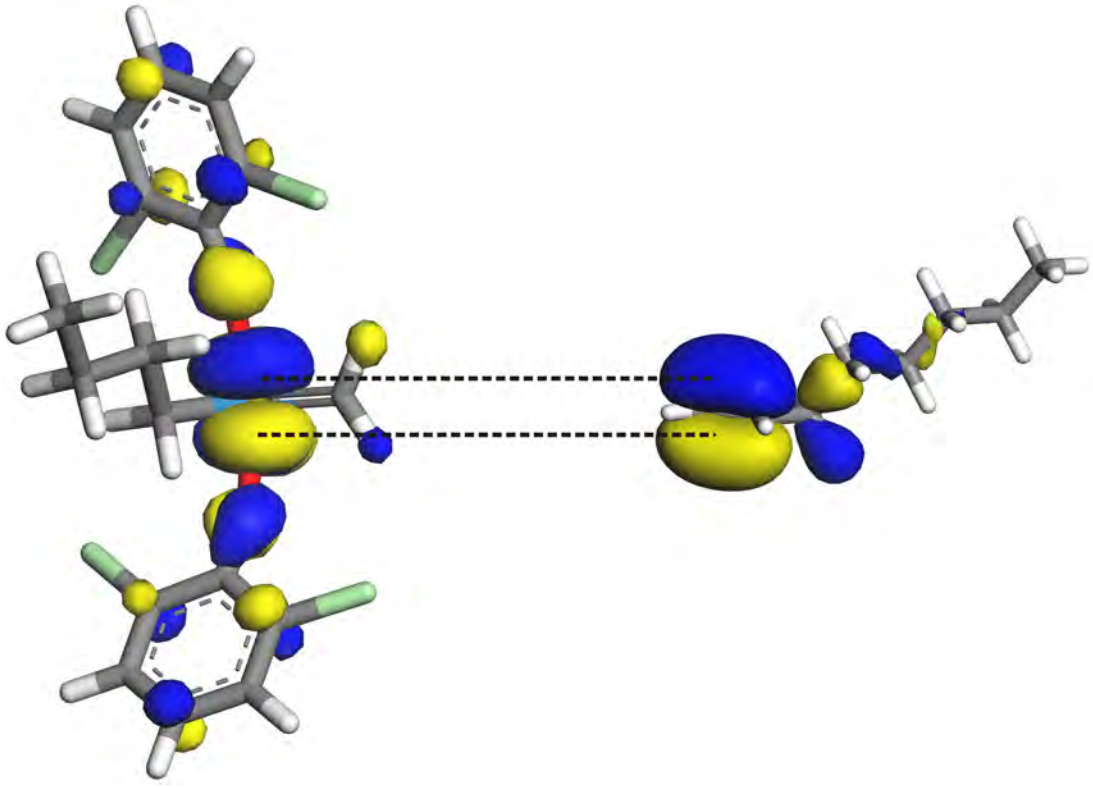

Figure 3.12 Symmetry and orientation of **20** and 1-octene.

The electronic energy profile of the catalytic cycle for the productive 1-octene conversion using the metal-carbenes **18** and **20** is shown in **Figure 3.13**. The energies of all the structures are normalised with respect to the heptylidene (**18**) and all the energy values in the profile are given in kcal/mol.

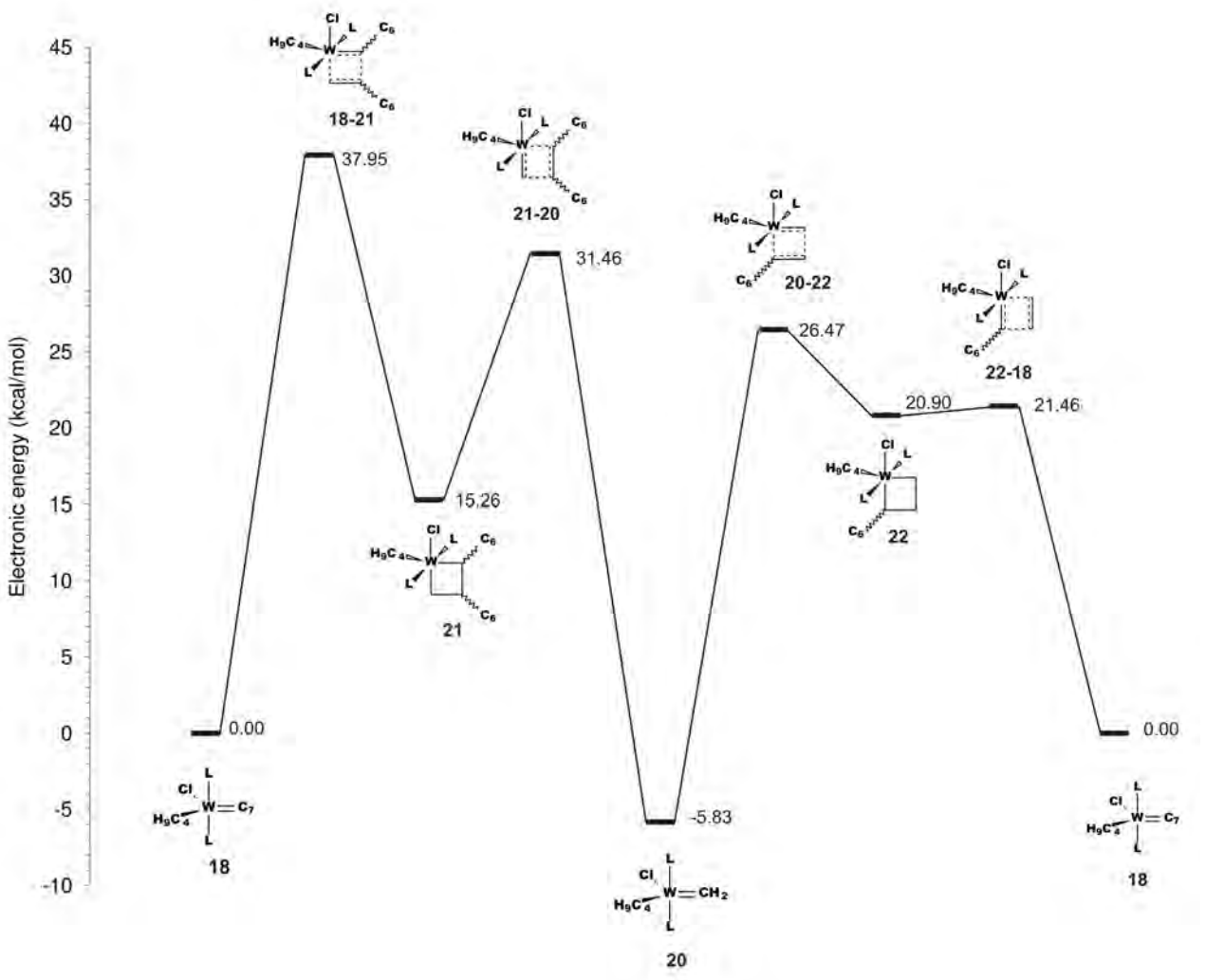

Figure 3.13 The energy profile of the catalytic cycle of 1-octene conversion by the metal carbenes **18** and **20**.

The formation of the metallacyclobutane (**21**) requires an activation energy of 37.95 kcal/mol and for this intermediate to form the methylidene **20**, 16.20 kcal/mol of energy barrier must be overcome and the first PMP, 7-tetradecene will be formed. The second metallacyclobutane (**22**) requires 32.3 kcal/mol of energy to be formed and to convert this intermediate back to the heptylidene (**18**), an energy barrier of 0.56 kcal/mol is required and the second PMP is formed namely ethene. The rate limiting step of the catalytic cycle is **18→(18-21)→21** which has the highest electronic energy of 37.95 kcal/mol. The catalytic cycle will be more possible to start at **20** which is also the more favoured route in the catalytic cycle, but as soon as the concentration of **18** is higher, the heptylidene route will then follow.

3.3.2 Beerens catalyst

The Beerens catalyst (**1**) is synthesised by the cross metathesis of four moles of the metal-carbene **16** and one mole of tetraallylsilane (**23**) (**Scheme 3.4**) and producing 1-pentene as a by-product.[5]

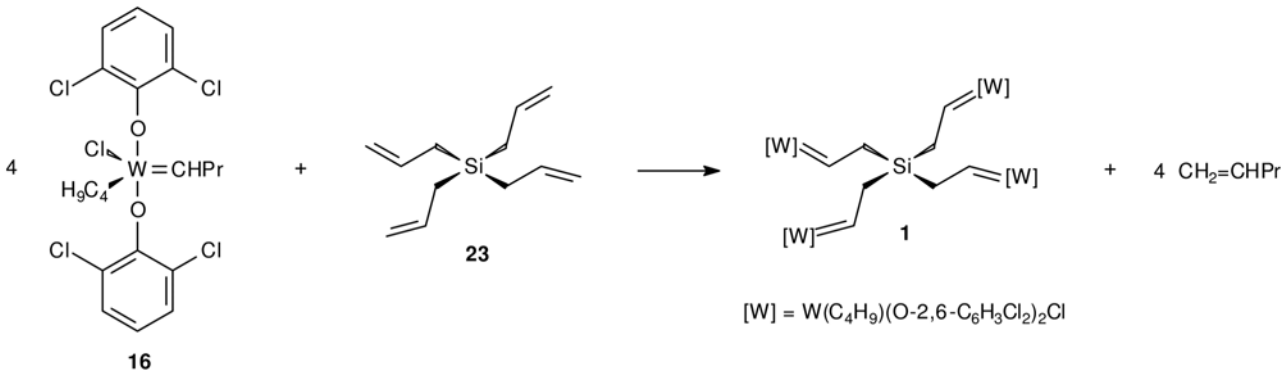

Scheme 3.4 Synthesis of the Beerens Catalyst **1**[5].

The frontier orbitals of **23** are shown in **Figure 3.14** and that of the metal-carbene (**16**) are shown in **Figure 3.5**. The smallest energy gap between the metal-carbene (**16**) LUMO and the tetraallylsilane (**23**) HOMO is indicated in **Table 3.6** as 0.068322 eV.

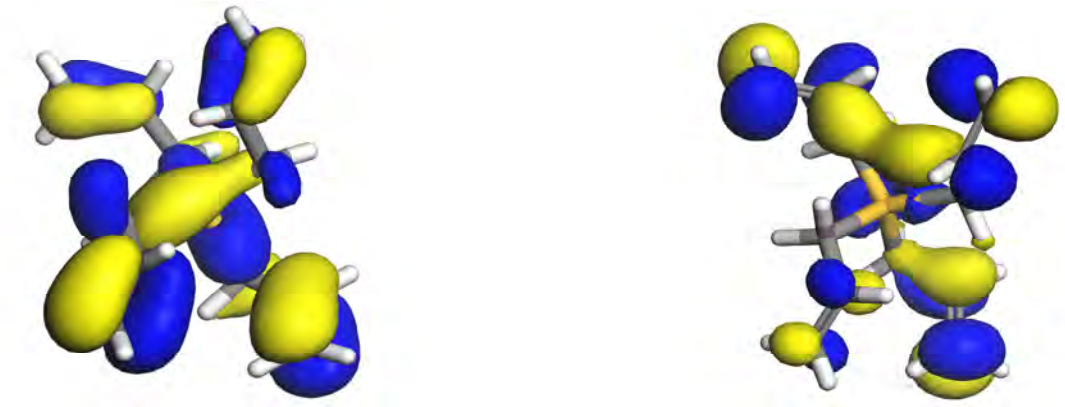

HOMO

E = -0.207362 eV

LUMO

E = -0.034566 eV

Figure 3.14 HOMO and LUMO of the tetraallylsilane **23**.

Table 3.6 Energies of the frontier orbitals of the metal-carbene (**16**) and tetraallylsilane (**23**)

	16	**23**
HOMO	-0.204498	-0.207362
LUMO	-0.139040	-0.034566
	16 HOMO vs. 23 LUMO	**16 LUMO vs. 23 HOMO**
E (eV)	-0.204498	-0.139040
E (eV)	-0.034566	-0.207362
Energy difference E (eV)	-0.169932	0.068322
Absolute values	0.169932	0.068322

Figure 3.15 shows how the orbitals of **16** and **23** will overlap to form **1** and 4 molecules of 1-pentene. The symmetry of the orbitals are the same allowing the orbitals to overlap and the approach of tetraallylsilane is direct onto the orbitals of the metal-carbene (**16**).

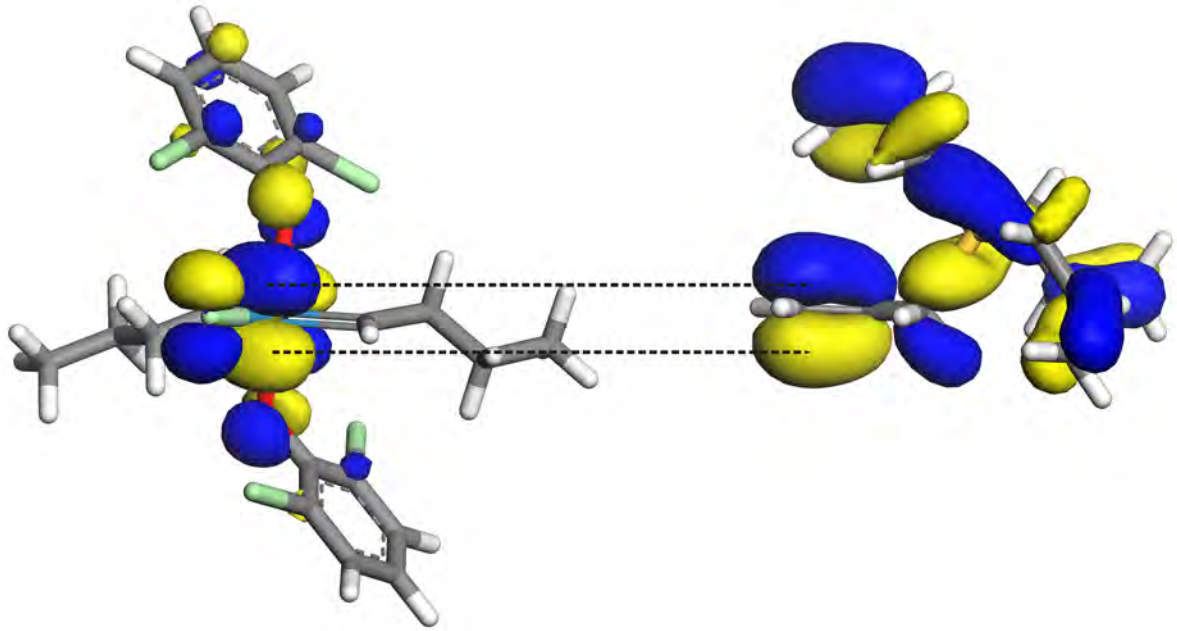

Figure 3.15 Symmetry and orientation of **16** and **23**.

The metathesis mechanism of the Basset's and Beerens's catalyst differ only in terms of the activation steps, the catalytic cycle is the same since the silane dendrimer/ligand of **1** is removed from the catalyst, leaving the catalyst to convert the 1-octene to PMPs, SMPs and IPs,as shown in **Figure 3.2**.

The two activation steps proposed for **1** are shown in **Scheme 3.5** below. **1** has four peripheries in which it can interact with 1-octene, in this study we only investigated the interaction of one arm/periphery of the catalyst (**1**) because of calculation time and method constraints.

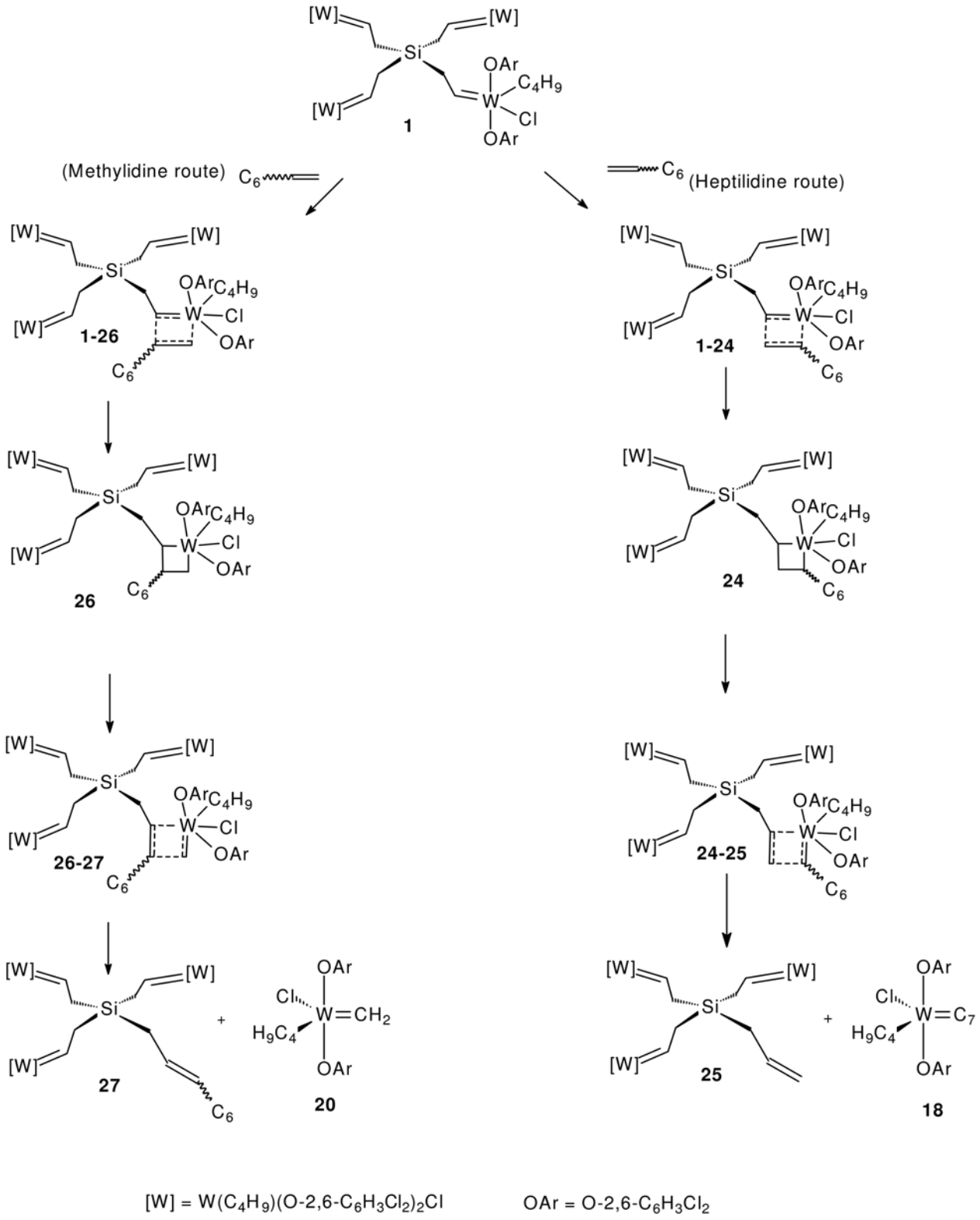

Scheme 3.5 Activation steps of the Beerens catalyst (**1**).

The frontier orbitals of **1** are shown in **Figure 3.16** and in **Table 3.7** the energies of the frontier orbitals of **1** and 1-octene are tabulated. From this table it is shown that the LUMO of **1** and HOMO

of 1-octene which has the smallest energy gap of 0.067778 eV, will overlap for the catalytic conversion.

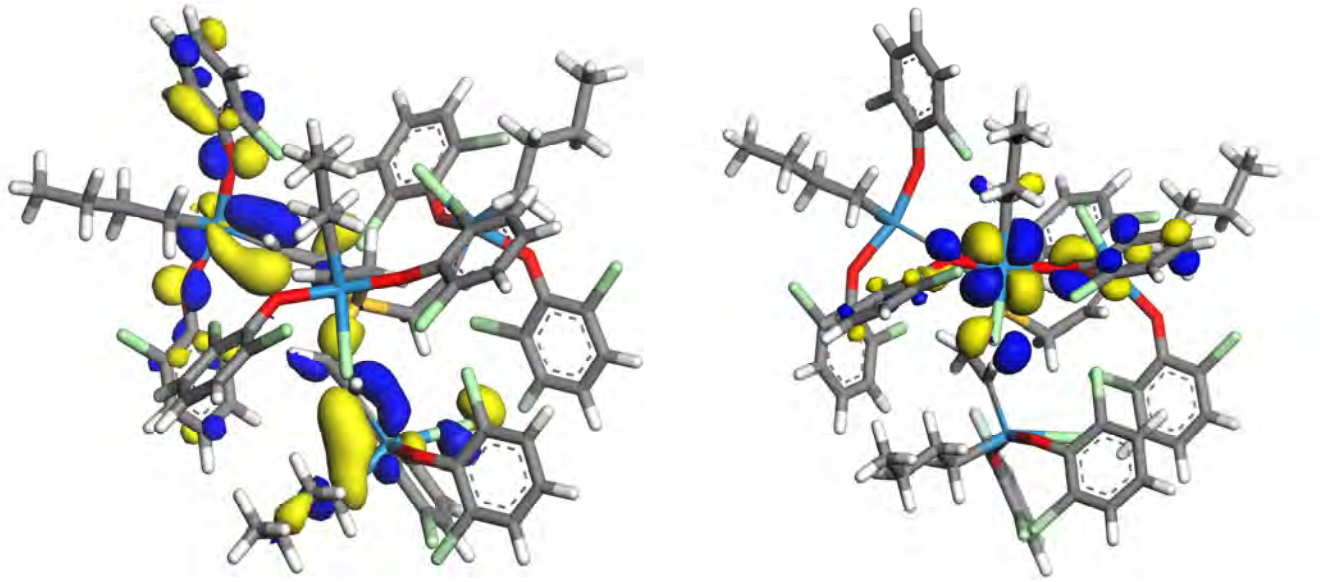

HOMO
E = -0.197119 eV

LUMO
E = -0.149484 eV

Figure 3.16 HOMO and LUMO of **1**.

Table 3.7 Energies of the frontier orbitals of **1** and 1-octene

	1	**1-octene**
HOMO (eV)	-0.197119	-0.217262
LUMO (eV)	-0.149484	-0.009538
	1 HOMO vs. 1-octene LUMO	**1 LUMO vs. 1-octene HOMO**
E (eV)	-0.197119	-0.149484
E (eV)	-0.009538	-0.217262
Energy difference (eV)	-0.187581	0.067778
Abs values	0.187581	0.067778

Figure 3.17 shows how the frontier orbitals of **1** and 1-octene will overlap in the activation step, 1-octene can approach from the chlorine side of **1** or from the side that is between one arm of **1** and butyl side. The first approach will lead to the heptylidene (**18**) and **25** and the latter will lead to the methylidene (**20**) and **27**. The HOMO and LUMO of **1** and 1-octene have the same symmetry and thus allow them to overlap with minimal steric hindrance.

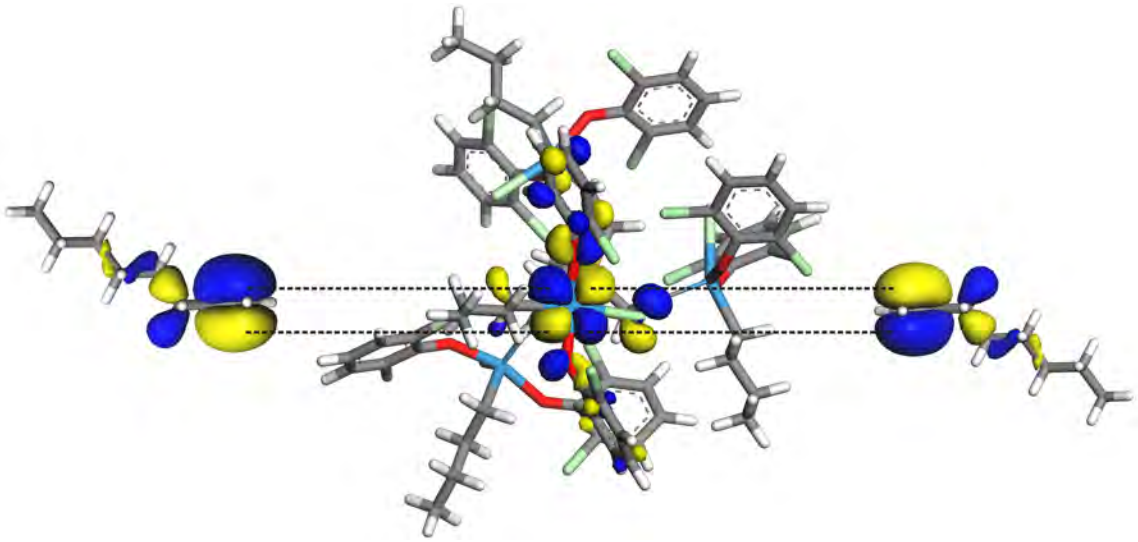

Figure 3.17 Symmetry and orientation of **1** and 1-octene.

The energy profile of 1-octene activation of **1** is shown in **Figure 3.18.** Both the heptylidene (**18**) and the methylidene (**20**) are presented in this profile and the energy values in this graph are normalised to the energy of **1** and the units are in kcal/mol.

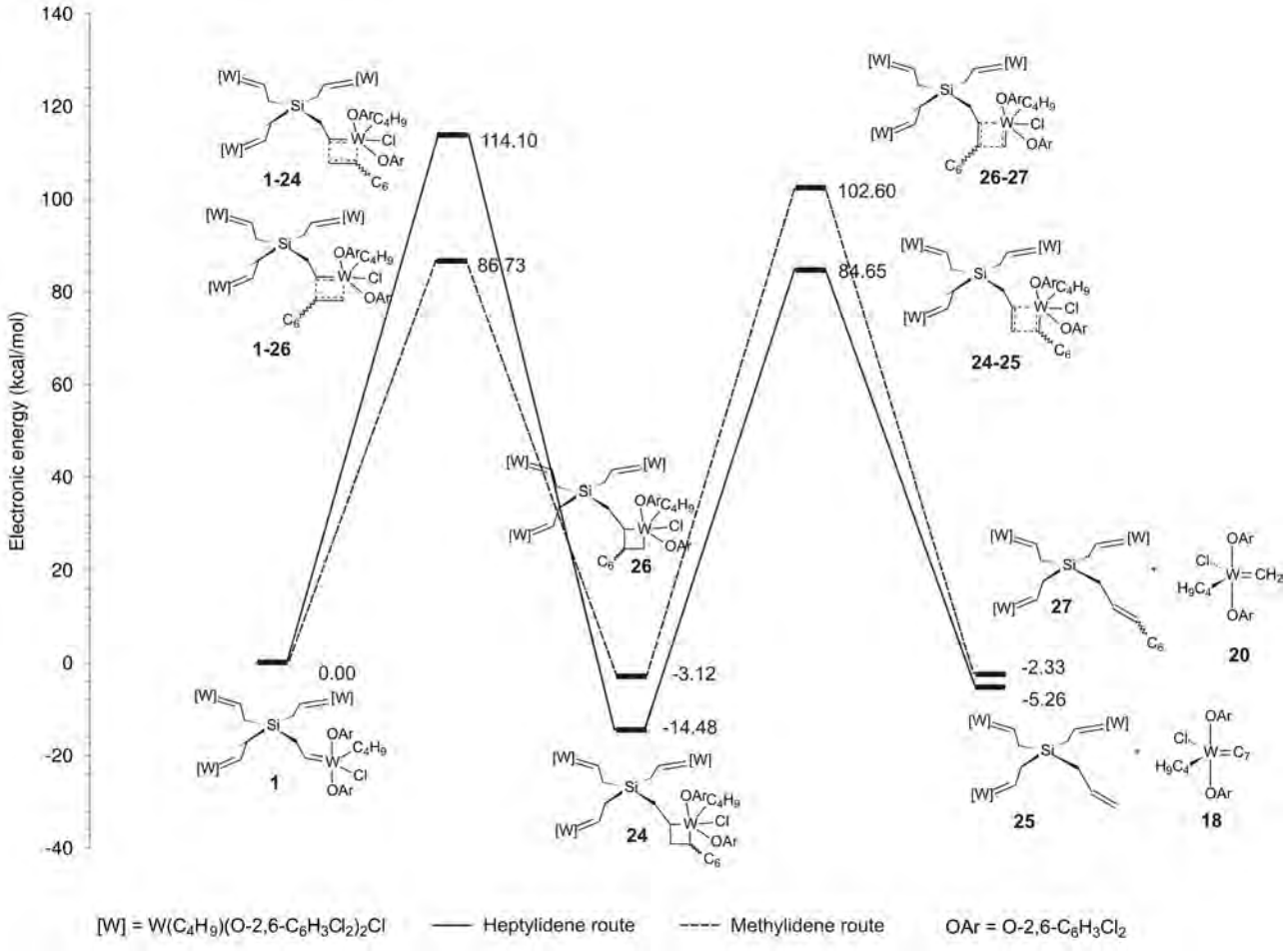

Figure 3.18 The energy profile of the activation steps of **1** by 1-octene.

The 1-octene activation of **1** requires 114.1 kcal/mol energy to form the metallacyclobutane (**24**). **25** and **18** will be formed by **24** overcoming an energy barrier of 99.13 kcal/mol. The methylidene route has the metallacyclobutane **26** which will be formed by activation energy of 86.73 kcal/mol. The methylidene species (**20** and **27**) will be formed by overcoming an energy barrier of 105.72 kcal/mol. The two activation steps are thermodynamically favoured since, the products (**18** and **25**) and (**20** and **27**) are lower in energy than their starting material **1**. The rate limiting step for the heptylidene route is **1→(1-24)→24** and for the methylidene route is **26→(26-27)→(20+27)**. The methylidene route will be most favoured because of its lower activation energy.

The energy profiles of both **1** in (**Figure 3.18**) and **16** in (**Figure 3.7**) shows that the methylidene route has lower activation energy. The energy of the intermediate (**19**) of the methylidene route in **16** is lower in energy than the intermediate (**17**) of the heptylidene route, while in **1**, the energy of the intermediate (**24**) of the heptylidene route is lower in energy than the intermediate (**26**) of the methylidene route. The heptylidene (**18**) is lower in energy than the methylidene (**20**) energy, making **20** the more stable active species in both the activation steps of **1** and **16**.

3.3.3 The G0-W_2 catalyst.

Scheme 3.6 shows the synthesis of **2**, four moles of **4** reacts with one mole of tetrallylsilane in chlorobenzene to give the intermediate (**28**). The intermediate reacts with 12 moles of tetrabutyltin and forms **2**, tributyltin chloride and butane.[6]

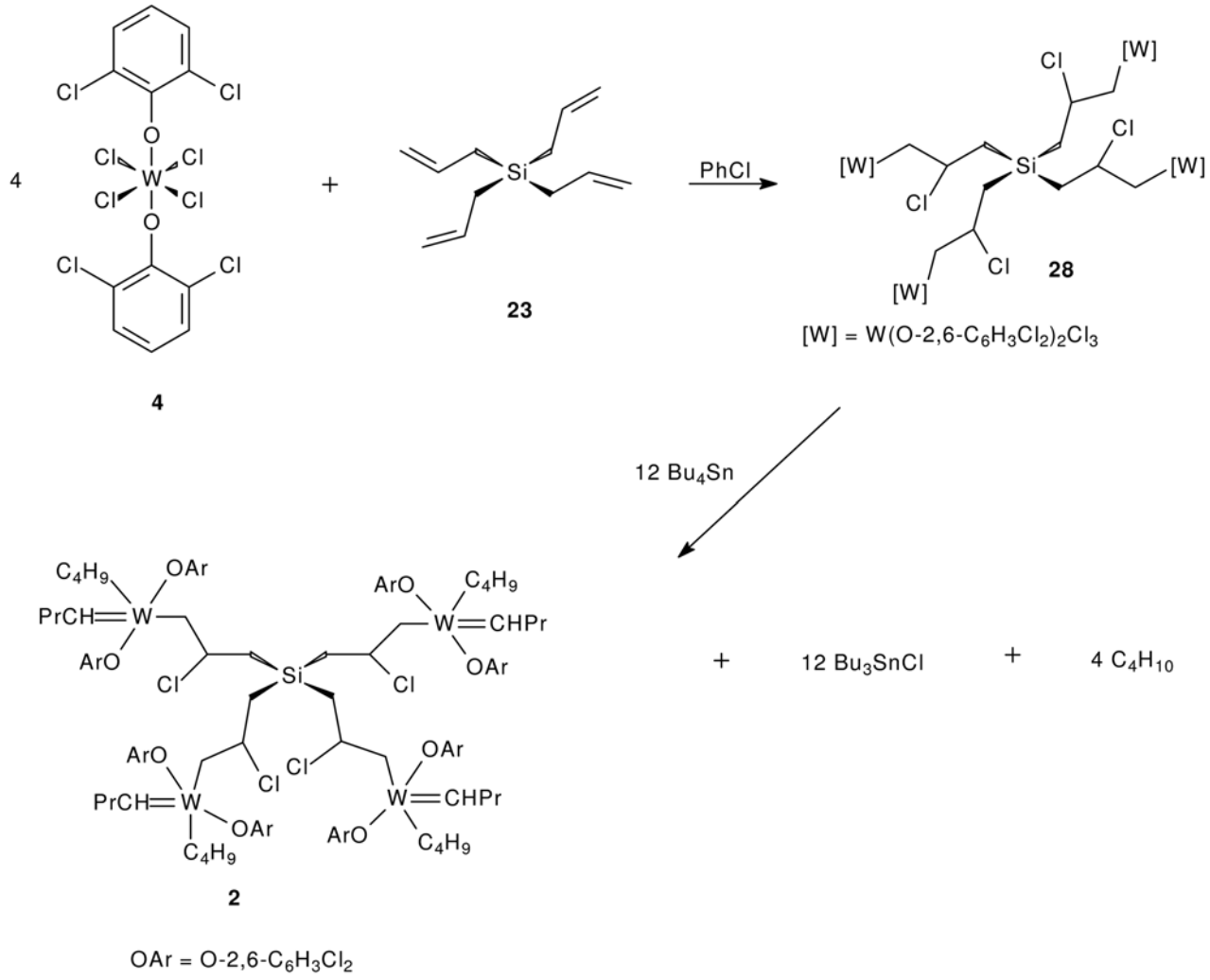

Scheme 3.6 Synthesis of **2**.[6]

The frontier orbitals of **4** and **23** are shown in **Figure 3.3** and **Figure 3.14** respectively. From **Table 3.8** the formation of **28** will occur from the overlap of **4** LUMO and **23** HOMO which have an energy gap of 0.011644 eV.

Table 3.8 Energies of the frontier orbitals of **4** and **23**

	4	**23**
HOMO (eV)	-0.233568	-0.207362
LUMO (eV)	-0.195718	-0.034566
	4 HOMO vs. 23 LUMO	**4 LUMO vs. 23 HOMO**
E (eV)	-0.233568	-0.195718
E (eV)	-0.034566	-0.207362
Energy difference (eV)	-0.199002	0.011644
Absolute values	0.199002	0.011644

Figure 3.18 shows the cross sectional view of the LUMOs of **4** and HOMOs of **23**, the symmetry of these orbitals are the same and that their orientation allows them to approach each other and overlap with minimal steric hindrance.

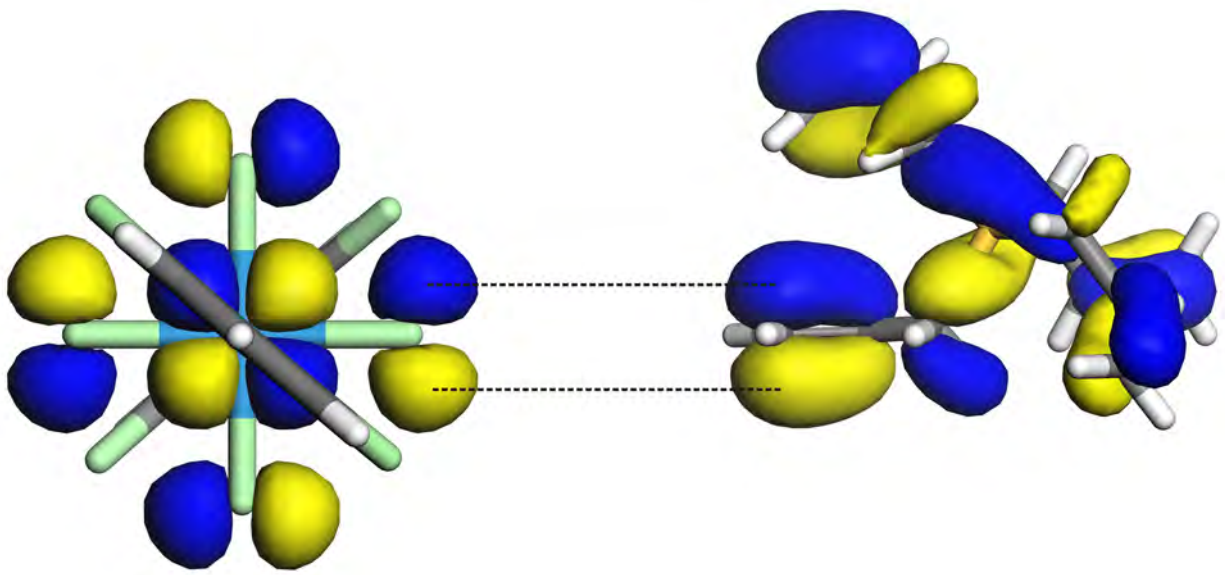

Figure 3.18 Symmetry and orientation of **4** and **23**.

Figure 3.19 shows the frontier orbitals of **28** and that of tetrabutyltin are shown in **Figure 3.4**. **Table 3.9** shows the energies of the frontier orbitals of **28** and the tetrabutyltin, and the overlap will occur between **28** LUMO and the tetrabutyltin (**23**) HOMO which have energy gap of 0.037636 eV.

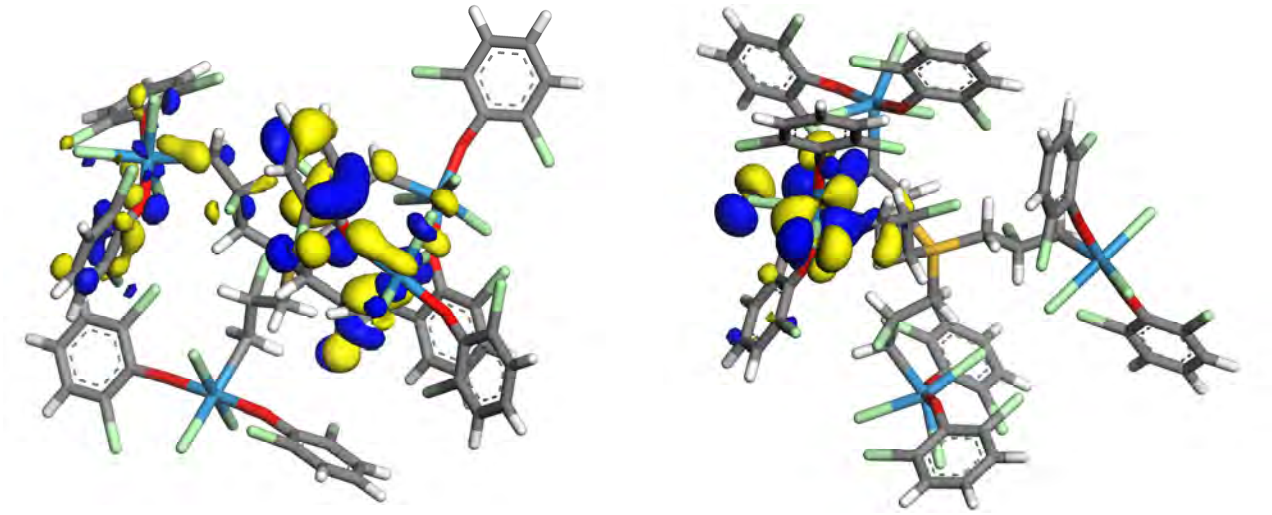

HOMO
E = -0.219944 eV

LUMO
E = -0.180478 eV

Figure 3.19 HOMO and LUMO of the **28** pre-catalyst.

Table 3.9 Energies of the frontier orbitals of tungsten pre-catalyst **28** and tetrabutyltin

	28	**Bu_4Sn**
HOMO (eV)	-0.219944	-0.218114
LUMO (eV)	-0.180478	0.01173
	28 HOMO vs. Bu_4Sn LUMO	**28 LUMO vs. Bu_4Sn HOMO**
E (eV)	-0.219944	-0.180478
E (eV)	0.01173	-0.218114
Energy difference (eV)	-0.231674	0.037636
Absolute values	0.231674	0.037636

Figure 3.20 shows the LUMOs of **28** and HOMOs of Bu_4Sn, the symmetry of these orbitals are also the same and that their orientation allows them to approach each other, and therefore there will be no hindrance for these two molecules to overlap. This interaction will lead to the formation of **2**, tributyltin chloride and butane (**Scheme 3.6**).

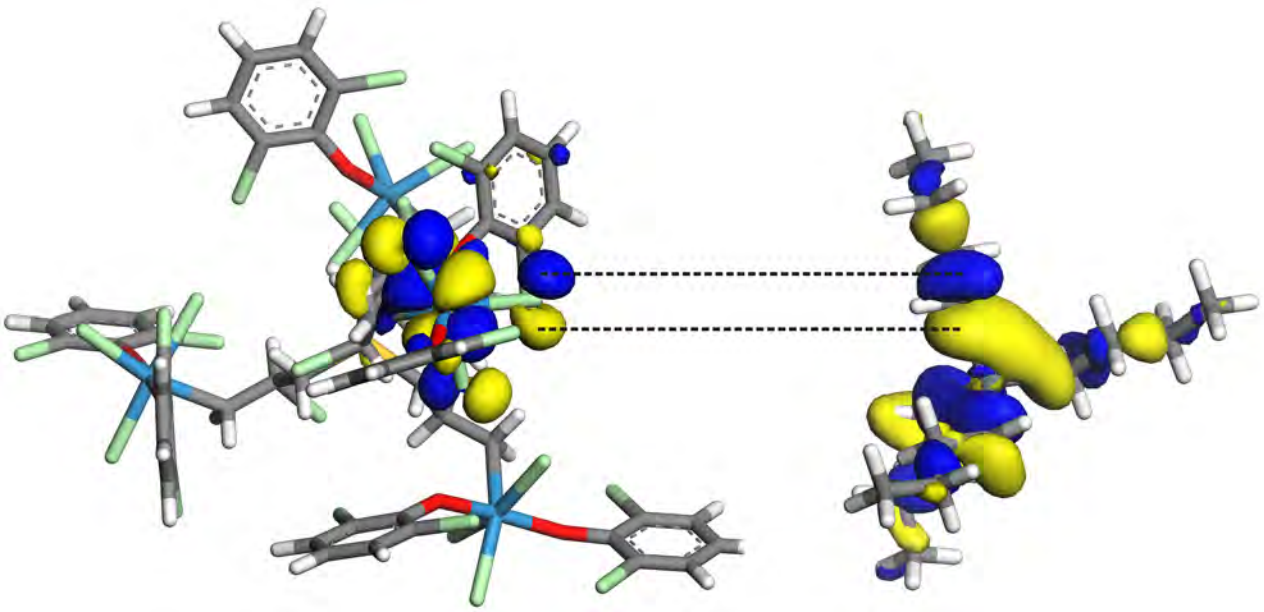

Figure 3.20 Symmetry and orientation of **28** and Bu_4Sn.

The mechanism of the 1-octene activation of **2** can be formulated as in **Scheme 3.7**. This activation leads to both the heptylidene (**30**) and the methylidene (**32**) species. In **Figure 3.21** is the two frontier orbitals of **2** with its orbital energies in eV.

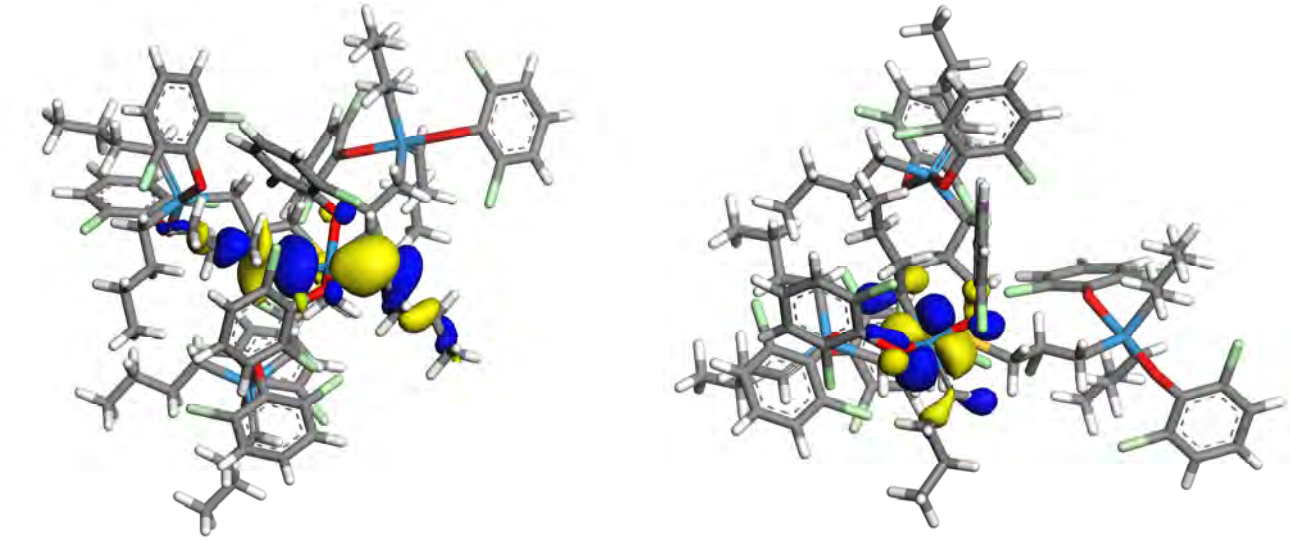

HOMO
E = -0.160319 eV

LUMO
E = -0.143185 eV

Figure 3.21 HOMO and LUMO of **2**.

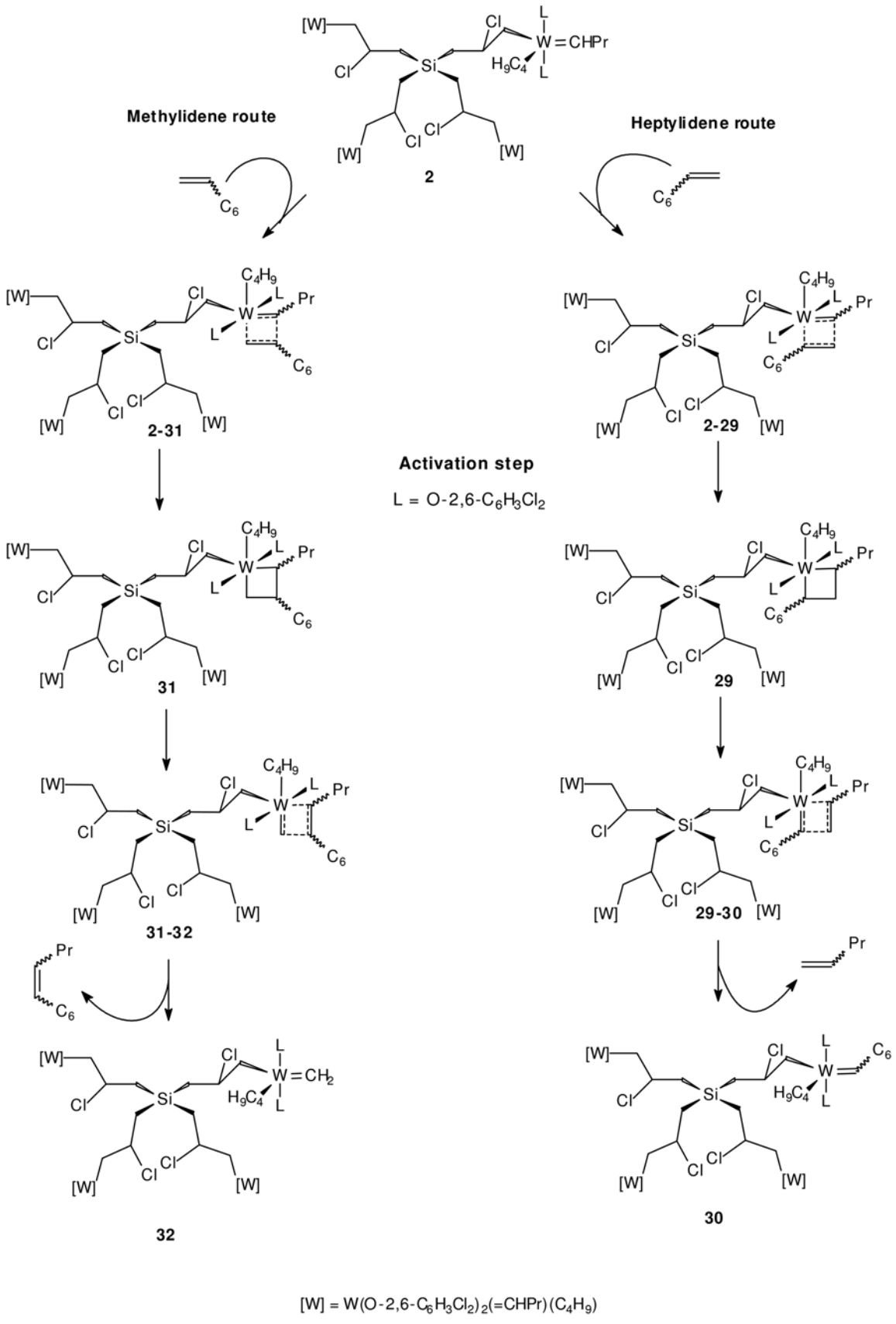

Scheme 3.7 The activation steps of **2**.

Table 3.10 shows that the most probable overlap between the frontier orbitals of **2** and 1-octene are the LUMO of **2** and the HOMO of 1-octene, with an energy gap of 0.074077 eV.

Table 3.10 Energies of the frontier orbitals of **2** and 1-octene.

	2	**1-octene**
HOMO (eV)	-0.160319	-0.217262
LUMO (eV)	-0.143185	-0.009538
	2 HOMO vs. 1-octene LUMO	**2 LUMO vs. 1-octene HOMO**
E (eV)	-0.160319	-0.143185
E (eV)	-0.009538	-0.217262
Energy difference (eV)	-0.150781	0.074077
Absolute values	0.150781	0.074077

Figure 3.22 shows the symmetry and orientation of **2** and 1-octene frontier orbitals, 1-octene can approach from the chlorine side of **2** or from the side that is between one arm of **2** and the butyl side. The first approach will lead to the heptylidene (**30**) and the latter will lead to the methylidene (**32**). The HOMOs and LUMOs of **2** and 1-octene have the same symmetry and thus allow them to overlap without any hindrance.

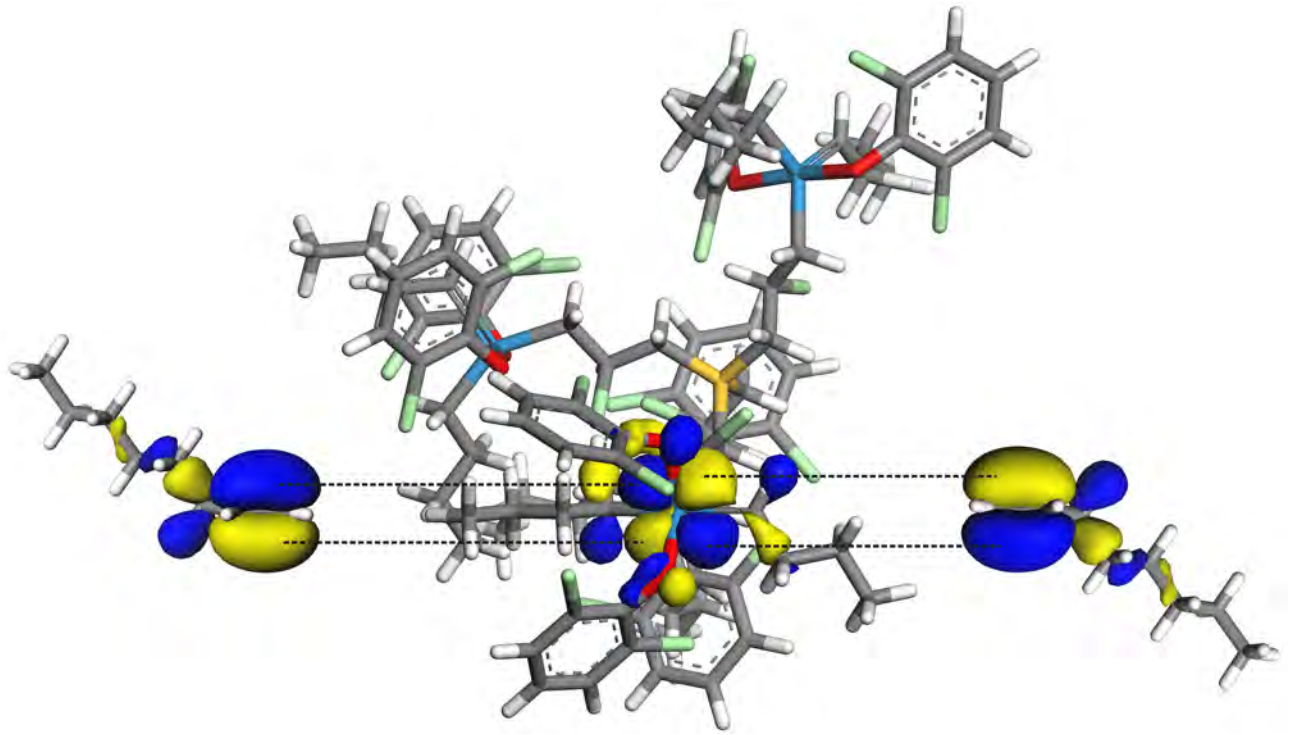

Figure 3.22 Symmetry and orientation of **2** and 1-octene.

Molecular modelling of **2**, specifically the PES scans were also done on one arm/periphery of the complex only because of computing time and method constrains. **Figure 3.23** gives the energy profile of the two activation steps involved in the productive metathesis of 1-octene with **2**, all the energies are normalised with respect to **2** and the units are given in kcal/mol.

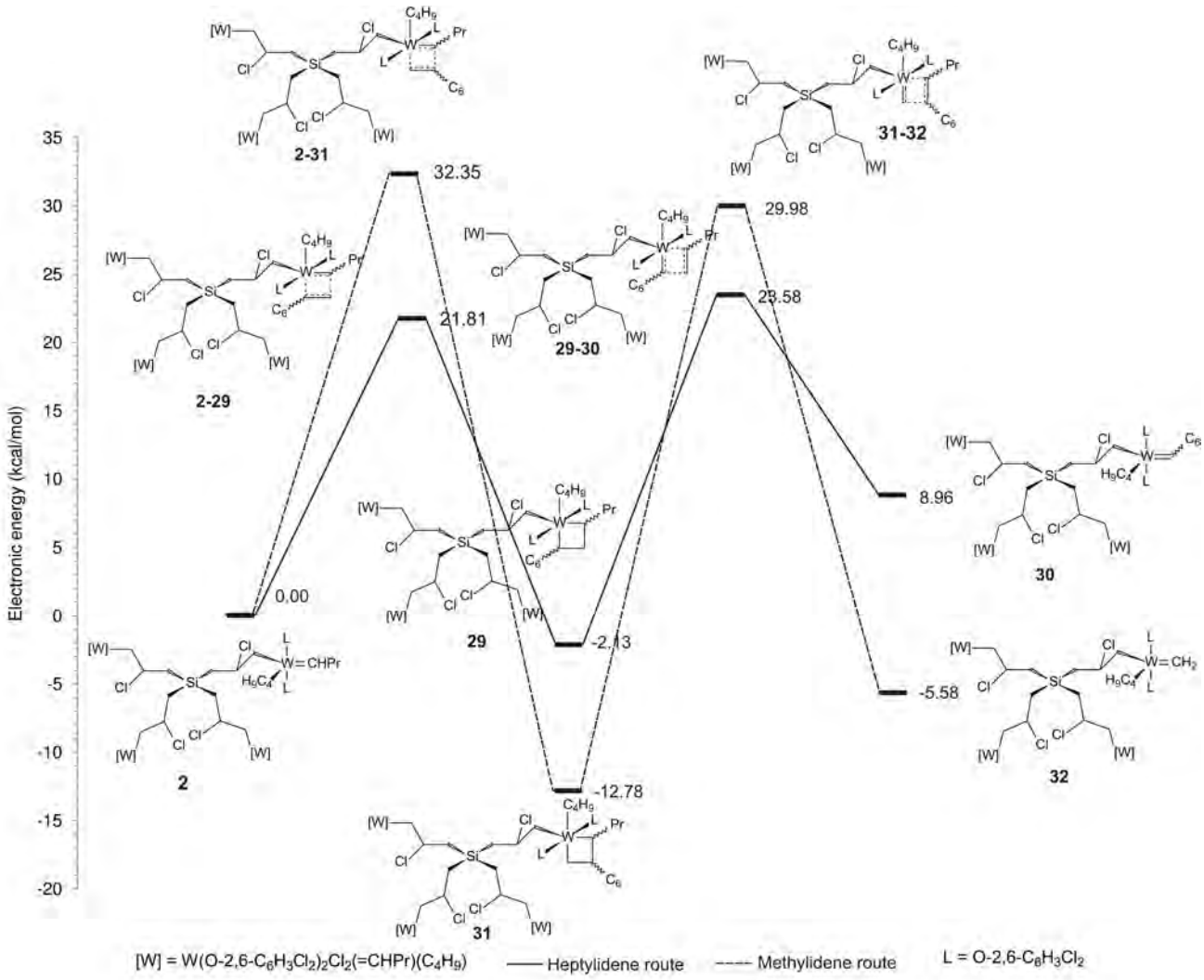

Figure 3.23 Energy profile of the activation steps of **2**.

In the heptylidene route, **2** requires an activation energy of 21.81 kcal/mol to form the metallacyclobutane (**29**). This metallacyclobutane has to overcome 25.71 kcal/mol of energy in order to form the heptylidene (**30**), which lies at 8.96 kcal/mol. **2** requires an activation energy of 32.35 kcal/mol to form the metallacyclobutane (**31**), this metallacyclobutane will have to overcome 42.76 kcal/mol of energy to form the methylidene (**32**), which lies at -5.58 kcal/mol. The methylidene route is thermodynamically favoured since their product **32** is lower in energy than its starting material **2** and the heptylidene is thermodynamically unfavoured. The rate limiting step of the heptylidene route is the step **2→(2-29)→29** and for the methylidene route is the step **31→(31-32)→32**, therefore the heptylidene route will be most favoured because of its lower activation energy.

The heptylidene route in the activation step of **2** has a lower activation energy than the methylidene route, but the metallacyclobutane (**31**) of the methylidene route is lower in energy than the metallacyclobutane (**29**) of the heptylidene route. **32** is lower in energy than **30**, which makes the methylidene species (**30**) to be more stable than the heptylidene species (**32**). The methylidene route has a higher probability to take place than the heptylidene route because of its lower activation energy.

The activation steps of the three catalytic systems considered namely; **16**, **1** and **2** are compared. The activation steps of **16** and **1** are similar because both have the methylidene route with the least activation energy, and that their heptylidene products (**18**) and (**18** + **25**) respectively are lower in energy than their methylidene products (**20**) and (**20** + **27**). The difference in these two energy profiles is their intermediates; the intermediate (**19**) of the methylidene route in **16** is lower in energy than the intermediate (**17**) of the heptylidene route. The intermediate (**24**) of the heptylidene route in **1** is lower in energy than the intermediate (**26**) of the methylidene route. The energy profile of **2** is similar with the energy profile of **16** only in their intermediates, because the intermediates (**19**) and (**31**) for the methylidene route are lower in energy than the intermediates (**17**) and (**29**) of the heptylidene route. However, the energy profile of **2** has the methylidene species (**32**) lower in energy than the heptylidene species (**30**).

Scheme 3.8 shows the catalytic cycle of **2** with 1-octene using only one arm of the dendritic periphery. The catalytic cycle has four transition states (**30-33**), (**33-32**), (**32-34**) and (**34-30**) and two intermediates (**33**) and (**34**). One half of the cycle leads to the methylidene (**32**) and produces the 7-tetradecene, the other half leads to the heptylidene (**30**) and produces ethene.

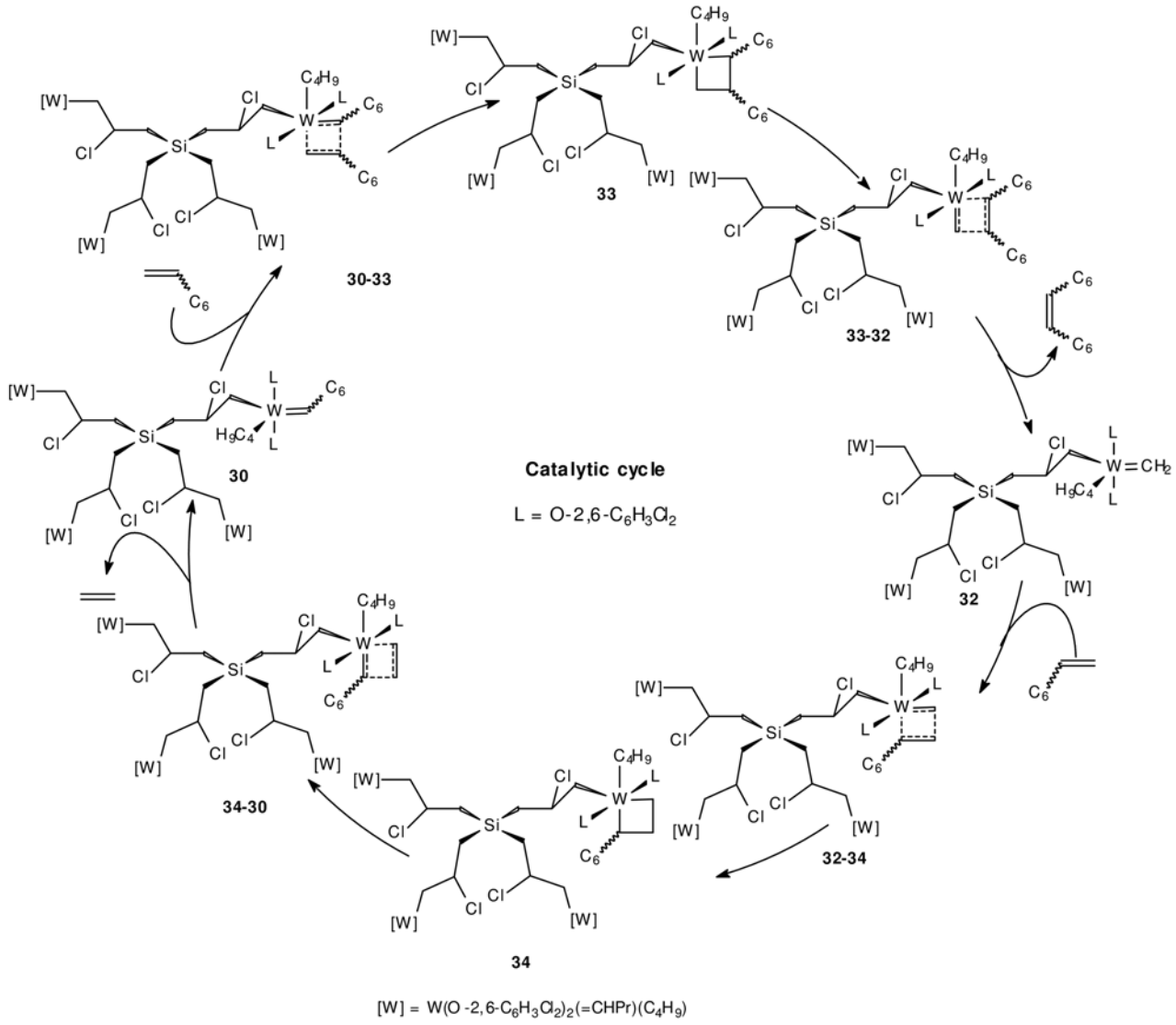

Scheme 3.8 The productive catalytic cycle of **2**.

Figure 3.24 shows the HOMO and LUMO of **30** which will overlap with 1-octene frontier orbitals shown in **Figure 3.6**. The orbitals's size, shape and geometry of these molecules will overlap to produce 7-tetradecene and **32**. This fact is in agreement with the frontier orbital energies given in **Table 3.11**, which indicates that the smallest energy gap is 0.085338 eV between the heptylidene (**30**) LUMO and 1-octene HOMO.

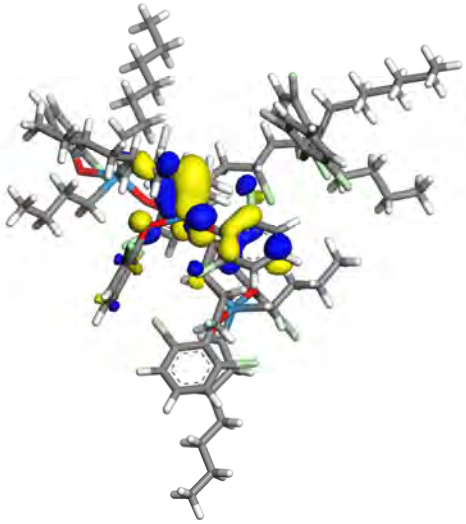

HOMO

E = -0.183131 eV

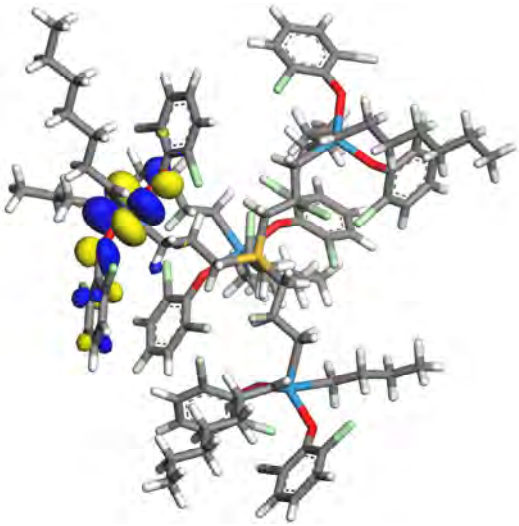

LUMO

E = -0.131924 eV

Figure 3.24 HOMO and LUMO of **30**.

Table 3.11 Energies of the frontier orbitals of **30** and 1-octene.

	30	**1-octene**
HOMO (eV)	-0.183131	-0.217262
LUMO (eV)	-0.131924	-0.009538
	30 HOMO vs. 1-octene LUMO	**30 LUMO vs. 1-octene HOMO**
E (eV)	-0.183131	-0.131924
E (eV)	-0.009538	-0.217262
Energy difference (eV)	-0.173593	0.085338
Absolute values	0.173593	0.085338

Figure 3.25 shows the LUMOs of **30** and HOMOs of 1-octene, the symmetry of these orbitals are the same and their orientation allows them to approach each other, there will be minimal steric hindrance for these two molecules to overlap. This interaction will lead to **32** and forming 7-tetradecene as shown in **Scheme 3.8**.

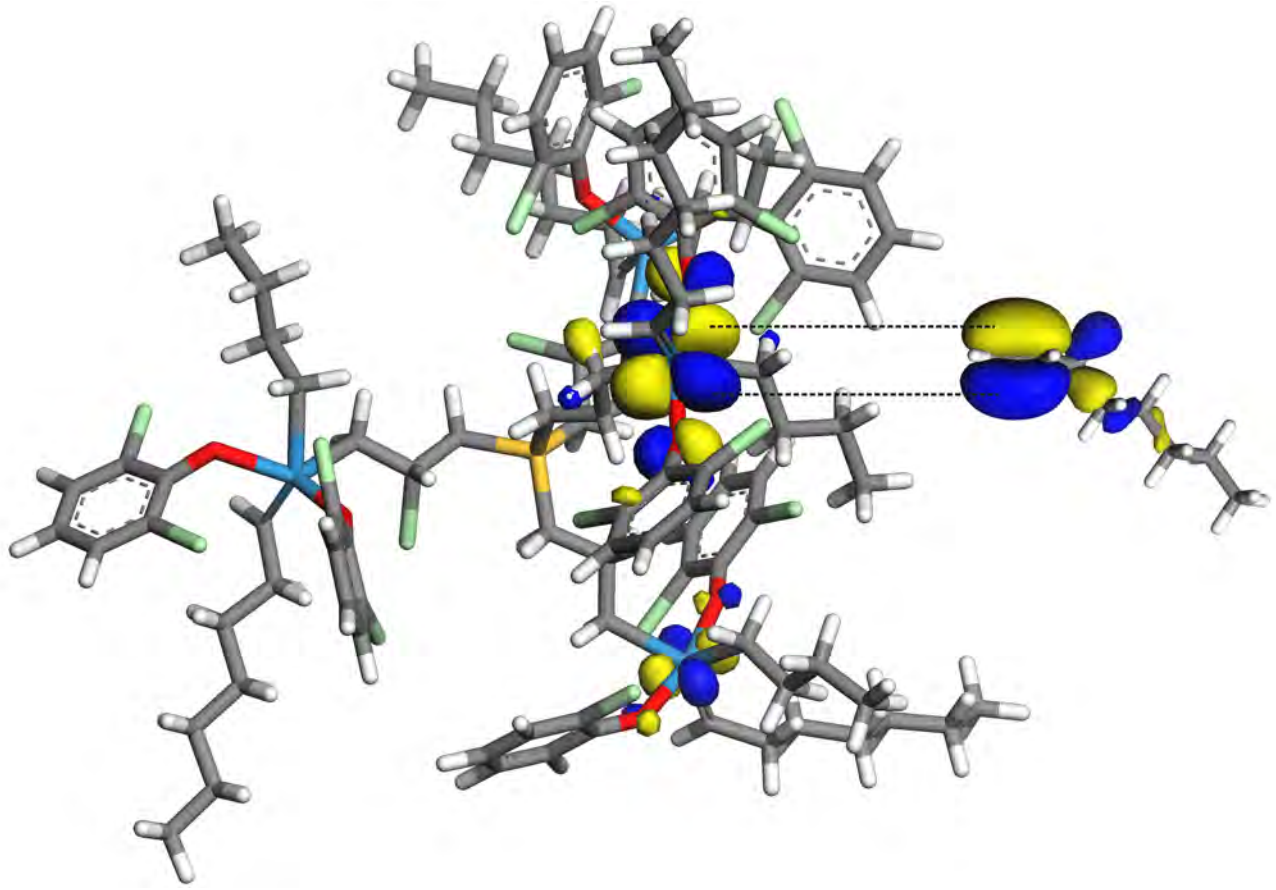

Figure 3.25 Symmetry and orientation of **30** and 1-octene.

Examination of the frontier orbitals of **32** shown in **Figure 3.26** and those of 1-octene in **Figure 3.6**, the orbitals will overlap by **32** LUMOs and the 1-octene HOMOs. **Table 3.12** shows the energies of the frontier orbitals of **32** and 1-octene, the smallest energy gap of 0.066495 eV, for **32** LUMO and 1-octene HOMO are the most probable orbitals to overlap for this interaction.

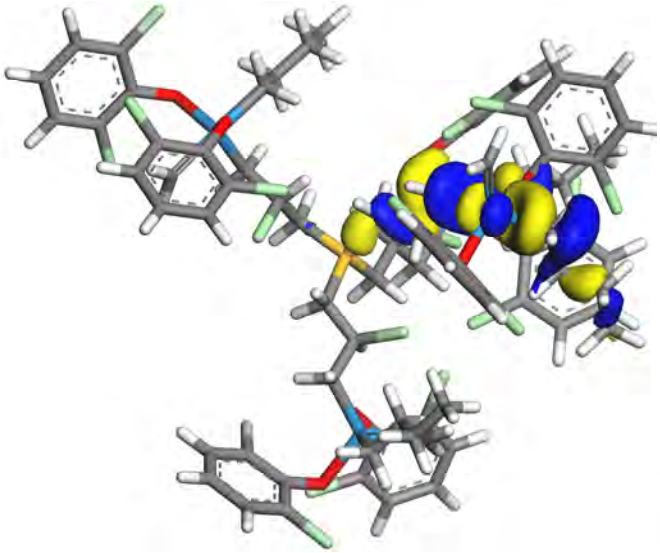

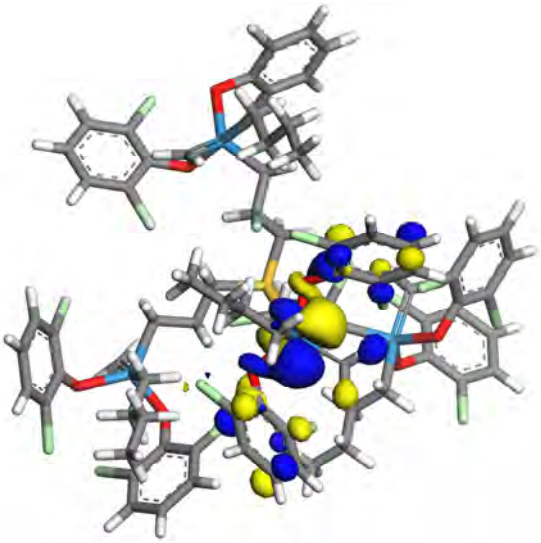

HOMO
E = -0.172492 eV

LUMO
E = -0.150767 eV

Figure 3.26 HOMO and LUMO **32**.

Table 3.12 Energies of the frontier orbitals of **32** and 1-octene.

	32	**1-octene**
HOMO (eV)	-0.172492	-0.217262
LUMO (eV)	-0.150767	-0.009538
	32 HOMO vs. 1-octene LUMO	**32 LUMO vs. 1-octene HOMO**
E (eV)	-0.172492	-0.150767
E (eV)	-0.009538	-0.217262
Energy difference (eV)	-0.162954	0.066495
Absolute values	0.162954	0.066495

Figure 3.27 shows the LUMOs of **32** and HOMOs of 1-octene, the symmetry of these orbitals are the same and their orientation allows them to approach each other, there will be no hindrance for these two molecules to overlap. This interaction will lead to **30** and forming ethene as shown in **Scheme 3.8**.

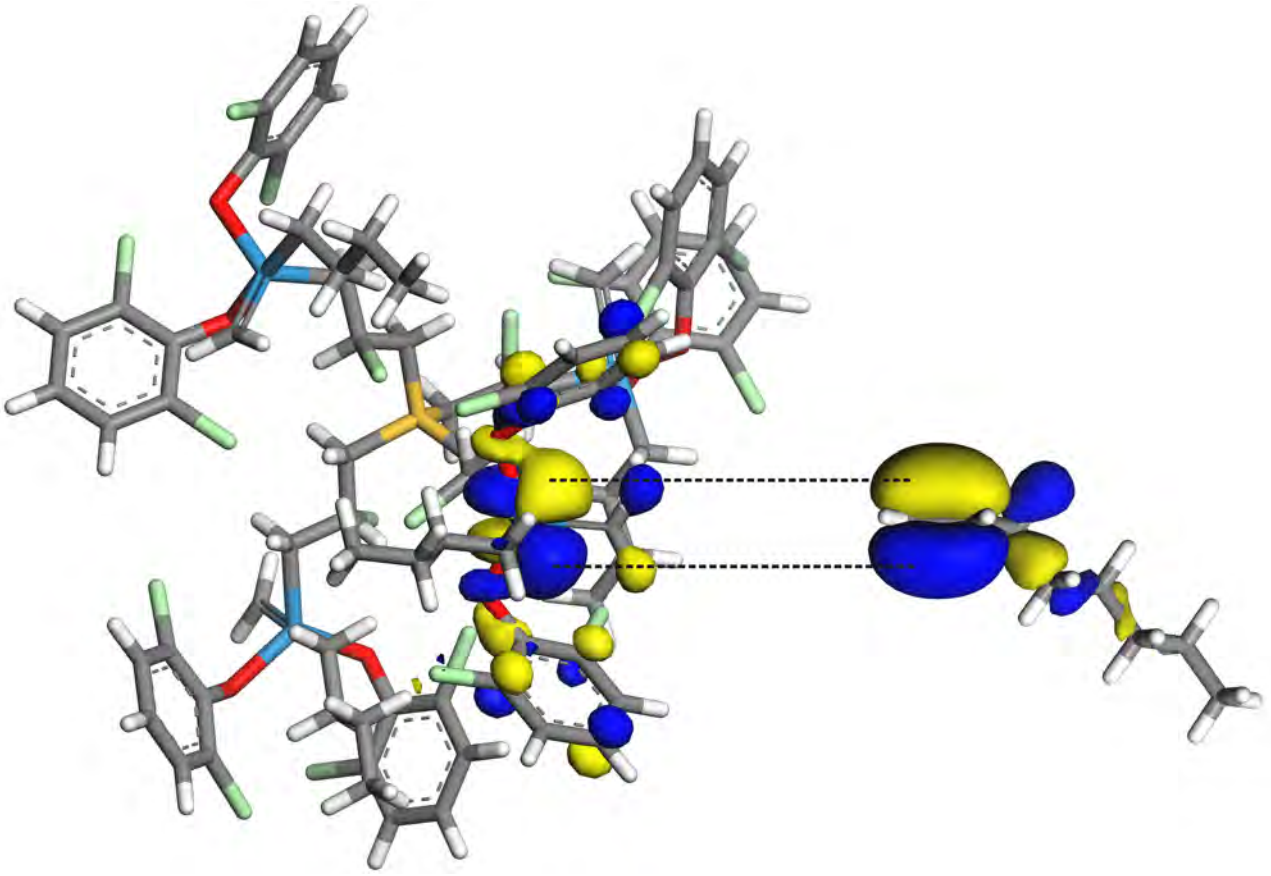

Figure 3.27 Symmetry and orientation of **32** and 1-octene.

The electronic energy profile of the catalytic cycle for the productive 1-octene conversion using the metal-carbenes (**30**) and (**32**) is shown in **Figure 3.28**. The energies of all the structures are normalised with respect to the **30** and all the energy values in the profile are given in kcal/mol units.

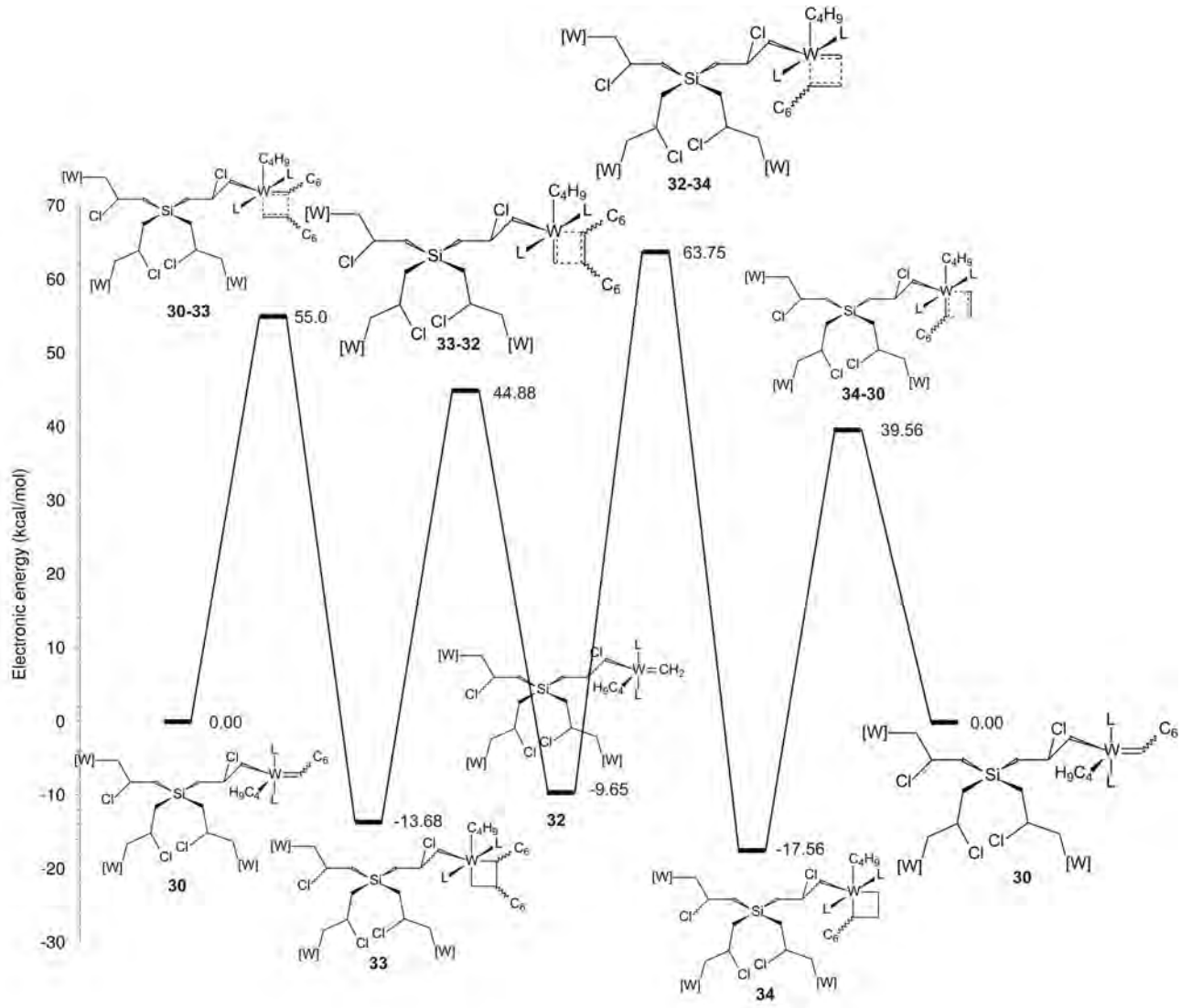

Figure 3.28 Energy profile of the catalytic cycle of **30** and **32**.

The formation of the metallacyclobutane (**33**) requires an activation energy of 55.0 kcal/mol, and for this intermediate to form **32** an energy barrier of 58.56 kcal/mol must be overcome and the first PMP, 7-tetradecene is formed. The second metallacyclobutane (**34**) requires 73.40 kcal/mol of activation energy to form and to convert this intermediate back to **30**, an energy barrier of 57.12 kcal/mol must be overcomed and the second PMP is generated, namely ethene. This cycle is thermodynamically favoured and **32** is more stable for it is lower in energy than **30**, and the rate limiting step is **32→(32-34)→34** which has the highest energy of 63.75 kcal/mol.

3.4 The carbocyclic ‘cage’ catalysts

In this study a method was used to attempt the synthesis of ‘cage’ carbocyclic catalysts **15** (**Scheme 5.2**) with the carbene on the outside (i.e., W between **3** and carbene). This meant that the W-complex will not dissociate from the dendrimers during metathesis reaction and that would make the recycling of the dendritic catalyst by nanomembrane process possible. The coordination of **12** or **3** to the $W(O\text{-}2,6\text{-}C_6H_3Cl_2)_2Cl_4$ system could not be achieved.

3.4.1 3,5-divinyl-4-oxahexacyclo[5.4.1.$0^{2,6}$.$0^{3,10}$.$0^{5,9}$.$0^{8,11}$]dodecane catalytic system

The step of the synthesis of the ‘cage’ catalyst bearing **12** as ligand is shown in **Scheme 3.9**. Examining the frontier orbitals of these interacting compounds i.e., **12** and **4**, the most probable overlap must occur between the LUMO of **4** and the HOMO of **12** which have the energy gap of 0.008457 eV (**Figure 3.29** and **Table 3.13**).

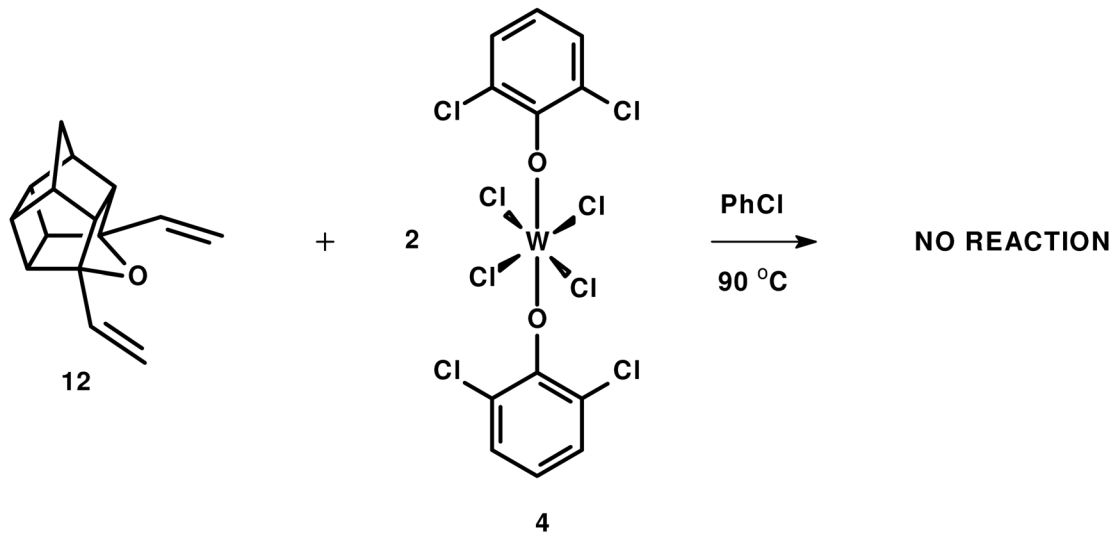

Scheme 3.9 Synthesis of the cage divinyl ether catalyst.

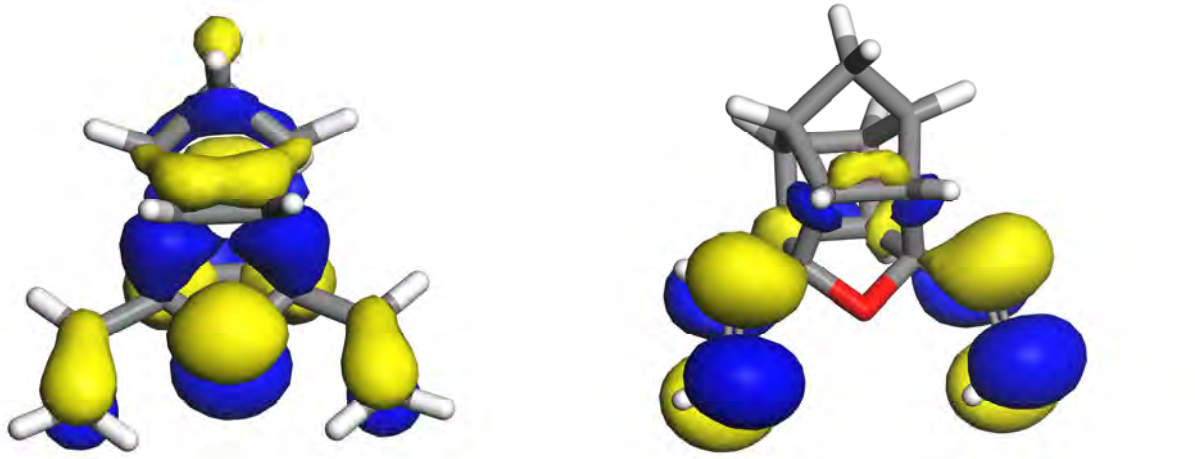

HOMO
E = -0.204175 eV

LUMO
E = -0.013281 eV

Figure 3.29 HOMO and LUMO of **12**.

Table 3.13 Energies of the frontier orbitals of **12** and **4**.

	12	**4**
HOMO (eV)	-0.204175	-0.233568
LUMO (eV)	-0.013281	-0.195718
	12 HOMO vs 4 LUMO	**12 LUMO vs 4 HOMO**
E (eV)	-0.204175	-0.013281
E (eV)	-0.195718	-0.233568
Energy difference (eV)	-0.008457	0.220287
Absolute values	0.008457	0.220287

The frontier orbitals have energy values associated with them and energy gaps could be calculated. However, the symmetry and orientation of the orbitals must also match for a coordination to occur between two compounds. **Figure 3.30** shows the symmetry and orientation of **4** and **12**, the orbitals size and shape of these two compounds does not match. The part of the orbitals responsible for overlap are distributed along two carbon atoms in the double bond of **12** and those of **4** are on one chlorine atom only. The shapes of the orbitals on **12** are *oval* in shape and those in **4** are *spherical* and the sizes of the two different orbitals on **4** and on **12** are not equal to permit an overlap and therefore no reaction takes place.

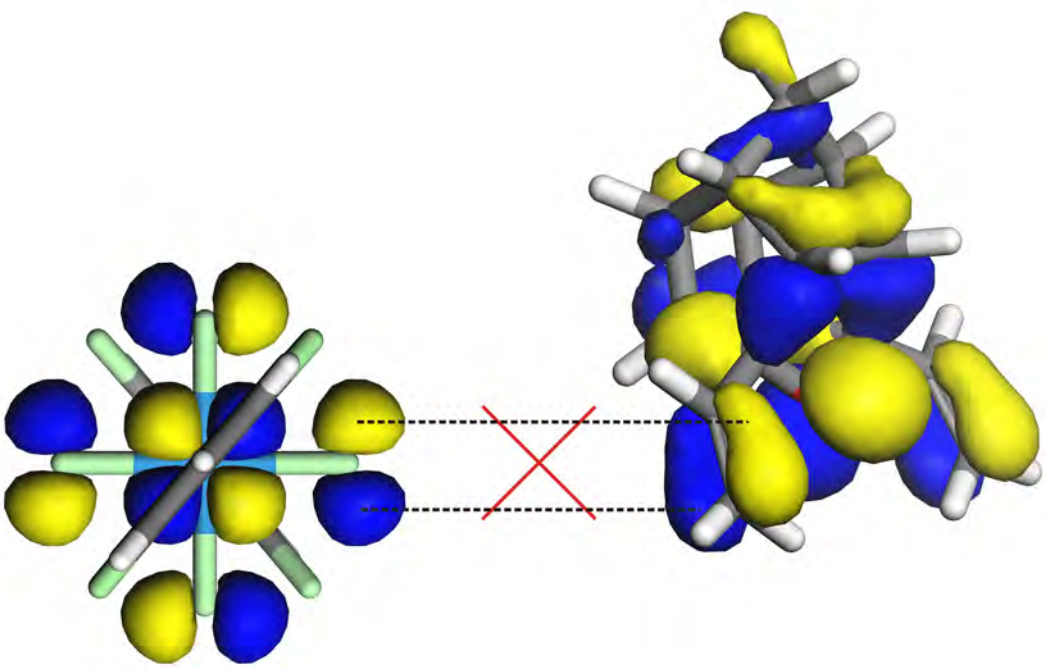

Figure 3.30 Symmetry and orientation of **4** and **12**.

3.4.2 3,5-diallyl-4-oxahexacyclo[5.4.1.$0^{2,6}$.$0^{3,10}$.$0^{5,9}$.$0^{8,11}$]dodecane catalytic system

The frontier orbitals of **3** are shown in **Figure 3.31** with their energies, and **Table 3.14** shows that the LUMO of **4** and HOMO of **3** must overlap with energy gap of 0.008867 eV to form a coordination.

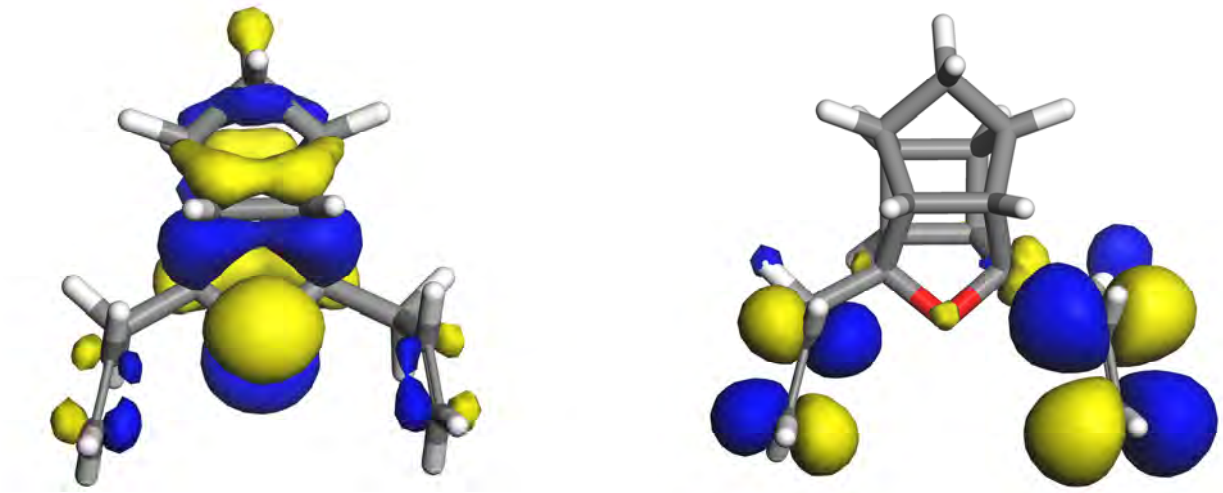

HOMO
E = -0.204585 eV

LUMO
E = -0.009307 eV

Figure 3.31 HOMO and LUMO of **3**.

Table 3.14 Energies of the frontier orbitals of **3** and **4**.

	3	**4**
HOMO (eV) **LUMO (eV)**	-0.204585 -0.009307	-0.233568 -0.195718
	3 HOMO vs 4 LUMO	**3 LUMO vs 4 HOMO**
E (eV) **E (eV)** **Energy difference (eV)** **Absolute values**	-0.204585 -0.195718 -0.008867 0.008867	-0.009307 -0.233568 0.224261 0.224261

Compound **3** showed a different interaction with **4**, the reaction was a chlorine addition reaction or electrophilic addition of the chlorine atoms on the double bonds of **3** instead of coupling to form the catalytic complex **14** which was the desired product (**Scheme 3.10**).The addition reaction lead to three identified chlorine compounds **35**, **36** and **37**. This result can be attributed to minute quantities of water present in the reaction mixture, since **3** was obtained as an oil instead of a powder or crystals in **§ 5.3.5**.

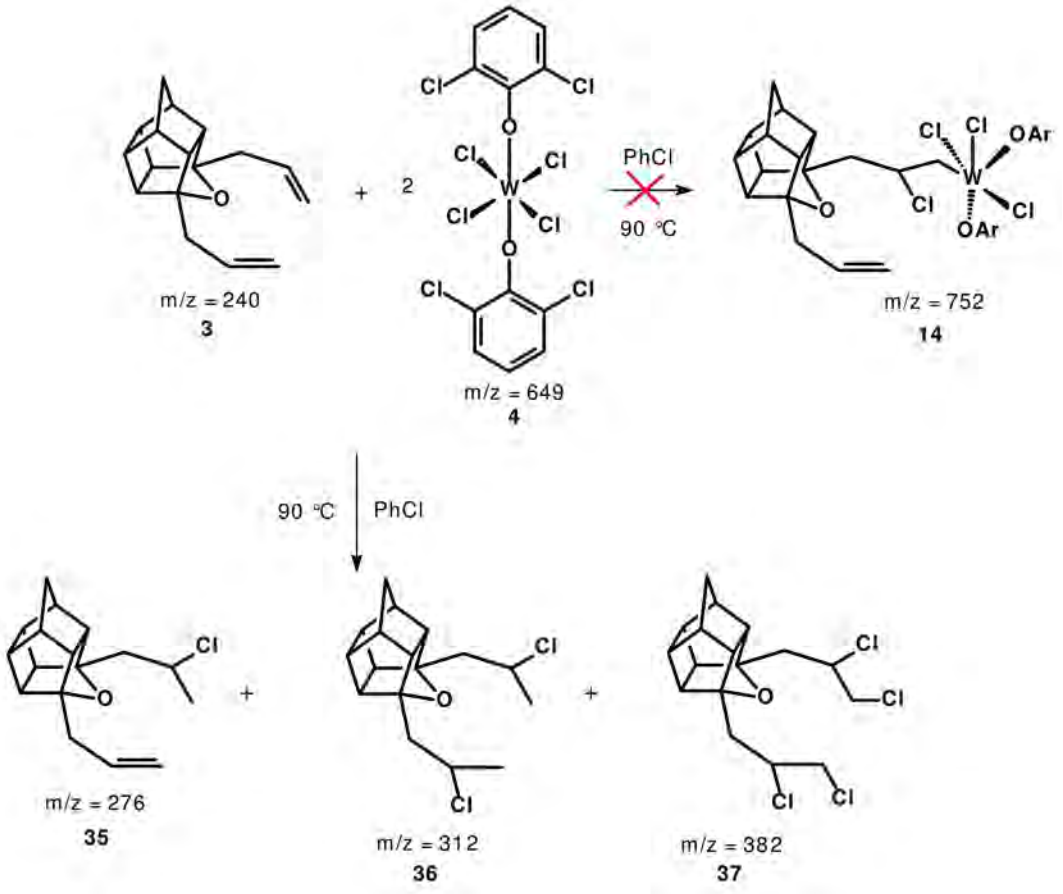

Scheme 3.10 Reaction of **3** and **4**.

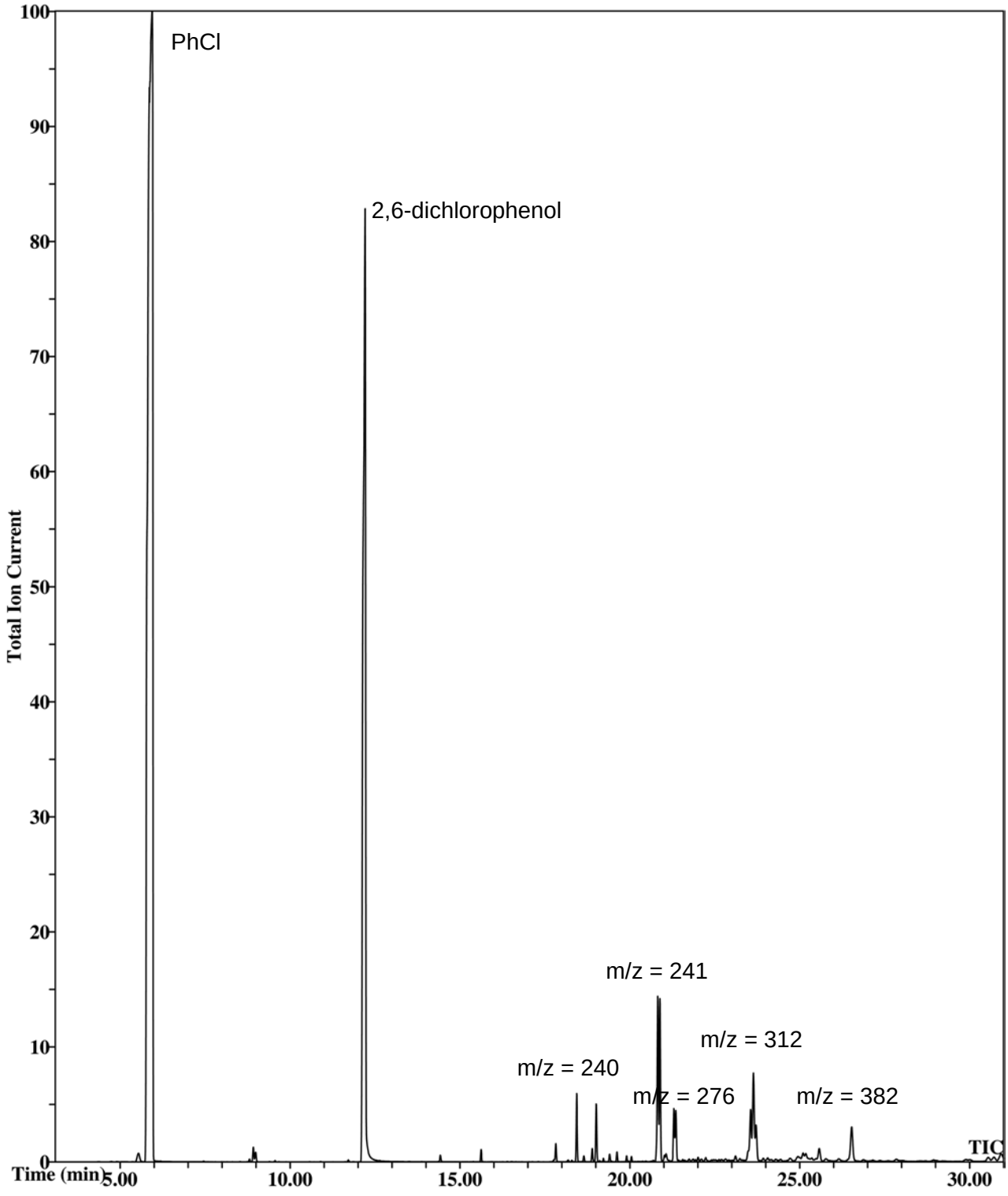

Figure 3.32 GC Chromatogram of the products obtained in the attempted synthesis of **14**.

Figure 3.32 shows the GC chromatogram of the products formed **35**, **36** and **37** (**Scheme 3.10)** during the synthesis of **14**. The most prominent peak at about 5.8 minutes is the internal standard chlorobenzene and the second dominating species is the 2,6-dichlorophenol. The peaks of **35**, **36** and **37** can all be read at 21.3, 23.3 and 26.5 minutes respectively with their mass per charge.

Another peak of the unreacted **3** can be read at 18.4 minutes. One last unidentified compound appears at 20.8 minutes with a mass to charge ratio of 241. The GC-MS spectra of these identified compounds are listed in the appendices section.

The energy gap between the frontier orbitals of **3** and **4** shows also that the two compounds can overlap. However, the orbital's size and shape of these two compounds does not match and does not allow them to coordinate. The orbitals are both round and are concentrated on only one atom in each compound. The part of the orbitals in **3** and in **4** that must overlap can only react to add chlorine atoms on the double bonds of **3** (**Figure 3.33**). The orbitals of both **3** and **4** are symmetrical and their orientation does allow them to interact but not to form a coordinate.

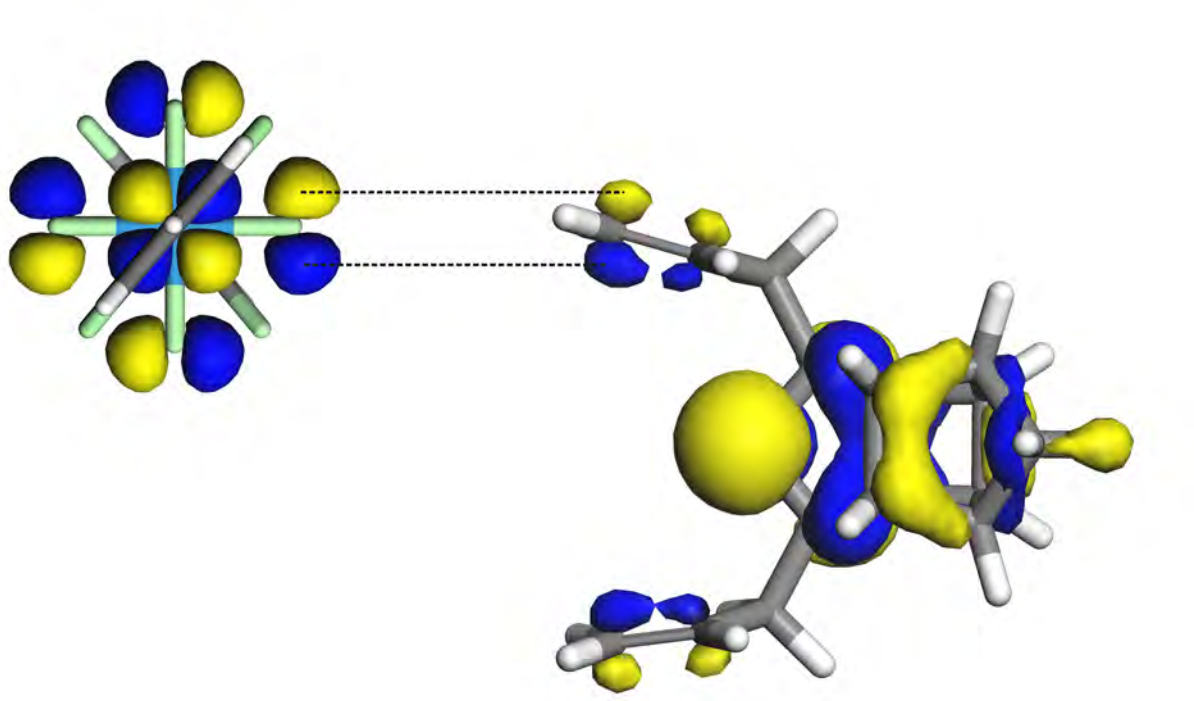

Figure 3.33 Symmetry and orientation of **4** and **3**.

Synthesis of **15** (**Scheme 5.2**) was unsuccessful; the next step was to test if there was activity when the reaction is run *in-situ*. The reaction was performed as discussed in **§ 5.4.2**. The GC chromatogram of the *in situ* 1-octene metathesis reaction between **3** and **4** (**Scheme 5.3**) at 210 minutes is given **Figure 3.34**. In this chromatogram, the most prominent peak is the internal standard which is chlorobenzene, followed by 1-octene, tetrabutyltin 2,6 dichlorophenol, and unreacted **3** peak can be read at 16.7 minutes. The reaction was monitored in 30 minutes intervals for 12 hours and no metathesis products were observed at any given time of the reaction.

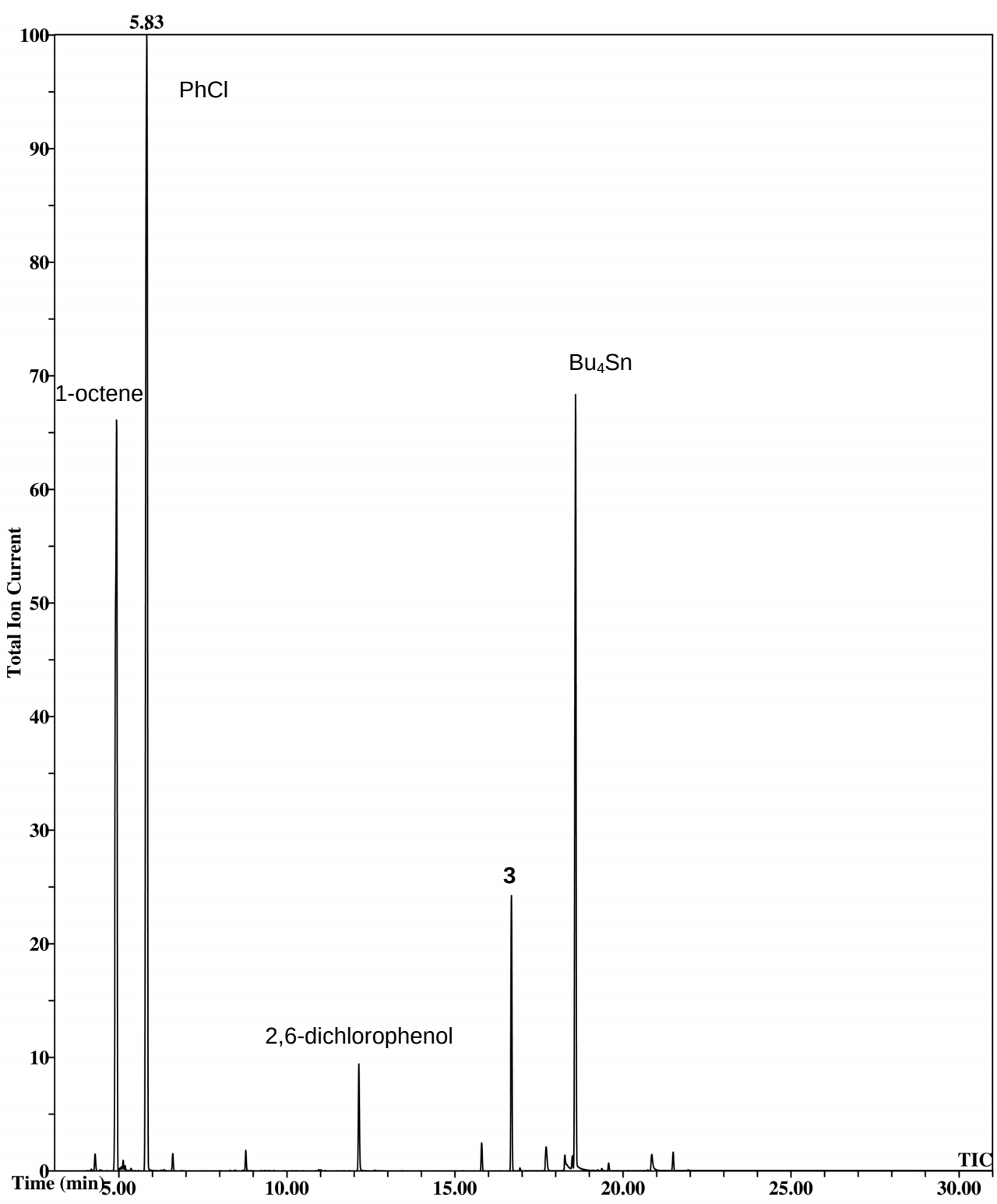

Figure 3.34 GC Chromatogram of the *in-situ* reaction between **3** and **4**.

3.5 References

1. Dodd HT and Rutt KJ, *J. Mol. Catal.*, 1982, **15**, 103
2. Quignard F, Leconte M and Basset J-M, *J. Mol. Catal*., 1986, **36**, 13
3. Vosloo HCM, Dickinson AJ and du Plessis JAK, *J. Mol. Catal.*, 1997, **115**, 199
4. van Schalkwyk C, Vosloo HCM and du Plessis JAK, *J. Mol. Catal.*, 1998, **133**, 167
5. Beerens H, Verpoort F and Verdonck L, *J. Mol. Catal.*, 2000, **159**, 197
6. Mbhele ZH, ***Experimental Investigation of Dendritic Catalysts for Alkene Metathesis***, MSc Dissertation, North-West University, 2006

Chapter 4. Conclusions

4.1 Introduction

The aim of this study was to investigate, theoretically and experimentally the $W(O\text{-}2,6\text{-}C_6H_3Cl_2)_2Cl_4$ catalyst and to synthesise 'cage' alicyclic ligands that will help retain the catalyst during the membrane separation process. Experimental work was done on the W-carbosilane dendritic catalysts **1** and **2**.[1,2] These catalysts have shown good activity, but their mode of formation and their reaction energy profiles have been unknown and inconclusive.[1,2] Synthesis of 'cage' carbocyclic catalysts was attempted and the results were negative.

4.2 Theoretical and experimental investigation of $W(O\text{-}2,6\text{-}C_6H_3Cl_2)_2Cl_4$

The conversion of 1-octene into PMPs, SMPs and IPs over a period of 210 minutes was in good comparison with literature results.[3] The PMP's reached 63.6 %, SMP's and IP's reaches 2.5 % and 0.9 % respectively, 1-octene was converted to 67 % of metathesis products in 30 minutes.

The coordination of the co-catalyst (Bu_4Sn) to the $W(O\text{-}2,6\text{-}C_6H_3Cl_2)_2Cl_4$ pre-catalyst to form the metal-carbene (**16**) occurs through an overlap of the pre-catalyst LUMO and the co-catalyst HOMO. The activation step *via* the methylidene route is more favoured because of its low activation energy, compared to that of the heptylidene route which is higher. However, the heptylidene route is thermodynamically favoured and **18** is a more stable species than **20**. The catalytic cycle is thermodynamically favoured since the methylidene (**20**) is lower in energy than the heptylidene (**18**). The orbitals symmetry and orientations of all the metal-carbenes and ligand/1-octene are in an accessible position for reactions to occur.

4.3 W-carbosilane dendritic catalysts

Compound **1** is formed through cross metathesis, from the overlap of the LUMO of the metal-carbene (**16**) and the HOMO of tetraallylsilane (**23**). The LUMO of **1** overlaps with the HOMO of 1-octene in the activation step and forms the heptylidene (**18**) and the methylidene (**20**), together with two silane by-products **25** and **27**. The HOMO and LUMO of **1** and 1-octene have the same symmetry and thus allow them to overlap without any steric hindrance. The two activation steps are thermodynamically favoured since, the products (**18** and **25**) and (**20** and **27**) are lower in energy than their starting material **1**; the methylidene route will be a much preferred route in the activation step because of its low activation energy. However, the heptylidene (**18**) and its by-product **25** are more stable.

Compound **2** is formed in two steps; the LUMO of W(O-2,6-$C_6H_3Cl_2)_2Cl_4$ overlaps with the HOMO of tetraallylsilane (**23**) to give the intermediate (**28**), which its LUMO will overlap with the Bu_4Sn HOMO to form **2**. The LUMO of **2** will undergo 1-octene activation with the HOMO of 1-octene leading to the heptylidene (**30**) and the methylidene (**32**). The orbitals's symmetry and orientation of **2** and 1-octene indicates a good coordination without any hindrance. The heptylidene route will be more favoured than the methylidene route because of its low activation energy, however the methylidene species (**32**) is thermodynamically more stable than the heptylidene species (**30**) and it is lower in energy than its starting material **2.**

4.4 Cage carbocyclic catalysts

The formation of the catalytic complexes using **12** or **3** as ligands with the W(O-2,6-$C_6H_3Cl_2)_2Cl_4$ system could not be obtained. Compound **3** reacts with **4**, and the reaction is a chlorine addition reaction or electrophilic addition of the chlorine atoms on the double bonds of the ligand instead of coupling to form the catalytic complex **14** which was the desired product. The orbitals of **12** are distributed along the double bonds and do not permit a coordination to occur. The formation of **35** and **36** are attributed to minute quantities of water present in the starting material. No metathesis products were observed in the *in-situ* reaction of **3** or **12** with W(O-2,6-$C_6H_3Cl_2)_2Cl_4$ as catalyst using 1-octene.

4.5 Recommendations

To fully and eloquently describe the theoretical metathesis behaviour of **1** and **2**, a PES scan method must be developed to comprehend all the four arms/peripheries of the catalysts. Experimental results of the 1-octene metathesis must be performed to compare properties such as kinetics and thermodynamics with the theoretical results. Synthesis of **3** and **12** and the *in-situ* metathesis reactions must be performed in an inert atmosphere such as glove boxes to prevent any presence of water in the products.

4.6 References

1. Beerens H, Verpoort F and Verdonck L, *J. Mol. Catal.*, 2000, **159**, 197
2. Mbhele ZH, *Experimental investigation of dendritic catalysts for alkene metathesis*, MSc-Dissertation, NWU, 2006
3. Vosloo HCM, Dickinson AJ and du Plessis JAK, *J. Mol. Catal.*, 1997, **115**, 199

Chapter 5. Experimental

5.1 Solvents and reagents

5.1.1 Solvents

Chlorobenzene (Merck) and chloroform (Merck) were dried with calcium chloride and stored over 4Å molecular sieves, benzene (Holpro), ethanol (Saarchem), dichloromethane (Labchem), hexane (Labchem), methanol (Merck), ethyl acetate (Saarchem), n-hexane (Labchem) were all used as obtained from the supplier. Tetrahydrofuran (Saarchem) was distilled under nitrogen from sodium with benzophenone as indicator before use and was stored over 4Å mol sieves.

5.1.2 Reagents

The alkene, 1-octene (Aldrich), was passed through a neutral alumina column for purification and was stored under a nitrogen atmosphere. Dicyclopentadiene (Fluka) was distilled and used immediately. p-Benzoquinone (Riedel-de Haën), allyl magnesium bromide (Aldrich), vinyl magnesium bromide (Aldrich), tetraallylsilane (Fluka), toluene-4-sulfonic acid (BDH), magnesium sulfate (Saarchem) were used as obtained from the supplier. Bu_4Sn (Aldrich), the phenolic compound
2,6-dichloro-phenol (Aldrich) was used as obtained from the supplier. All the gasses used for purification and drying of solvents were supplied by Afrox.

5.2 Apparatus

An experimental setup (**Figure 5.1**) was used for the synthesis of the 2,6-disubstituted aryloxide tungsten(VI) pre-catalyst **4**.

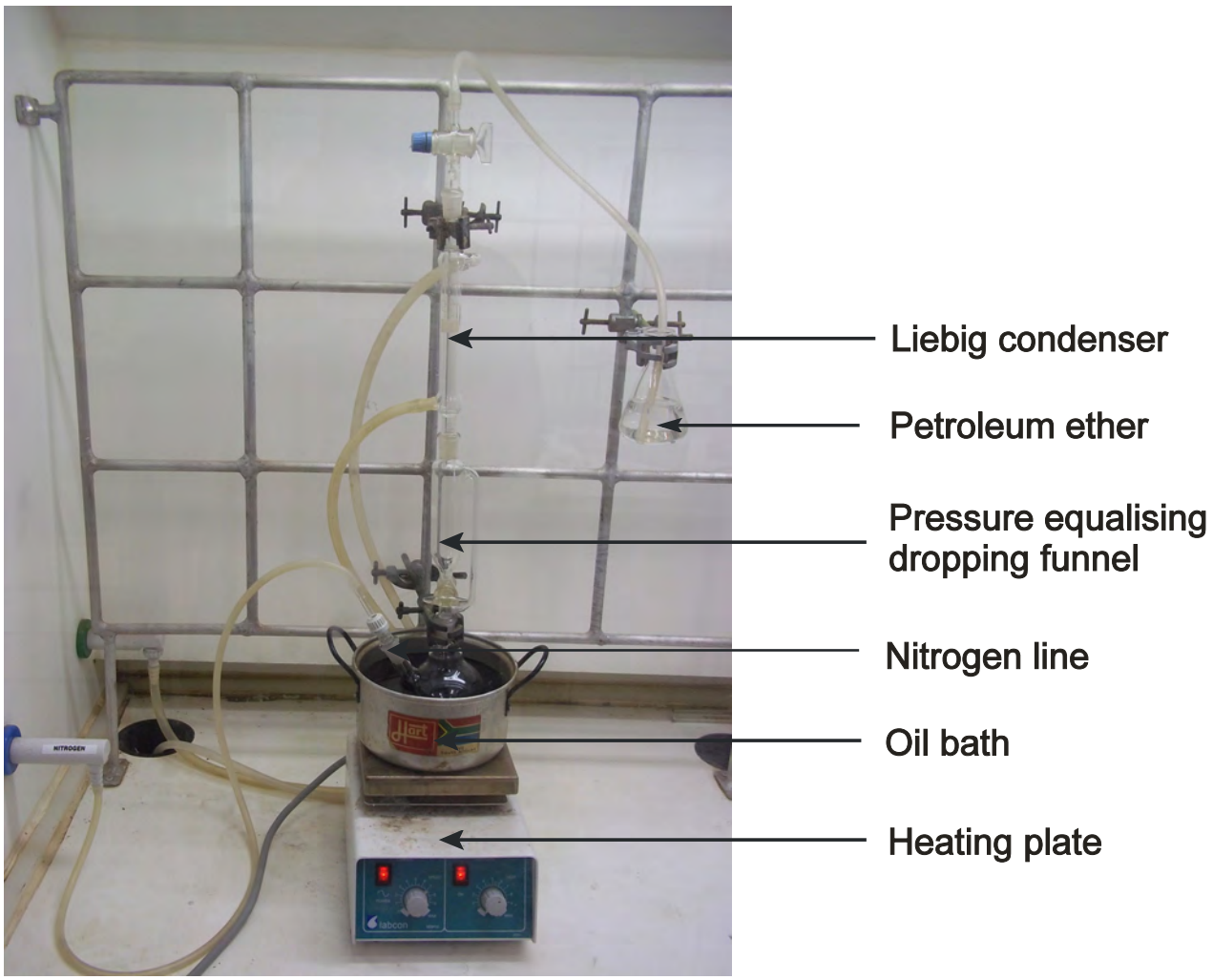

Figure 5.1 Experimental setup for the synthesis of $W(O\text{-}2,6\text{-}C_6H_3Cl_2)_2Cl_4$ (**4**).

The metathesis reactions were carried out by small scale setup shown in **Figure 5.2**. 5 mL glass mini reactors with plastic screw tops that have a small opening on top for the syringe needle (the screw tops can be turned open and close by a stop cock) and Hamilton-gastight syringes were used for the reactions. The mini reactor containing a small magnet insulated with plastic was heated in an aluminium block on a hot plate with **4**, Bu_4Sn, 1-octene and PhCl as an internal standard.

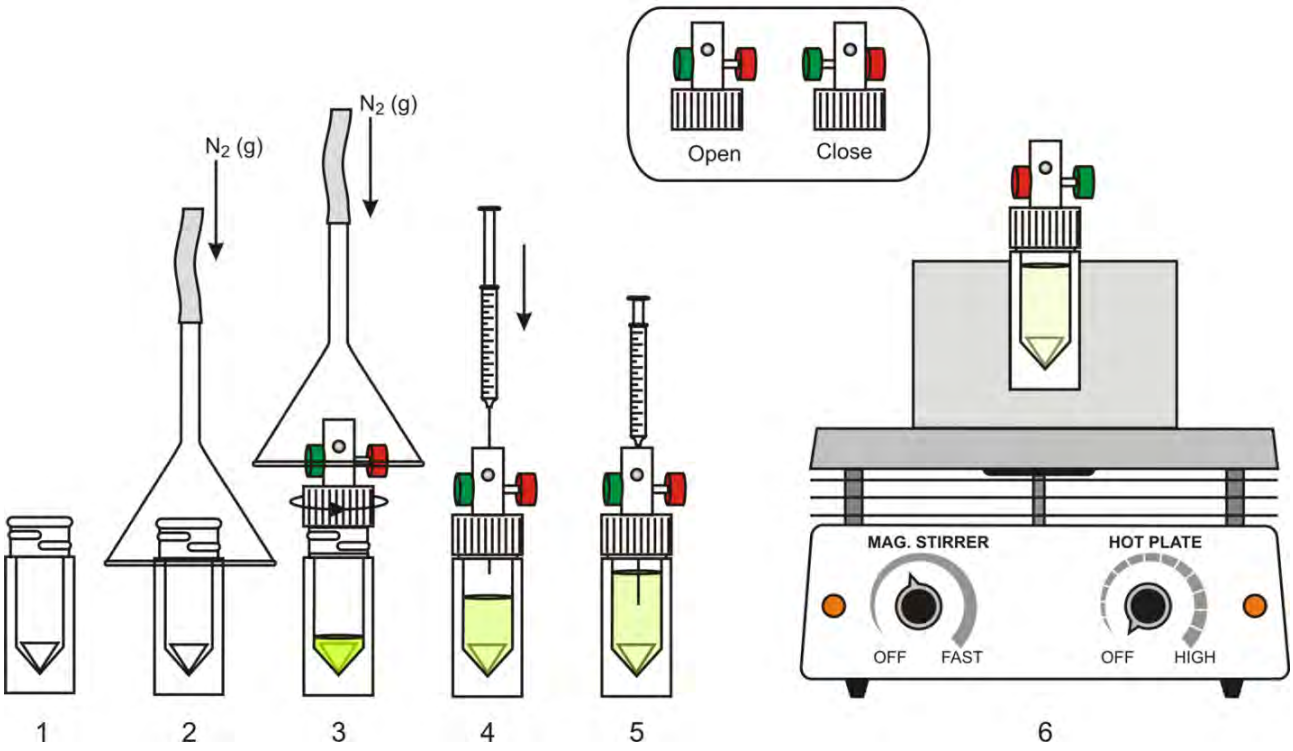

Figure 5.2 An illustration of catalytic reaction procedure followed for all metathesis reactions in this study.

5.3 Experimental procedure

The synthesis of **3** and **12** ligands is shown in **Scheme 2.3**. The procedure involves a reaction of a 1:1 mole ratio of cyclopentadiene with p-Benzoquinone to give the adduct **7**, upon irradiation of **7** in methanol compound **8** is formed. Compound **8** was reacted with an excess of vinylmagnesium bromide or allylmagnesium bromide in THF to form **11** or **13** respectively. Both **11** and **13** were reacted with dilute hydrochloric acid to give the expected **12** and **3**. All the spectra of the synthesised compounds can be found in the appendices section.

5.3.1 Synthesis of pentacyclo[5.4.0.0^{2,6}.0^{3,10}.0^{5,9}]undecane-8,11-dione (8)[1]

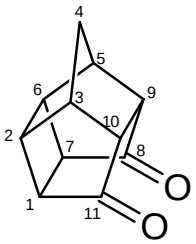

Equivalent molar amounts of cyclopentadiene and p-benzoquinone were used. Cyclopentadiene (11 mL) was added slowly (10 mL per min) into a solution of p-benzoquinone (18 g) in 150 mL benzene. The reaction was stirred for 12 hours in the dark, covered with aluminium foil. The reaction was monitored with TLC, with benzene-chloroform-diethylether (1:2:1) as eluent to make sure that all the p-benzoquinone is used up in the reaction. The reaction solution was concentrated in *vacuo* and the residue was recrystallised from petroleum ether, light yellow adduct was obtained (18.5 g, 81%). A solution of the adduct (3.08 g; 0,23 mol) in 300 mL ethyl acetate was irradiated for 12 hours with a Hanovia medium-pressure Hg lamp (Pyrex filter). The solution was concentrated, whereupon 'cage' dione crystallized as a white, microcrystalline solid (2.95 g, 78 %).

Melting point : 236-237°C.

Infrared spectrum : ν_{max} 3 000, 1 756, 1 068 cm^{-1}

Mass spectrum : m/z 174 (M^+)

^{1}H NMR spectrum : ($CDCl_3$, 600 MHz) δ_H 1.95 ppm (d, 2 x H), 2.79 ppm (s, 2 x H), 3.15 ppm (q, 2 x H), 2.91 ppm (q, 2 x H), 2.68 ppm (d, 2 x H)

^{13}C NMR spectrum : ($CDCl_3$, 600 MHz) δ_C 38.7 ppm (2 x $C_{2,6}$), 43.8 ppm (2 x $C_{1,7}$), 44.6 ppm (2 x $C_{3,5}$), 40.5 ppm (1 x C_4), 212.1 ppm (2 x $C_{8,11}$), 54.7 ppm (2 x $C_{9,10}$)

5.3.2 Synthesis of *exo*-8-*exo*-11-divinylpentacyclo[5.4.0.0^{2,6}.0^{3,10}.0^{5,9}]undecane-*endo*-8-*endo*-11-diol (11)[2]

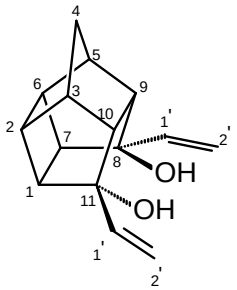

To a solution of **8** (**Scheme 2.3**) (1.00 g, 5.74 mmol) in dry THF (10 mL) under nitrogen was added with stirring a 1 molar solution vinylmagnesium bromide in dry THF (22.9 mL, 22.9 mmol). The resulting solution was stirred at ambient temperature for 3 h and then it was heated to 50 °C and was stirred at that temperature for an additional 12 h. The reaction mixture was cooled to 0 °C *via* application of an external ice-water bath, and the reaction was quenched *via* addition of cold

saturated aqueous NH_4Cl (10 mL). The resulting aqueous suspension was extracted with EtOAc (3 x 30 mL), and the combined organic layers were washed with water (10 mL). The organic layer was dried ($MgSO_4$) and filtered, and the filtrate was concentrated in *vacuo*. Dark brown oil was obtained (0.74 g, 59 %).

Infrared spectrum : ν_{max} 2969, 1412, 1271, 1116, 1069, 989, 915, 672 cm^{-1}

Mass spectrum : m/z 207 (M^+)

^{1}H NMR spectrum : ($CDCl_3$, 600 MHz) δ_H 2.44 ppm (d, 2 x H), 2.45 ppm (t, 2 x H), 2.36 ppm (q, 2 x H), 1.07 ppm (t, 2 x H), 2.15 ppm (d, 2 x H), 1.97-2.24 ppm (d, 2 x H), 5.90 ppm (t, 2 x H), 5.01 ppm (d, 2 x H), 5.30 ppm (s, 2 x OH)

^{13}C NMR spectrum : ($CDCl_3$, 600 MHz) δ_C 40.0 ppm (2 x $C_{2,6}$), 42.8 ppm (2 x $C_{1,7}$), 44.0 ppm (2 x $C_{3,5}$), 33.9 ppm (1 x C_4), 72.2 ppm (1 x C_8), 49.1 ppm (2 x $C_{9,10}$), 77.2 ppm (1 x C_{11}), 44.0 ppm (2 x $C_{1'}$), 133.8 ppm (2 x $C_{2'}$)

5.3.3 Synthesis of 3,5-divinyl-4-oxahexacyclo[5.4.1.$0^{2,6}$.$0^{3,10}$.$0^{5,9}$.$0^{8,11}$]dodecane (12)[2]

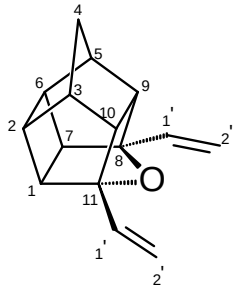

The diol **11** (1.00 g) was refluxed in dilute HCl for one hour. The solution was allowed to cool to ambient temperature and it was extracted with diethyl-ether. The extract was neutralised with sodium bicarbonate solution and dried with sodium sulphate. The solution was concentrated in *vacuo* and a light brown oil was obtained (0.56 g, 66 %).

Infrared spectrum : ν_{max} 2968, 1412, 1271, 1068, 915, 672 cm^{-1}

Mass spectrum : m/z 212 (M^+)

^{1}H NMR spectrum : ($CDCl_3$, 600 MHz) δ_H 2.44 ppm (d, 2 x H), 2.45 ppm (t, 2 x H), 2.36 ppm (q, 2 x H), 1.07 ppm (t, 2 x H), 2.15 ppm (d, 2 x H), 1.97-2.24 ppm (d, 2 x H), 5.90 ppm (t, 2 x H), 5.01 ppm (d, 2 x H)

^{13}C NMR spectrum : ($CDCl_3$, 600 MHz) δ_C 40.0 ppm (2 x $C_{2,6}$), 42.8 ppm (2 x $C_{1,7}$), 44.0 ppm (2 x $C_{3,5}$), 33.9 ppm (1 x C_4), 72.2 ppm (1 x C_8), 49.1 ppm (2 x $C_{9,10}$), 77.2 ppm (1 x C_{11}), 44.0 ppm (2 x $C_{1'}$), 133.8 ppm (2 x $C_{2'}$)

5.3.4 Synthesis of *exo*-8-*exo*-11-diallylpentacyclo[5.4.0.0^{2,6}.0^{3,10}.0^{5,9}]undecane-*endo*-8-*endo*-11-diol (13)[3]

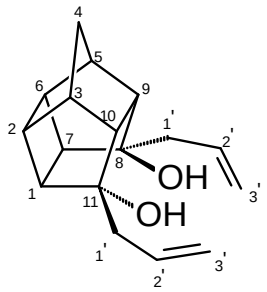

A mechanically stirred suspension of allyl-magnesium bromide (15 mL of a 0.392 *M* solution in dry THF, excess) was cooled to 0 ˚C using an external ice bath. To this suspension, **8** (1.10 g; 336 mmol) in 75 mL dry THF was added dropwise with vigorous stirring at 0 ˚C over a period of 2 hours. After the addition of **8** had been completed, the external ice-water bath was removed, and the reaction mixture was allowed to warm gradually to ambient temperature while stirring under nitrogen for 24 hours. The reaction was quenched by dropwise addition of saturated aqueous NH_4Cl solution until a pH of *ca*. 6-7 was reached. The layers were separated, and the aqueous layer was extracted with EtOAc (2 x 50 mL). The combined organic extracts were dried with $MgSO_4$ and filtered, and the filtrate was concentrated in *vacuo*. The residue was recrystallized from hexane, thereby affording **13** as a brown oil, (0.44 g, 51 %).

Infrared spectrum : ν_{max} 3071, 2955, 1639, 1436, 1282, 1154, 1050, 911 cm^{-1}

Mass spectrum : m/z 217 (M^+)

^{1}H NMR spectrum : ($CDCl_3$, 600 MHz) δ_H 2.44 ppm (d, 2 x H), 2.45 ppm (t, 2 x H), 2.36 ppm (q, 2 x H), 1.07 ppm (t, 2 x H), 2.15 ppm (d, 2 x H), 1.97-2.24 ppm (d, 2 x H), 5.90 ppm (t, 2 x H), 5.01 ppm (d, 2 x H), 5.30 ppm (s, 2 x OH)

^{13}C NMR spectrum : ($CDCl_3$, 600 MHz) δ_C 40.0 ppm (2 x $C_{2,6}$), 42.8 ppm (2 x $C_{1,7}$), 44.0 ppm (2 x $C_{3,5}$), 33.9 ppm (1 x C_4), 72.2 ppm (1 x C_8), 49.1 ppm (2 x $C_{9,10}$), 77.2 ppm (1 x C_{11}), 44.0 ppm (2 x $C_{1'}$), 133.8 ppm (2 x $C_{2'}$), 117.9 ppm (2 x $C_{3'}$)

5.3.5 Synthesis of 3,5-diallyl-4-oxahexacyclo[5.4.1.$0^{2,6}$.$0^{3,10}$.$0^{5,9}$.$0^{8,11}$]dodecane (3)[3]

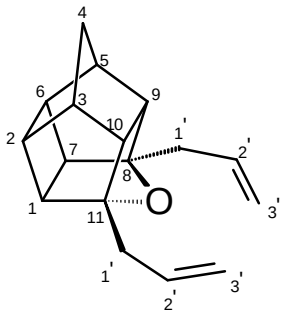

The diol **13** (1.00 g) was refluxed in dilute HCl for one hour. The solution was allowed to cool to ambient temperature and it was extracted with diethyl-ether. The extract was neutralised with $NaHCO_3$ solution and dried with $NaSO_4$. The solution was concentrated in *vacuo* and a light brown oil was obtained **3** (0.49 g, 55 %).

Infrared spectrum : ν_{max} 2959, 1639, 1437, 1293, 993, 908 cm^{-1}

Mass spectrum : m/z 240 (M^+)

^{1}H NMR spectrum : ($CDCl_3$, 600 MHz) δ_H 2.44 ppm (d, 2 x H), 2.45 ppm (t, 2 x H), 2.36 ppm (q, 2 x H), 1.07 ppm (t, 2 x H), 2.15 ppm (d, 2 x H), 1.97-2.24 ppm (d, 2 x H), 5.90 ppm (t, 2 x H), 5.01 ppm (d, 2 x H)

^{13}C NMR spectrum : ($CDCl_3$, 600 MHz) δ_C 40.0 ppm (2 x $C_{2,6}$), 42.8 ppm (2 x $C_{1,7}$), 44.0 ppm (2 x $C_{3,5}$), 33.9 ppm (1 x C_4), 72.2 ppm (1 x C_8), 49.1 ppm (2 x $C_{9,10}$), 77.2 ppm (1 x C_{11}), 44.0 ppm (2 x $C_{1'}$), 133.8 ppm (2 x $C_{2'}$), 117.9 ppm (2 x $C_{3'}$)

5.3.6 Purification of WCl_6

WCl_6 was transferred into a round bottom flask under N_2. It was then heated at a temperature of 250 ˚C, and tungsten oxide compounds (yellowish-red) which have a sublimation temperature lower than that of WCl_6 were removed by a constant nitrogen flow. WCl_6 was heated under N_2 until all tungsten oxides have been removed; dark-purple crystals of WCl_6 remained in the flask. WCl_6 was stored under argon to avoid oxidation indicated by colour change from dark-purple to yellow. The crystals were used in the preparation of $W(O\text{-}2,6\text{-}C_6H_3Cl_2)_2Cl_4$ complex.

5.3.7 Synthesis of $W(O\text{-}2,6\text{-}C_6H_3Cl_2)_2Cl_4$[4]

A solution of $HO\text{-}2,6\text{-}C_6H_3Cl_2$ (0.839 g; 5.1 mmol) in 20 mL chloroform was added to a solution of WCl_6 (1.02 g; 2.56 mmol) suspended in 20 mL of chloroform in a round bottom flask. The reaction mixture was stirred under reflux for 4 hours. During the reaction, the reaction mixture turned from red to dark red. Filtration of the mixture followed by recrystallisation from ethanol gave $W(O\text{-}2,6\text{-}C_6H_3Cl_2)_2Cl_4$ (1.4 g; 85%) as black microcrystals with a green lusture. The synthesis was carried out under inert environment.

Infrared spectrum : ν_{max} 1 556, 1 436, 1 246, 1 099, 915, 777 cm^{-1}

5.3.8 Synthesis of 'cage' compound catalysts[6]

$W(O\text{-}2,6\text{-}C_6H_3Cl_2)_2Cl_4$ complex (0.30 g; 3.08 x 10^{-4} mol) was added into a mini reactor (1, 2 and 3 in **Figure 5.2**) under nitrogen. Dry chlorobenzene (0.3 mL) was added as a solvent to the complex, using a Hamilton-gastight syringe (4 and 5 in **Figure 5.2**). The reaction mixture was heated at 85°C for 10 minutes (6 in **Figure 5.2**). 'Cage' diallyl ether ligand **3** (0.074 g; 3.08 x 10^{-4} mol) dissolved in chlorobenzene (0.3 mL) was added to the mixture (4 and 5 in **Figure 5.2**). The solution was heated and stirred for 90 minutes under nitrogen (6 in **Figure 5.2**). **Scheme 5.2** shows the synthetic route of the cage diallyl ether catalyst **15**, the coordination of **3** and **4** to produce **14** that will be alkylated with Bu_4Sn to **15** could not be obtained.

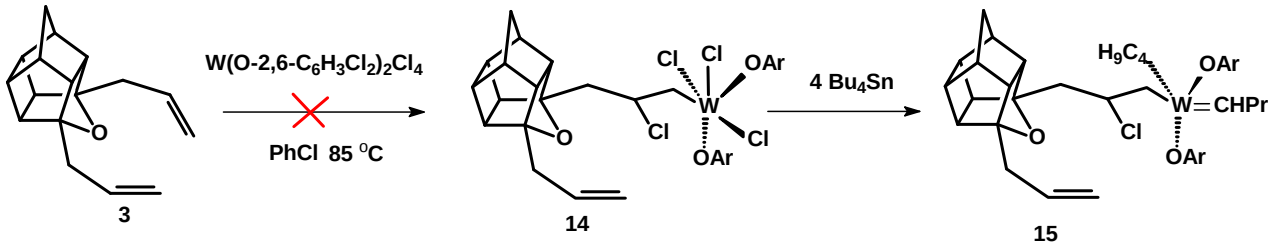

Scheme 5.2 Synthesis of **15**.[6]

5.4 Metathesis reactions

5.4.1 $W(O\text{-}2,6\text{-}C_6H_3Cl_2)_2Cl_4$ complex[5]

The tungsten(VI) aryloxide complex **4** (0.016 g; 2.5 x 10^{-5} mol) was transferred under nitrogen into a 5 mL mini reactor (1, 2 and 3 in **Figure 5.2**). Chlorobenzene (0.3 mL) was added as a solvent to the complex, using a Hamilton-gastight syringe (4 and 5 in **Figure 5.2**). The mixture was heated at 85 °C for 10 minutes (6 in **Figure 5.2**). Bu_4Sn, the co-catalyst, (0.025 mL; 0.75 x 10^{-5} mol) was added (4 and 5 in **Figure 5.2**) to the heated mixture. The reaction mixture was heated at 85 °C for 20 minutes (6 in **Figure 5.2**). After 20 minutes which is the activation time, 1-octene (0.5 mL; 2.5 x 10^{-3} mol) was added (4 and 5 in **Figure 5.2**). The reaction mixture was stirred at 85 °C (6 in **Figure 5.2**) and followed with a GC for 210 minutes.

5.4.2 'Cage' compound catalysts

The next step was the same reaction when it is run *in situ*. $W(O\text{-}2,6\text{-}C_6H_3Cl_2)_2Cl_4$ (0.30 g; 3.08 x 10^{-4} mol) was added into a mini reactor (1, 2 and 3 in **Figure 5.2**) under nitrogen. Dry chlorobenzene (0.3 mL) was added as a solvent to the complex, using a Hamilton-gastight syringe (4 and 5 in **Figure 5.2**). The reaction mixture was heated at 85 °C for 10 minutes (6 in **Figure 5.2**). 'Cage' diallyl ether. **3** ligand (0.074 g; 3.08 x 10^{-4} mol) dissolved in chlorobenzene (0.3 mL) was added to the mixture (4 and 5 in **Figure 5.2**). The solution was heated and stirred for 90 minutes under nitrogen (6 in **Figure 5.2**). Bu_4Sn (0.025 ml; 0.075 x 10^{-4} mol) was added by using a Hamilton-gastight syringe (4 and 5 in **Figure 5.2**) and heated for further 90 minutes. 1-Octene (0.5 ml; 2.5 x 10^{-3} mol) was added and the reaction was followed with a GC, **Scheme 5.3** shows the reaction of the in situ metathesis of **3** with 1-octene.

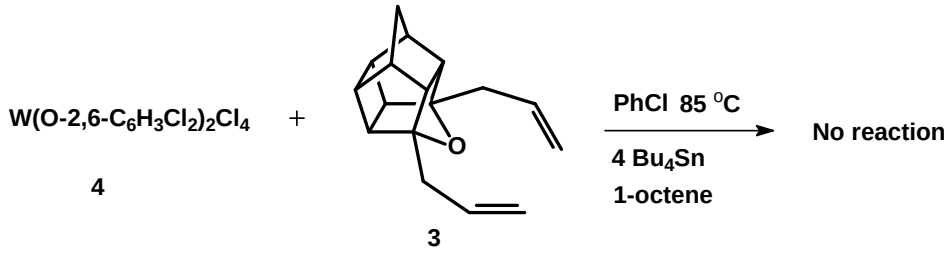

Scheme 5.3 *in situ* metathesis of the cage diallyl ether catalyst.

The reactions in **Scheme 5.2** and in **Scheme 5.3** were also performed with **12** as a ligand using the same reaction conditions and the same results were obtained.

5.5 Analysis

5.5.1 Gas Chromatography (GC)

GC analyses were performed on an HP 6890 gas chromatography equipped with a Phenomenex 80646 (ZB-1) column (50.0 m x 250 μm x 0.50 μm) and flame ionisation detector (FID). The following temperature programme and analytical conditions were used.

Oven programme:

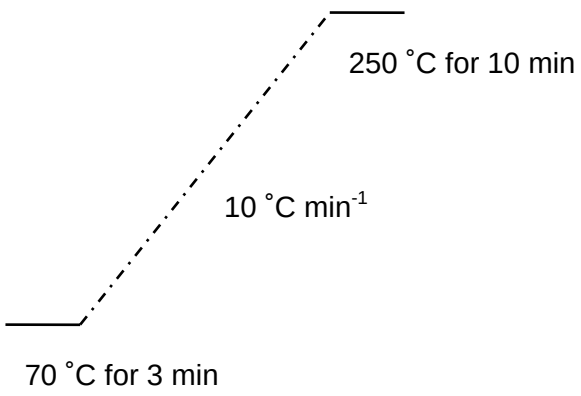

Inlet temperature:	250˚C
Detector temperature:	250 ˚C
N_2 carrier gas flow:	1.2 mL/min
Fuel gas flow	
H_2 flow rate:	40 mL/min
Air flow rate:	450 mL/min
Injection volume:	0.2 μL
Split ratio:	50:1

Chlorobenzene was used as the internal standard to determine the mole percentage of 1-octene converted to the primary metathesis products, secondary metathesis products and isomerisation products. The GC response factor (Rf) was calculated from a calibration curve plotted as $A_{chlorobenzene}/A_{octene}$ against $V_{chlorobenzene}/V_{octene}$ (**Figure 5.3**). A response factor of 0.9933 for 1-octene was calculated from the slope of the calibration curve.

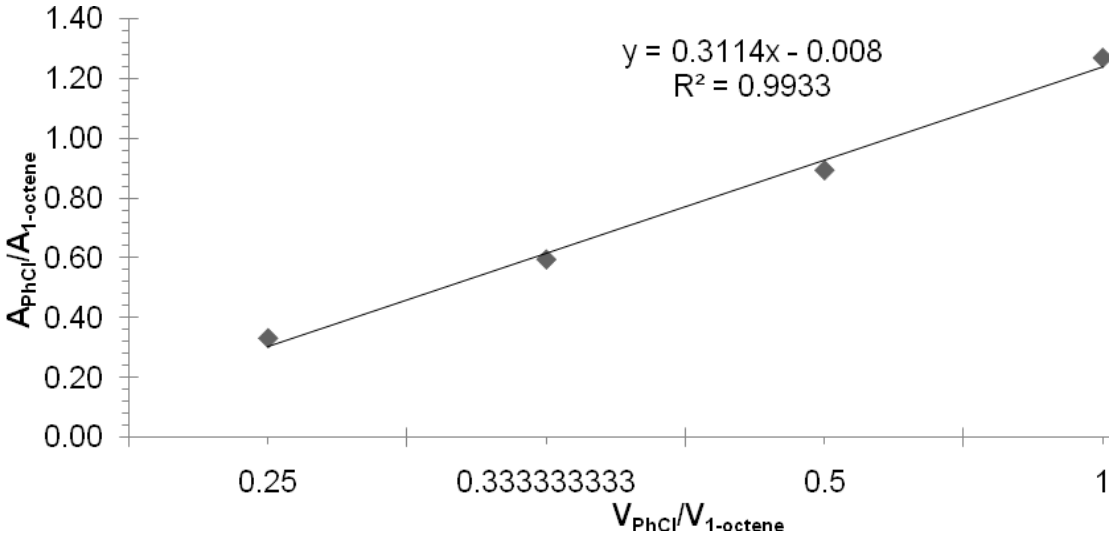

Figure 5.3 Calibration curve for determining the response factor.

Equation 5.1 was used to determine the mol percentage conversion of 1-octene to 7-tetradecene:

$$\text{mol\%}C_8 = 100 \times R_f \times \frac{V_{is}}{V_{C8}} \times \frac{A_{C8}}{A_{is}} \qquad (5.1)$$

Where

C_8 = 1-octene
R_f = GC response factor
V_{is} = Volume of the internal standard at t = 0
V_{C8} = Volume of the 1-octene at t = 0
A_{C8} = Area of 1-octene
A_{is} = Area of the internal standard

Equation 5.2 was used to determine the mol percentage of 7-tetradecene formed during the reaction:

$$\text{mol\%}C_n = 2 \times R_f \times \left(V_{is} \frac{A_{Cn}}{A_{is}} \right) \times \frac{\rho_{Cn}}{M_{Cn}} \times \left(\frac{M_{C8}}{\rho_{C8} \times V_{C8}} \right) \times 100 \qquad (5.2)$$

Where

C_n = Alkene

R_f = GC response actor

V_{is} = Volume of the internal standard at t = 0

V_{C8} = Volume of the 1-octene at t = 0

A_{Cn} = Area of the alkene

A_{is} = Area of the internal standard

M_{Cn} = Molecular mass of C_n

M_{C8} = Molecular mass of 1-octene

ρ_{Cn} = Density of C_n

ρ_{C8} = Density of 1-octene

5.5.2 Gas Chromatography-Mass Spectrometry (GC-MS)

MS analyses were performed on an HP 6890 GC-MS equipped with a PE-001 capillary column (60 m x 0.32 mm x 1.00 µm, Elite Methyl Siloxane) connected to an Autospec Micromass Time-of-Flight (TOF) mass spectrometer. The NIST database of the OPUS v 3.6 X software was used for characterisation of the products identified during analysis. The temperature programme and analytical conditions used were similar to those used in GC. 100 mg of the sample was weighed and dissolved in 2 mL diethyl-ether in a GC vial for analysis.

5.5.3 Infrared spectroscopy (IR)

The IR spectra were recorded using a FTIR Bruker Tensor 27 equiped with a diamond ATR. The software OPUS version 6.5 was used for data analysis.

5.5.4 Nuclear Magnetic Resonance spectroscopy (NMR)

A Bruker Advance III Ultra Shield 600 MHz Nuclear Magnetic Resonance spectrometer (NMR); for the ^{1}H and ^{13}C spectroscopy was used. TopSpin 2.1 Version 2.1.1 was used for processing commands and parameters as well as data acquisition. Approximately 40 mg of the sample was dissolved in 0.7 mL of $CDCl_3$ in an NMR tube.

5.6 Computational details

5.6.1 Hardware

There were two types of hardware used for this study:

i) 52 CPU cluster (HP Proliant CP4000 Linux Beowulf with Procurve Gb/E Interconnect on computer nodes):
1 x Master node: HP DL385 - 2 x 2.8 MHz AMD Opteron 64, 2 GB RAM, 2 x 72 GB HDD
12 x Compute nodes: HP DL145G2 - 2 x 2.8 MHz AMD Opteron 64, 2 GB RAM, 2 x 36 GB HDD
Operating system on compute nodes: Redhat Enterprise Linux 4
Cluster operating system: HPC CMU v3.0 cluster

ii) 336 CPU Cluster[7]
1 x Master Node: HP BL460C G6 - 2 Quad Core 2.93 GHz, 16GB RAM, 2 146 GB HDD
40 X Compute Nodes :HP BL460C G6 - 2 Quad Core 2.93 GHz, 16GB RAM, 2 146 GB HDD, ProLiant BL2x220c G5, HP BL460C G1
1 x HP EVA 4400 SAN 3TB
1X Storage Server :HP BL460C G6
Operating system on compute nodes: Scientific Linux SL release 5.3
Cluster operating system : Rocks 5.2 - Scientific Linux SL release 5.3

5.6.2 Software

All molecular modelling calculations were performed using the Accelrys Material Studio 5.0. Geometric optimizations and determinations of properties were calculated with the Density Functional Theory (DFT) method DMol^3 using the GGA functional PW91 together with the following specifications:

- A medium quality of convergence tolerance using 2 x 10^{-5} Ha (Energy), 0,004 Ha/Å (Max. force) and 0.005 Å (Max. displacement)
- A medium Self Consistent Field (SCF) of 1 x 10^{-5} Ha using a maximum of 1000 SCF cycles and octupole multipolar expansion
- A Double Numeric Polarized (DNP) basis set

5.7 References

1. Cookson RC, Crundwell E, Hill RR and Hudec J, *J. Chem. Soc.*, 1964, 3062
2. Marchand AP, Kumar KA, McKim AS, Mlinaric-Majerski K and Kragol G, *Tetrahedron*, 1997, **53(10)**, 3467
3. Marchand AP, Huang Z, Chen Z, Hariprakasha HK, Namboothiri INN, Brodbelt JS and Reyzer ML, *J. Heterocyclic. Chem*., 2001, **38**, 1361
4. Quignard F, Leconte M, Basset J. Hsu L, Alexander JJ and Shore SG, *Inorg. Chem*., 1987, **26**, 4272
5. Vosloo HCM, Dickinson AJ and du Plessis JAK, *J. Mol. Catal. A, Chem*., 1997, **115**, 199
6. Mbhele ZH, *Experimental investigation of dendritic catalysts for alkene metathesis*, MSc-Dissertation, NWU, 2006
7. North-West University High Performance Computer Centre http://efundi.nwu.ac.za/access/wiki/site/4ba488f2-2b27-43be-b5f4f1d97148ec98/home.html Year 2010 [Date of access: August 2010]

Appendices

Appendix A: IR spectra

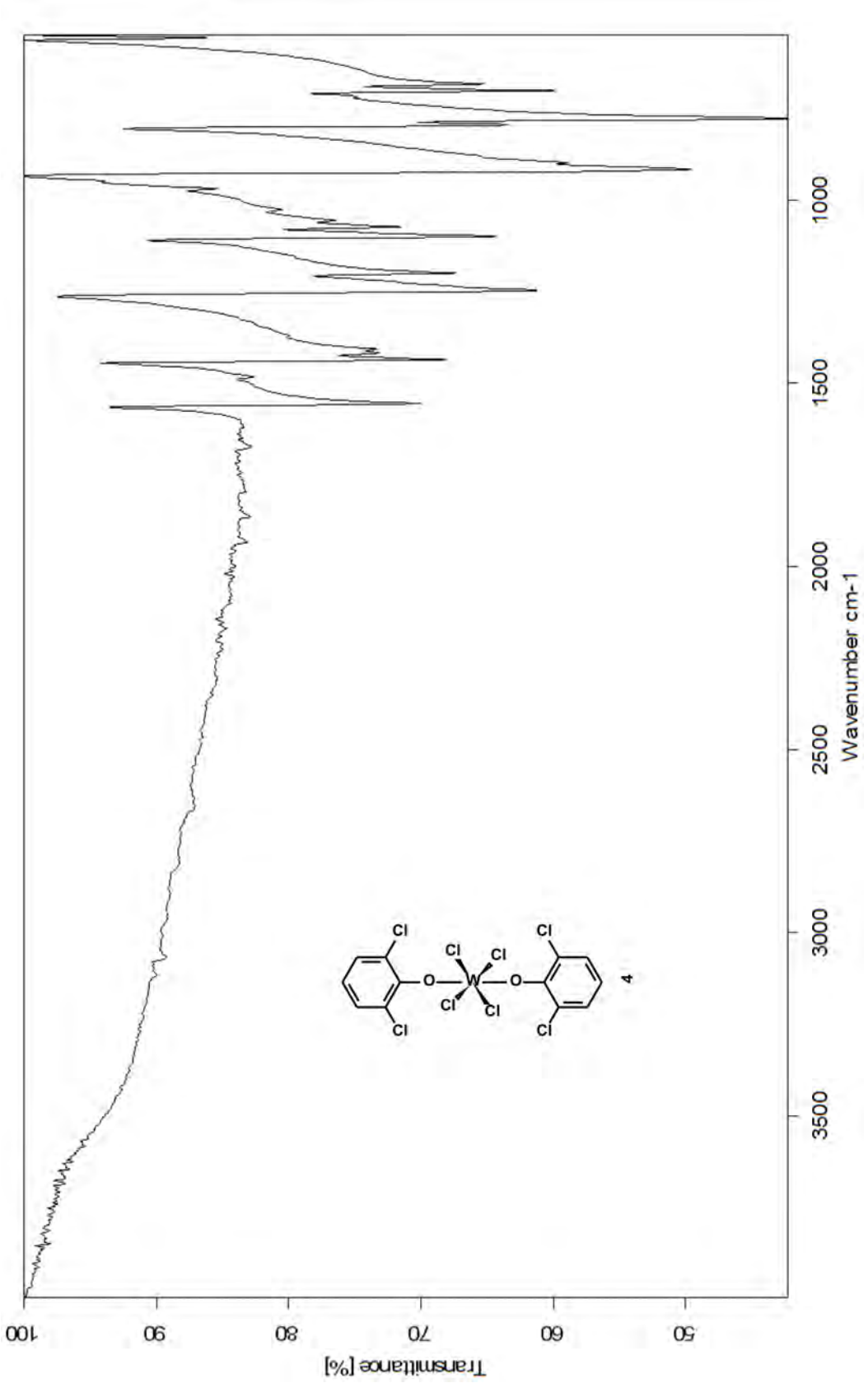

IR spectrum of **4**.

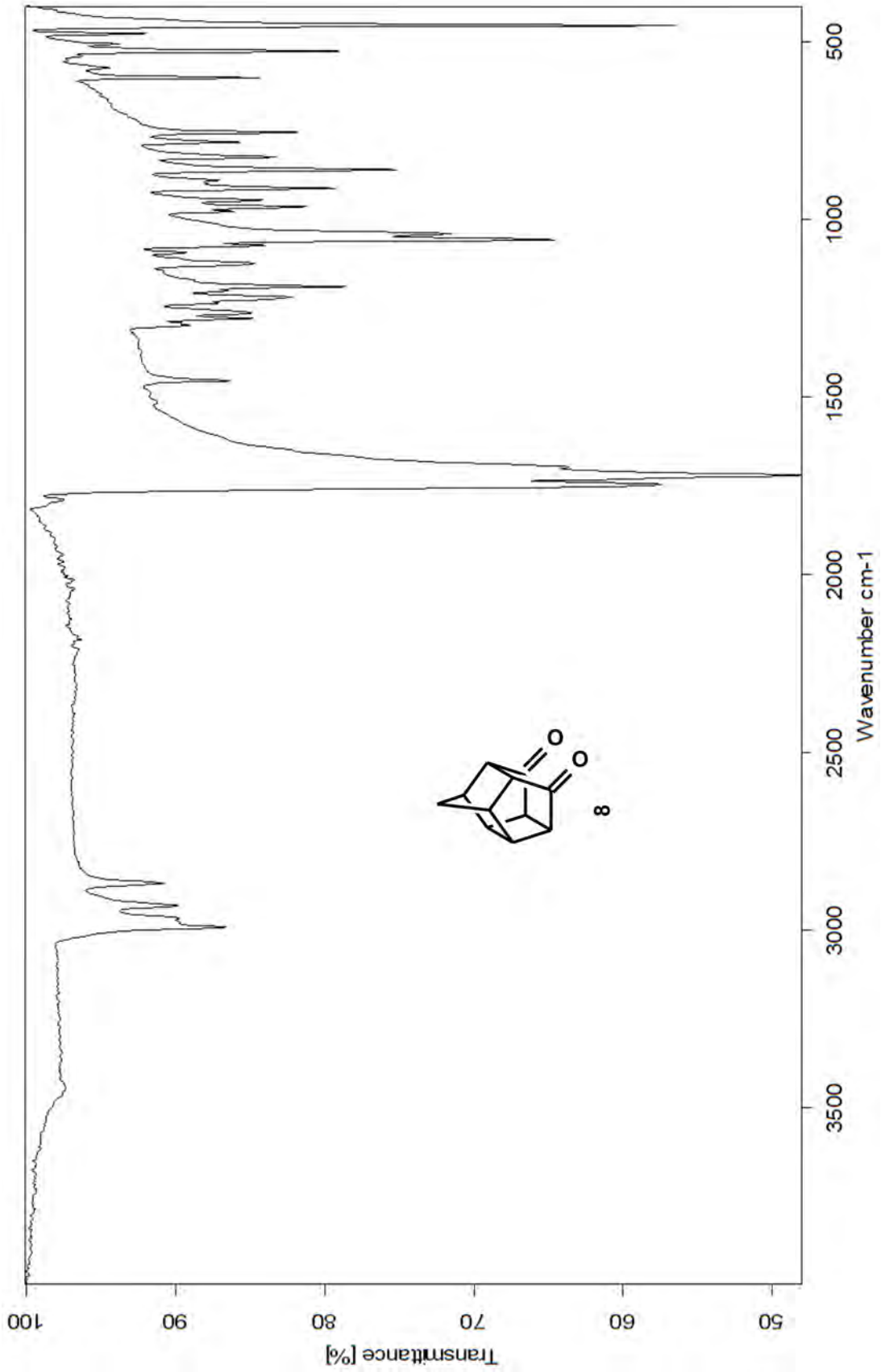

IR spectrum of **8**.

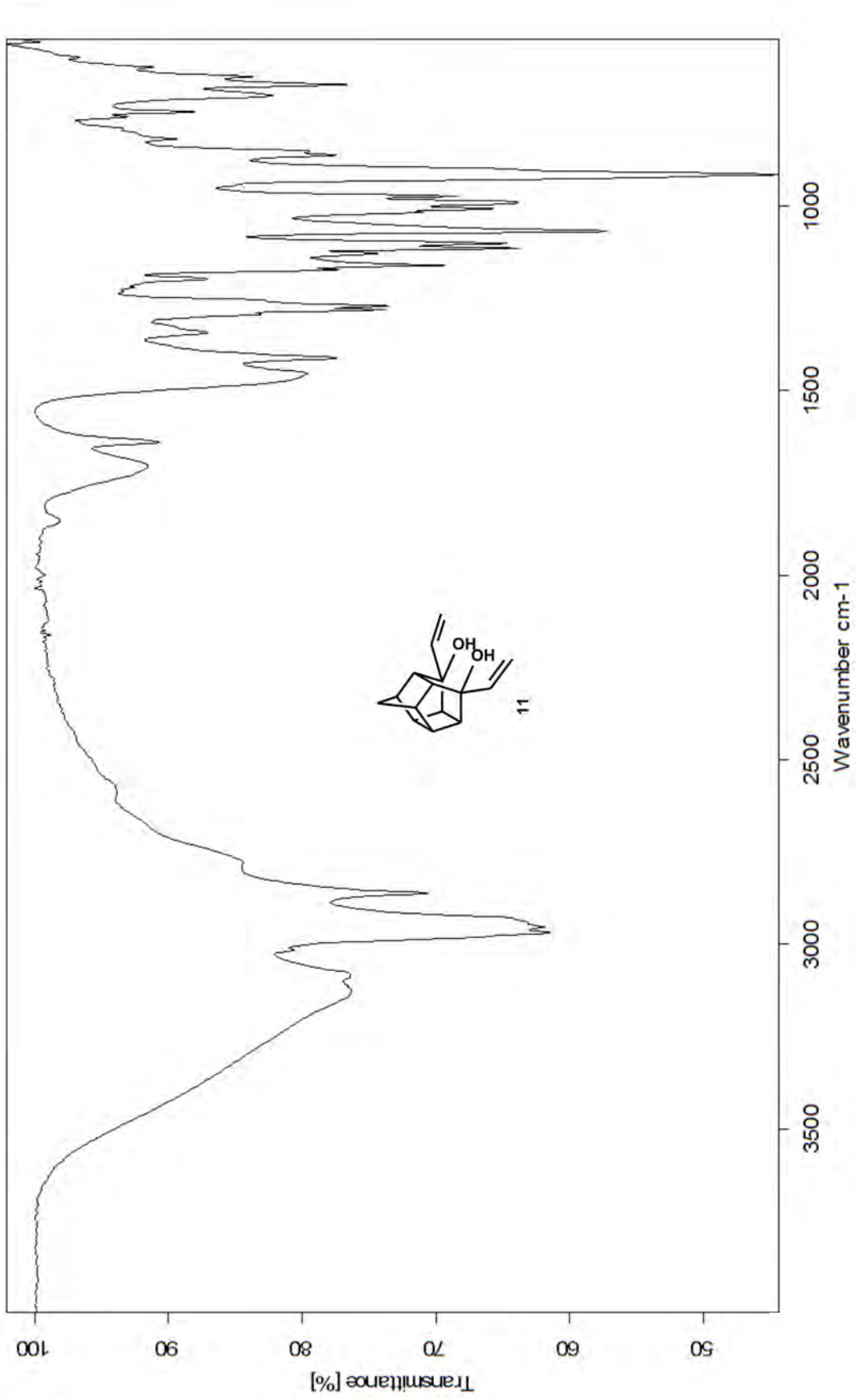

IR spectrum of **11**.

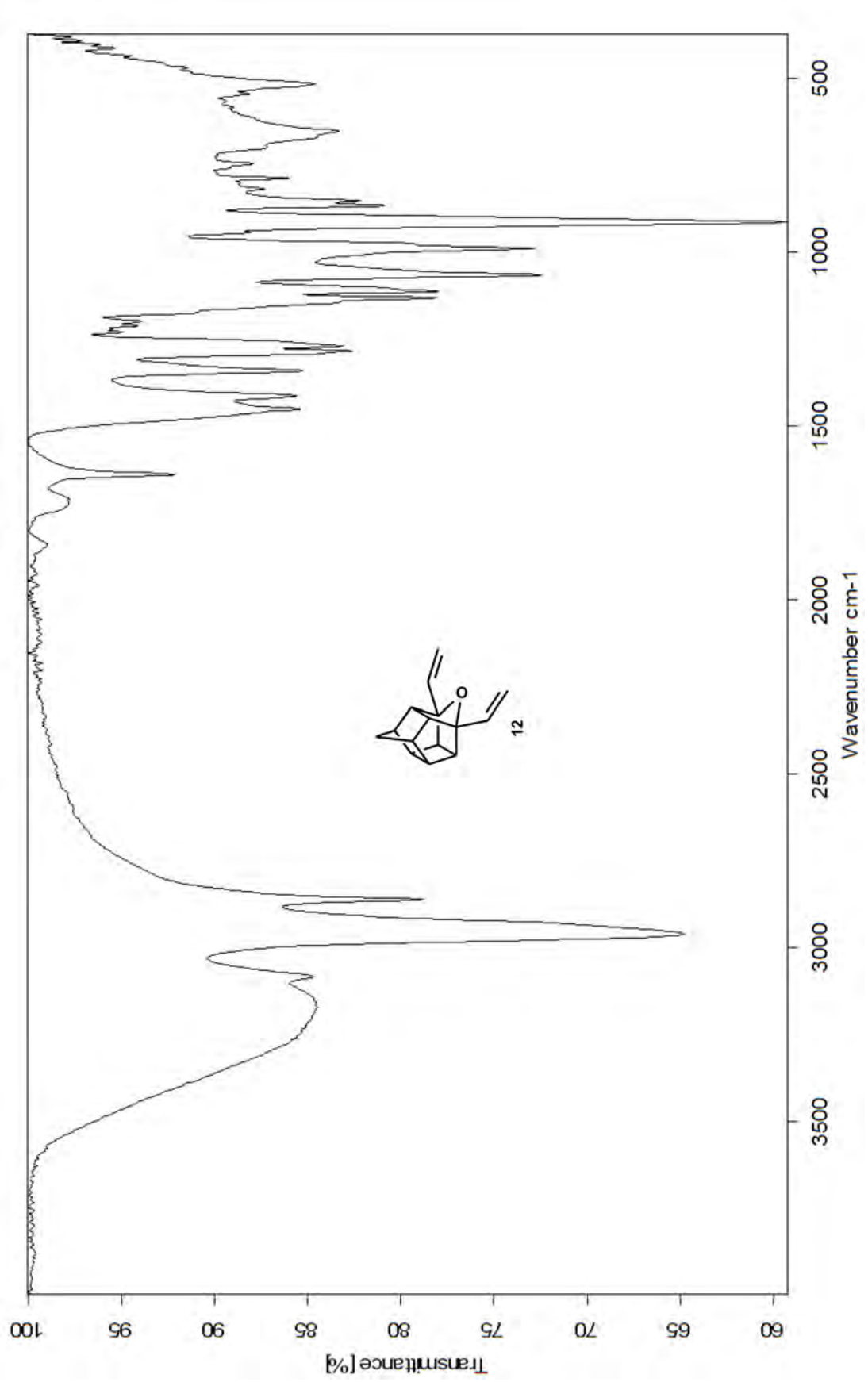

IR spectrum of **12**.

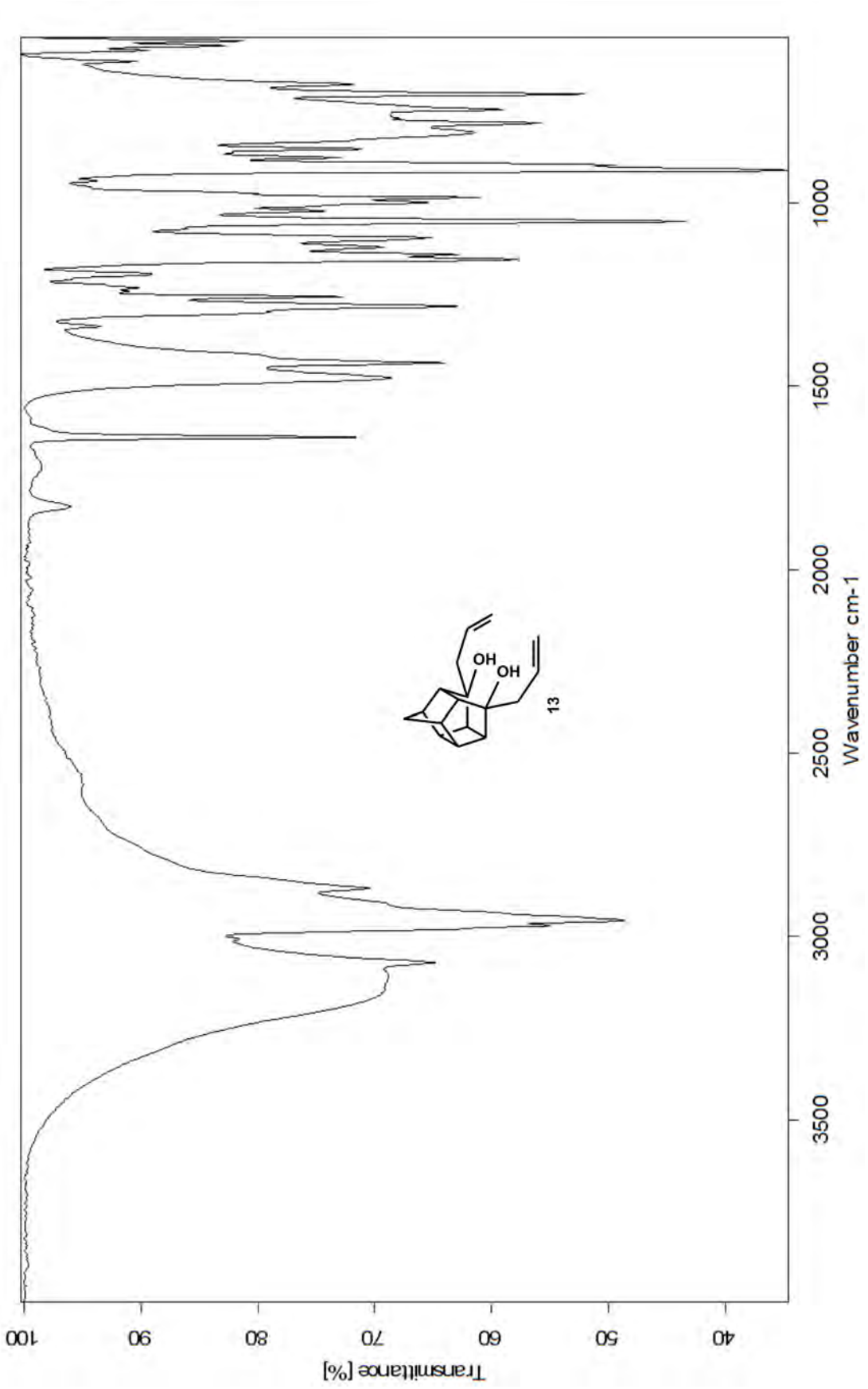

IR spectrum of **13**.

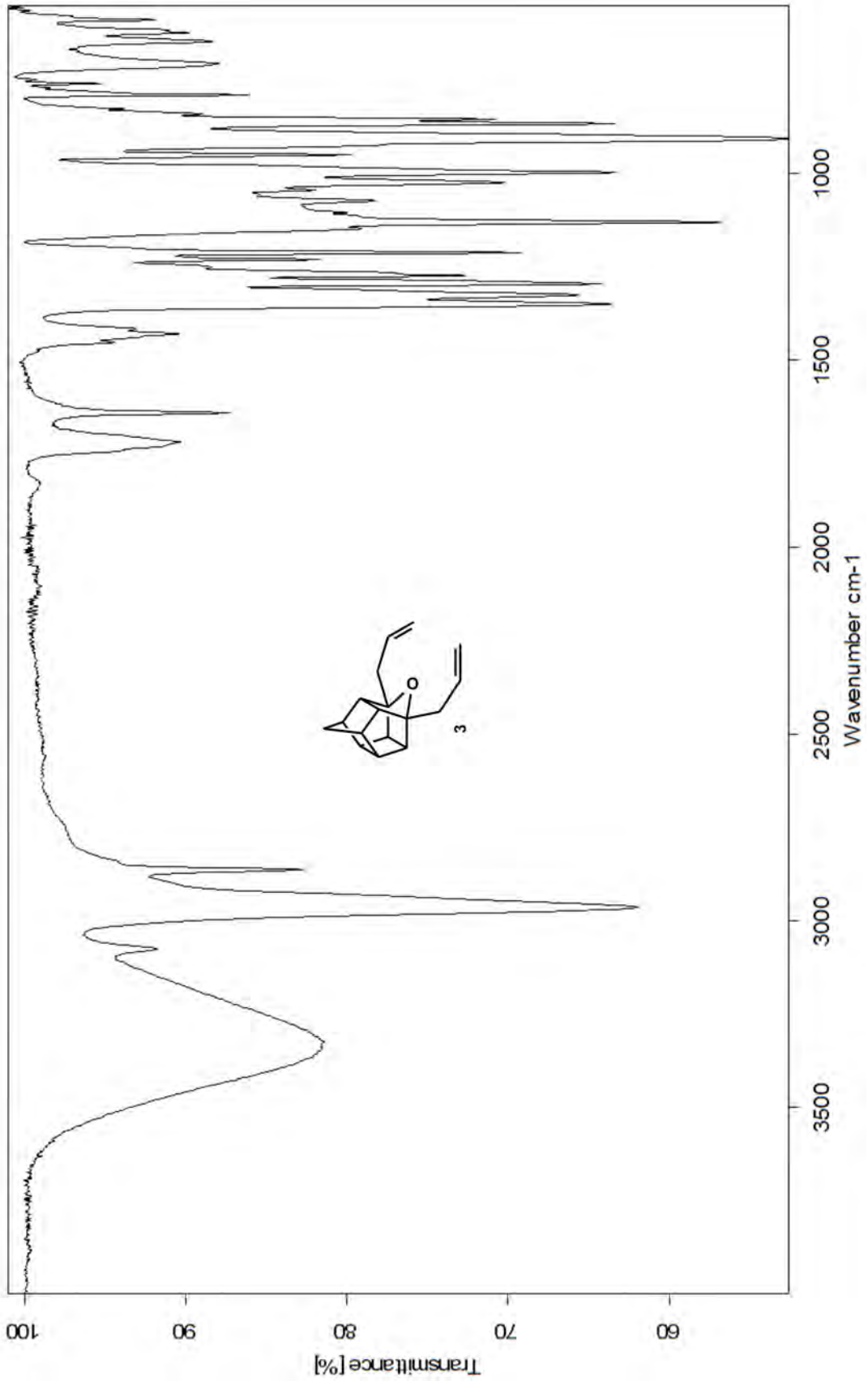

IR spectrum of **3**.

Appendix B: GC-MS spectra

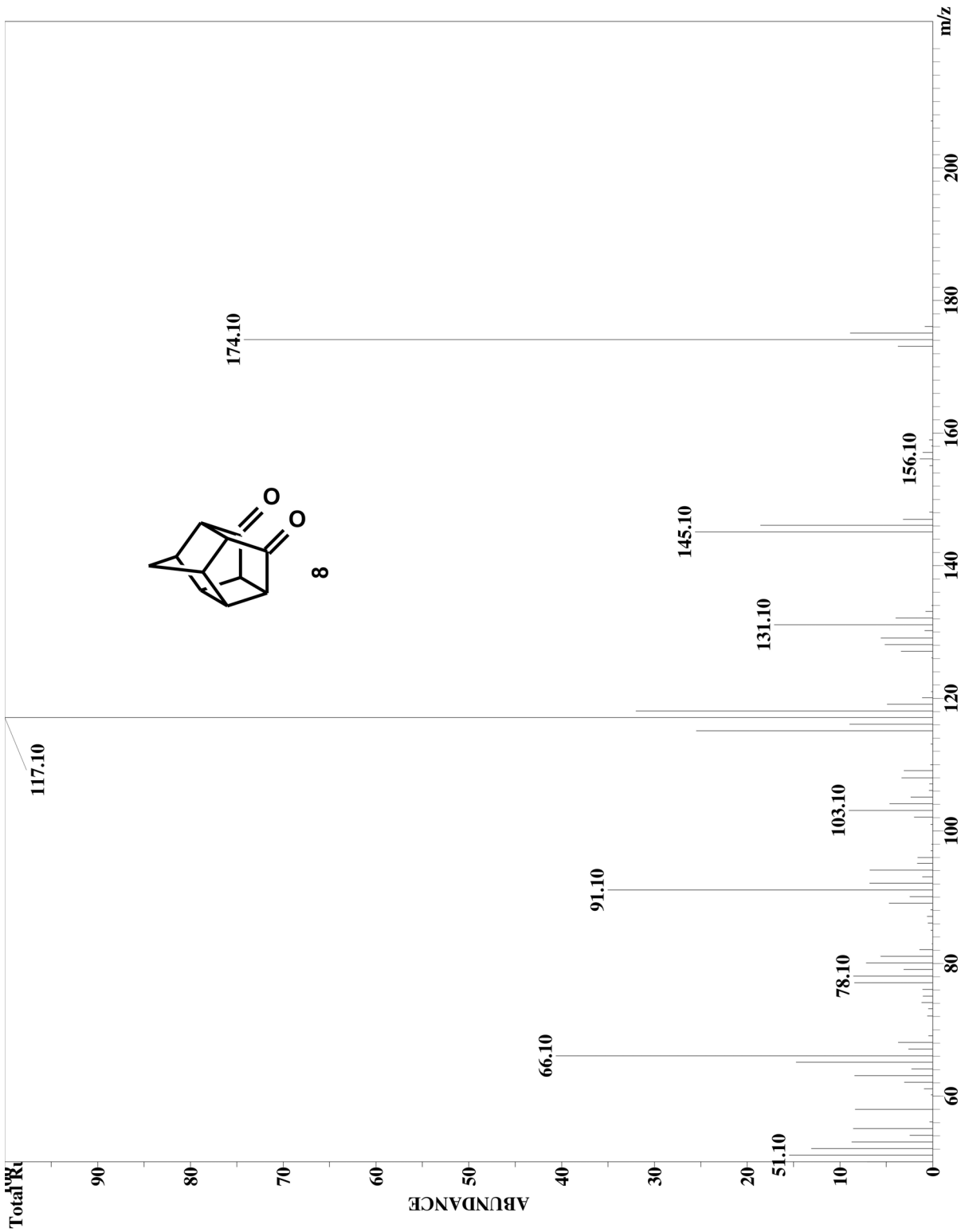

GC-MS spectrum of **8**.

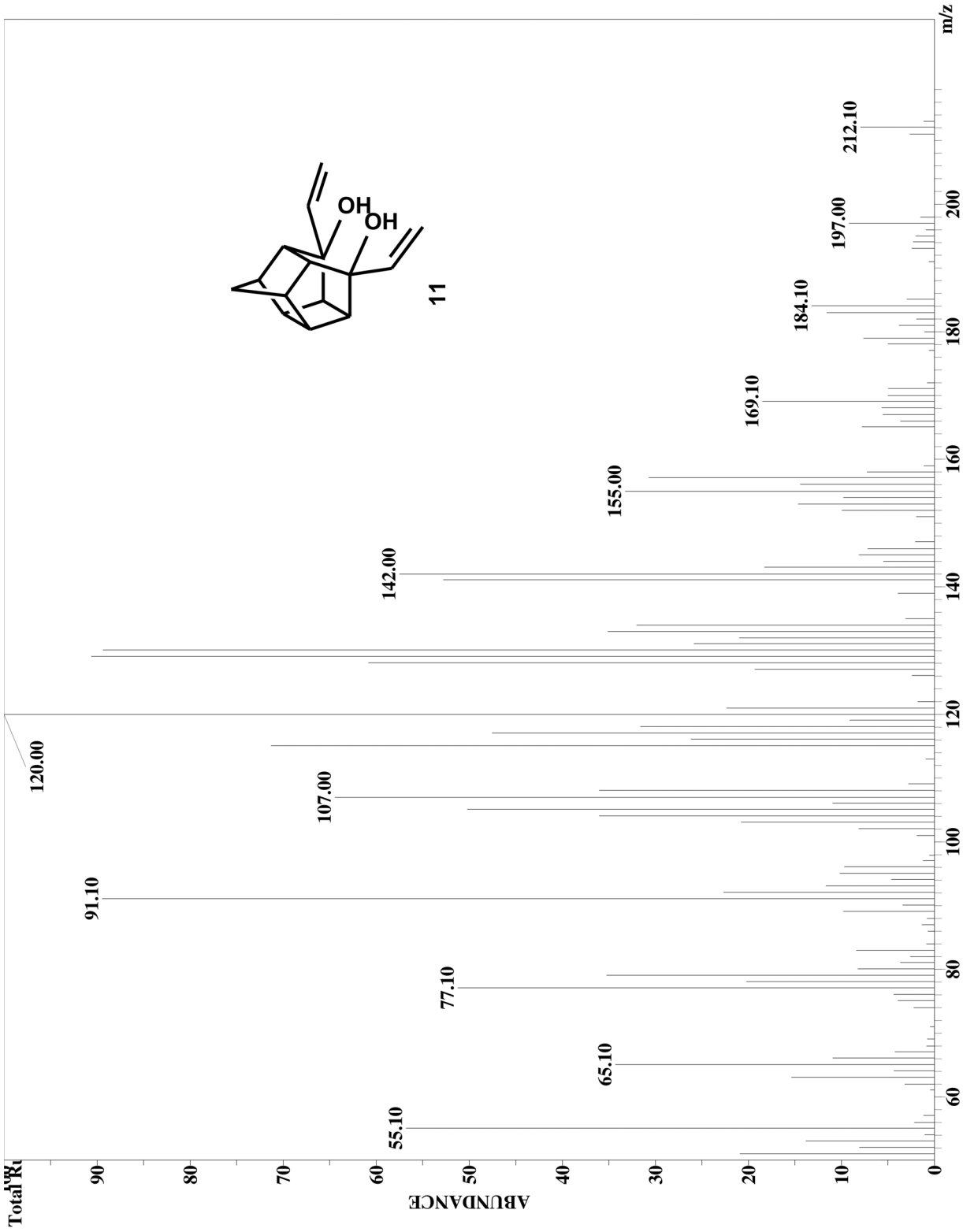

GC-MS spectrum of **11**.

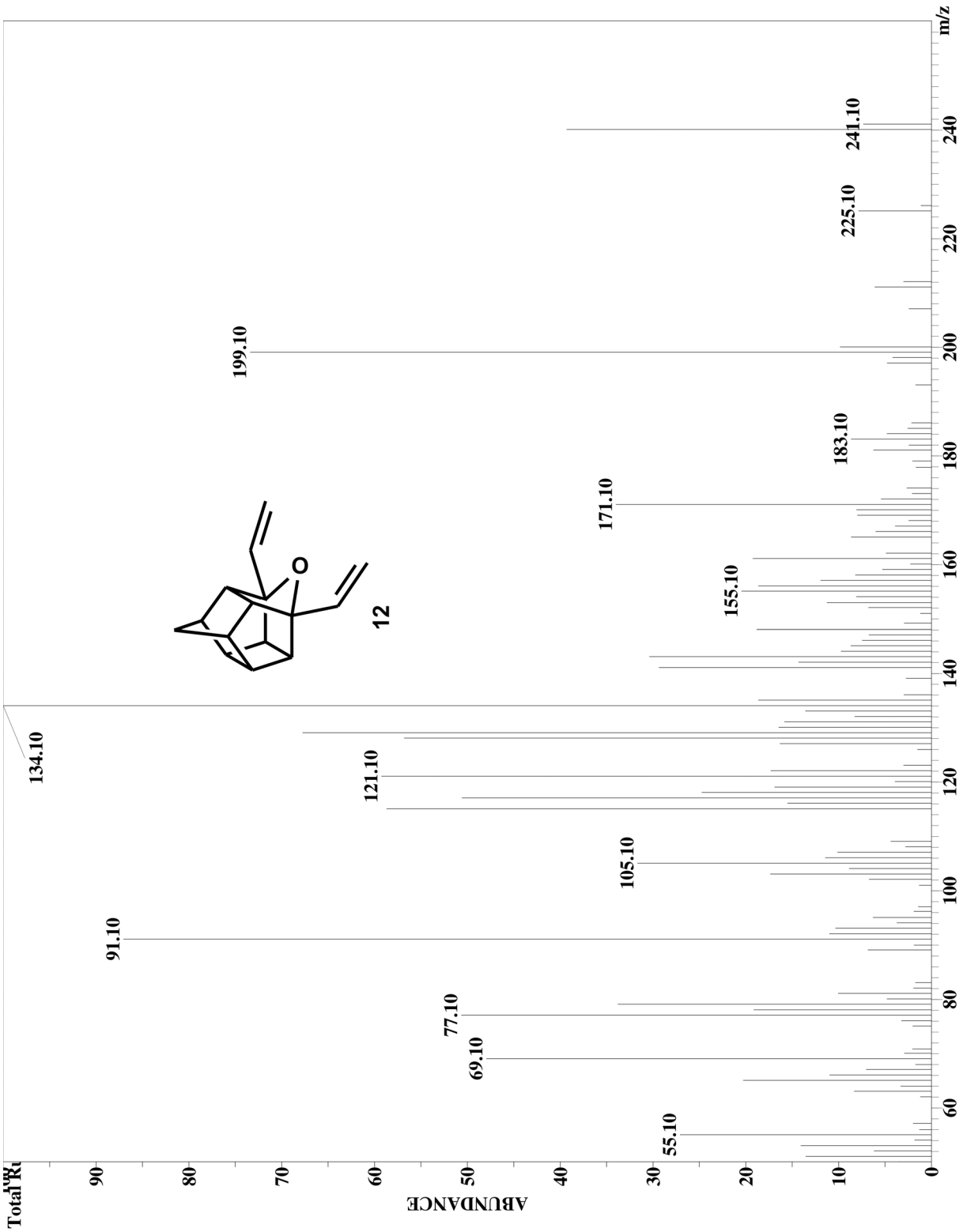

GC-MS spectrum of **12**.

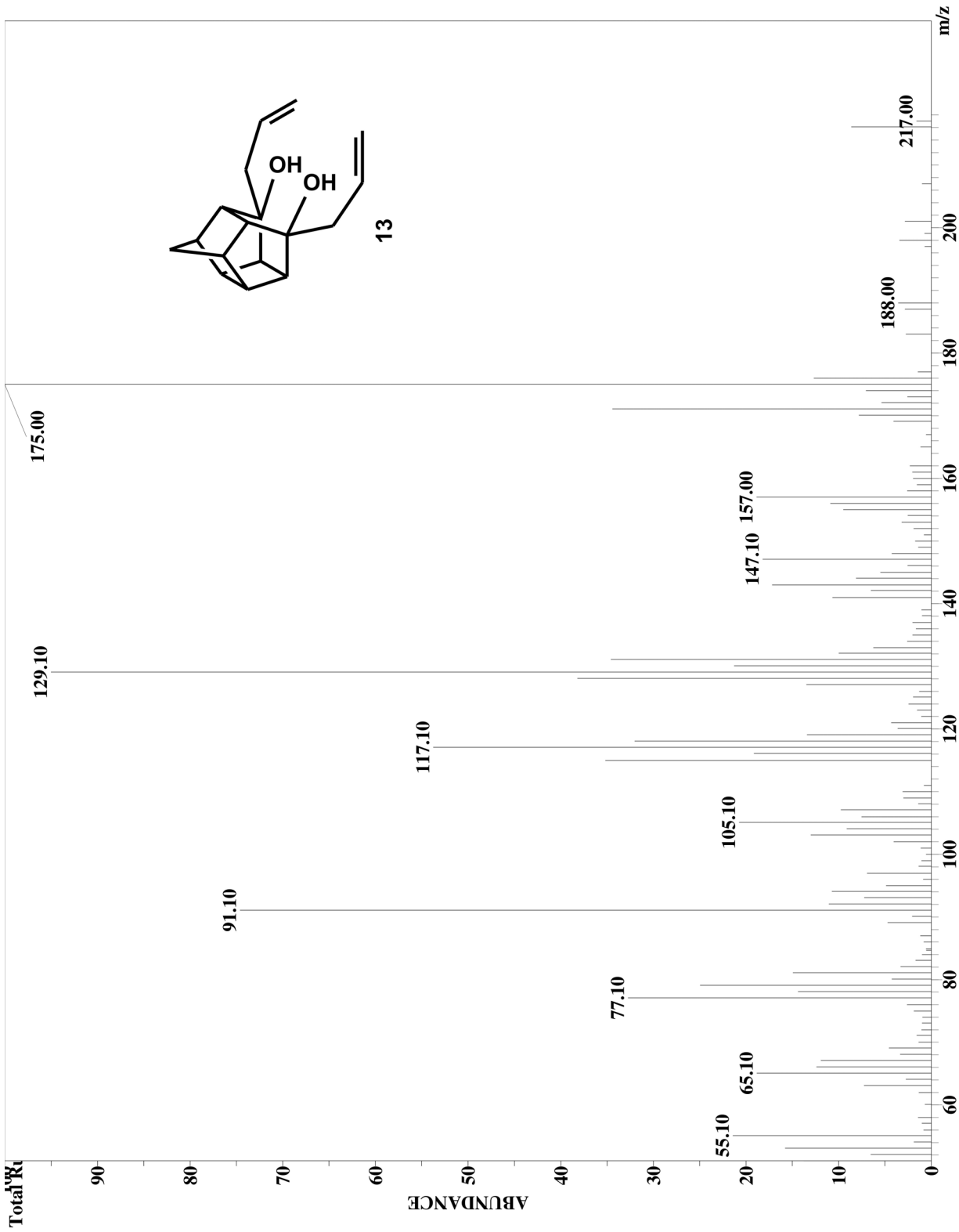

GC-MS spectrum of **13**.

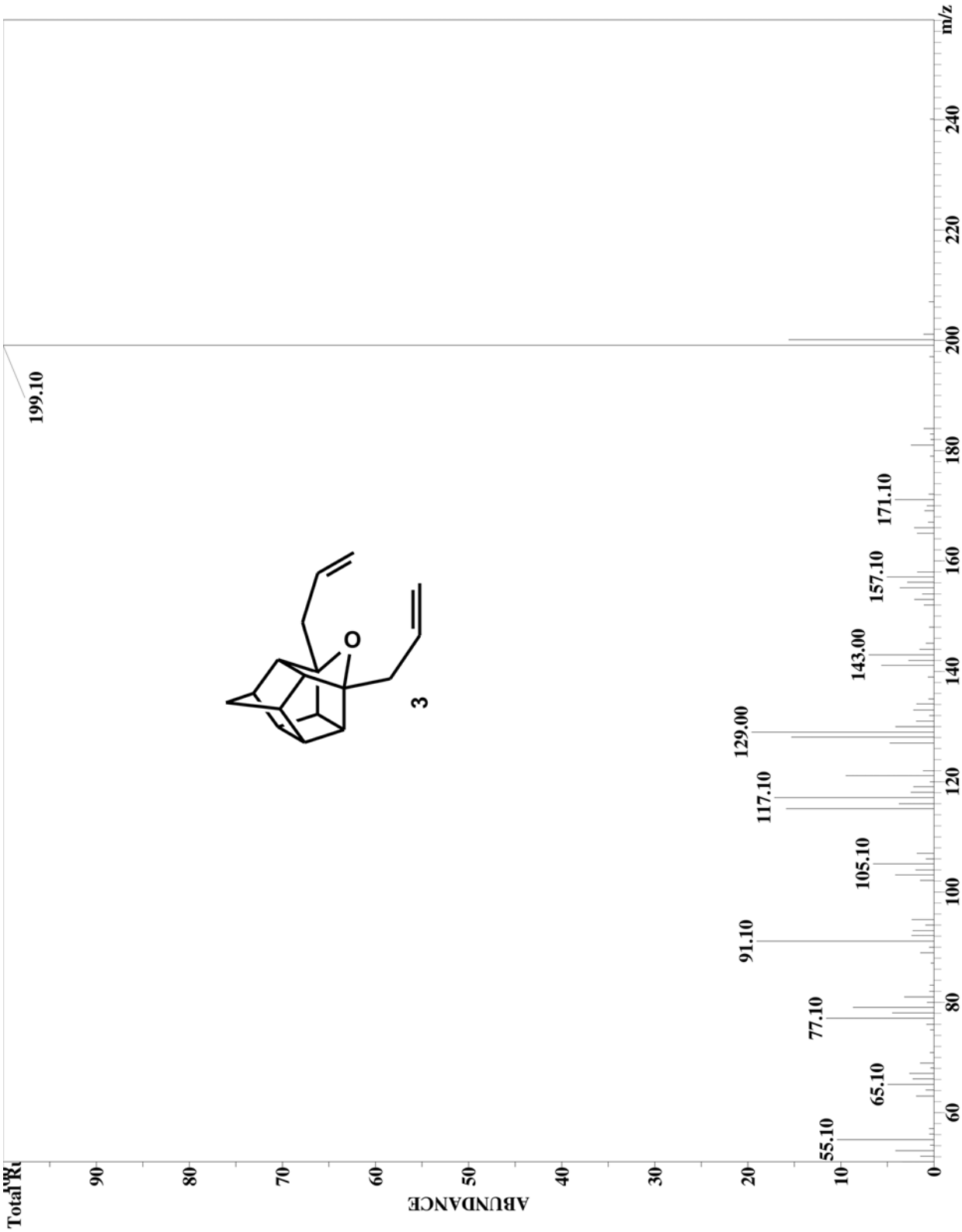

GC-MS spectrum of **3**.

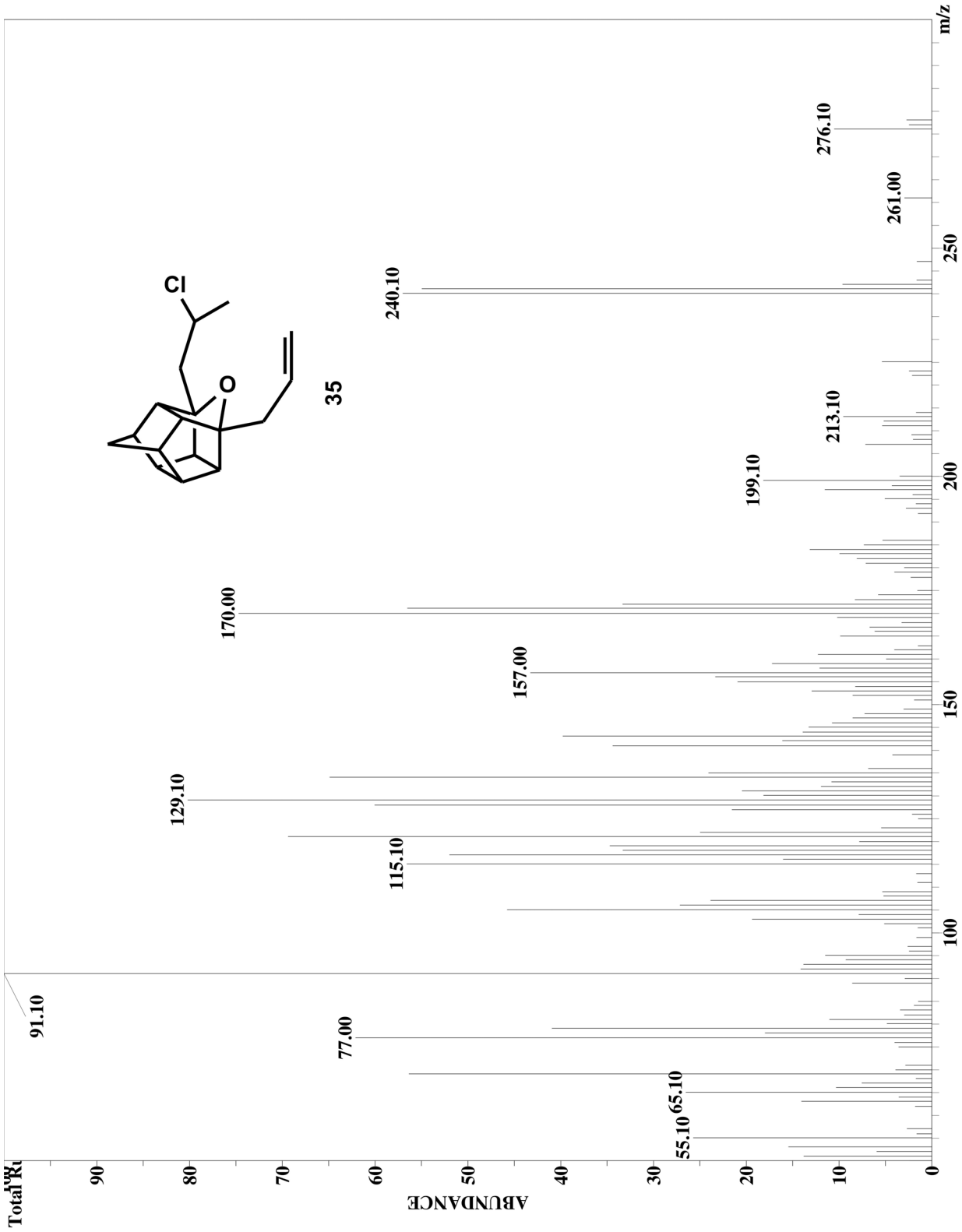

GC-MS spectrum of **35**.

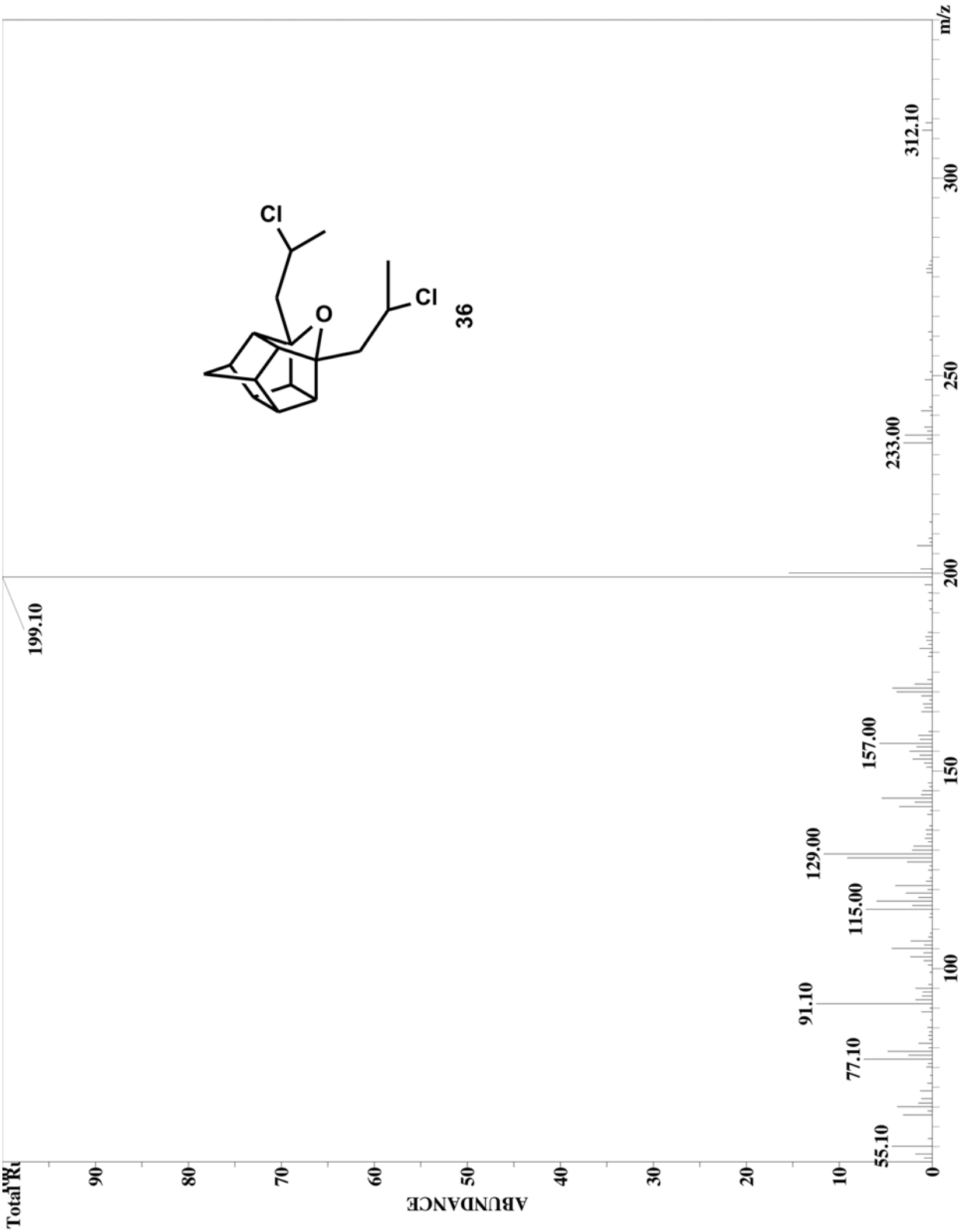

GC-MS spectrum of **36**.

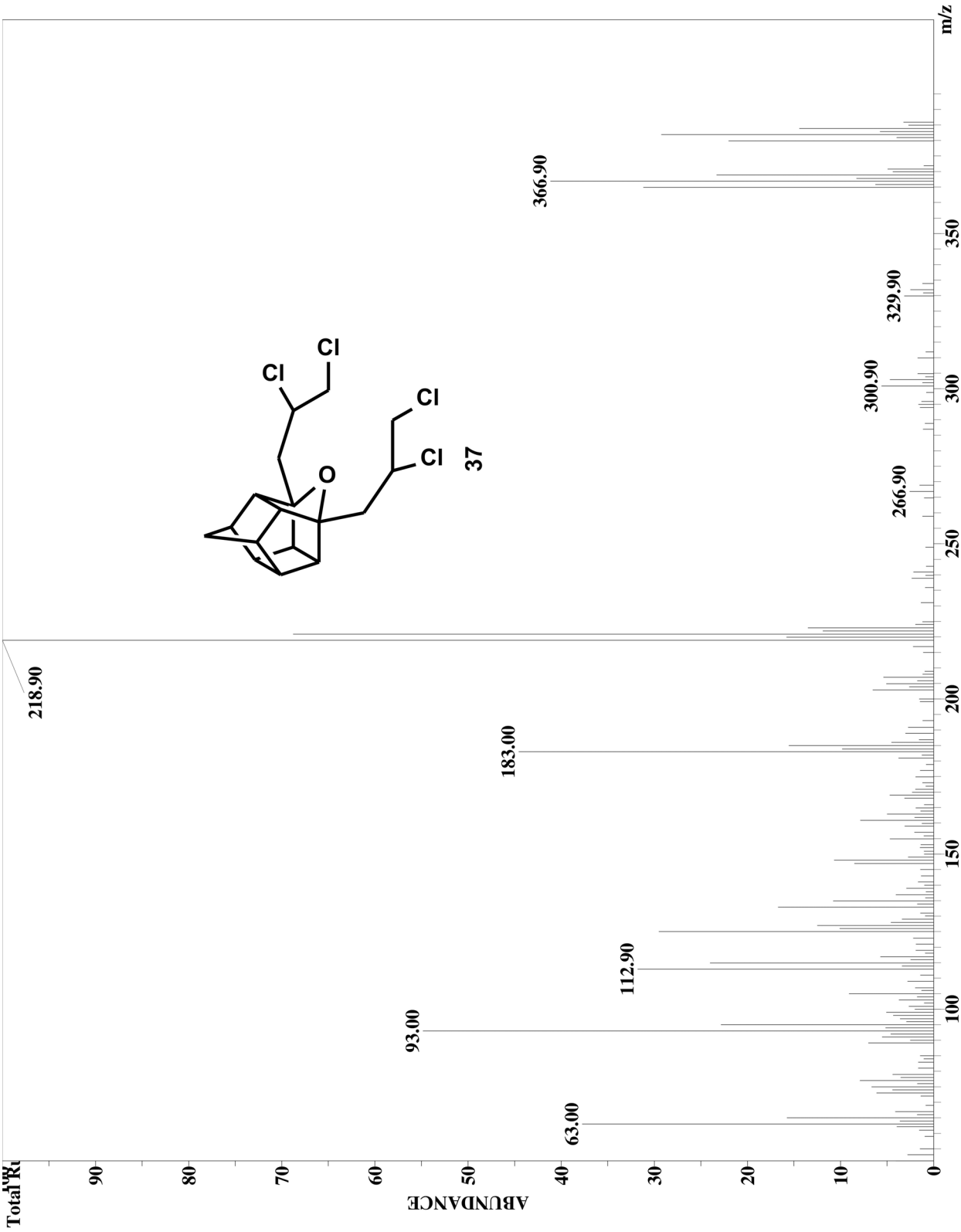

GC-MS spectrum of **37**.

Appendix C: ^{1}H NMR spectra

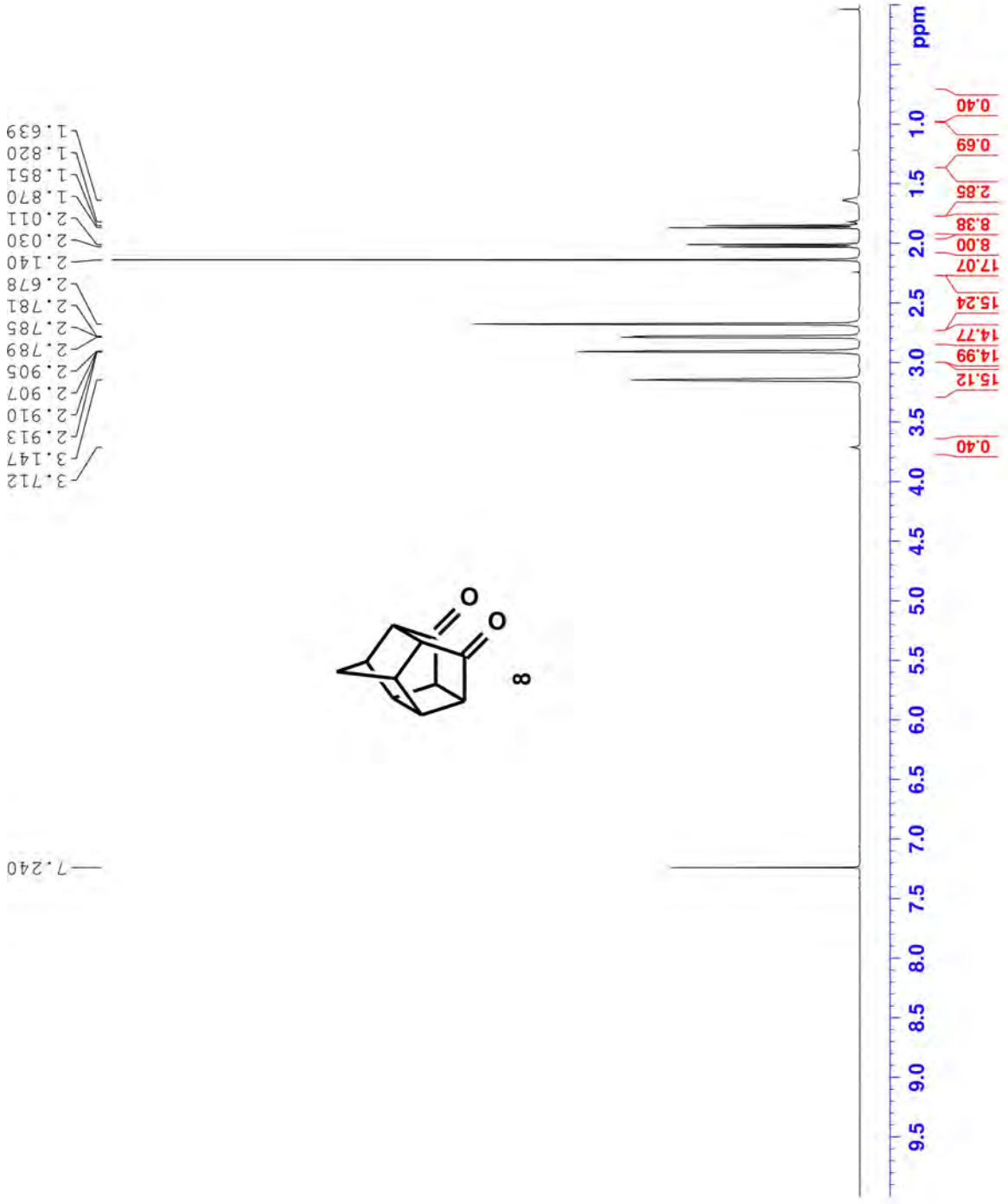

^{1}H NMR spectrum of **8**.

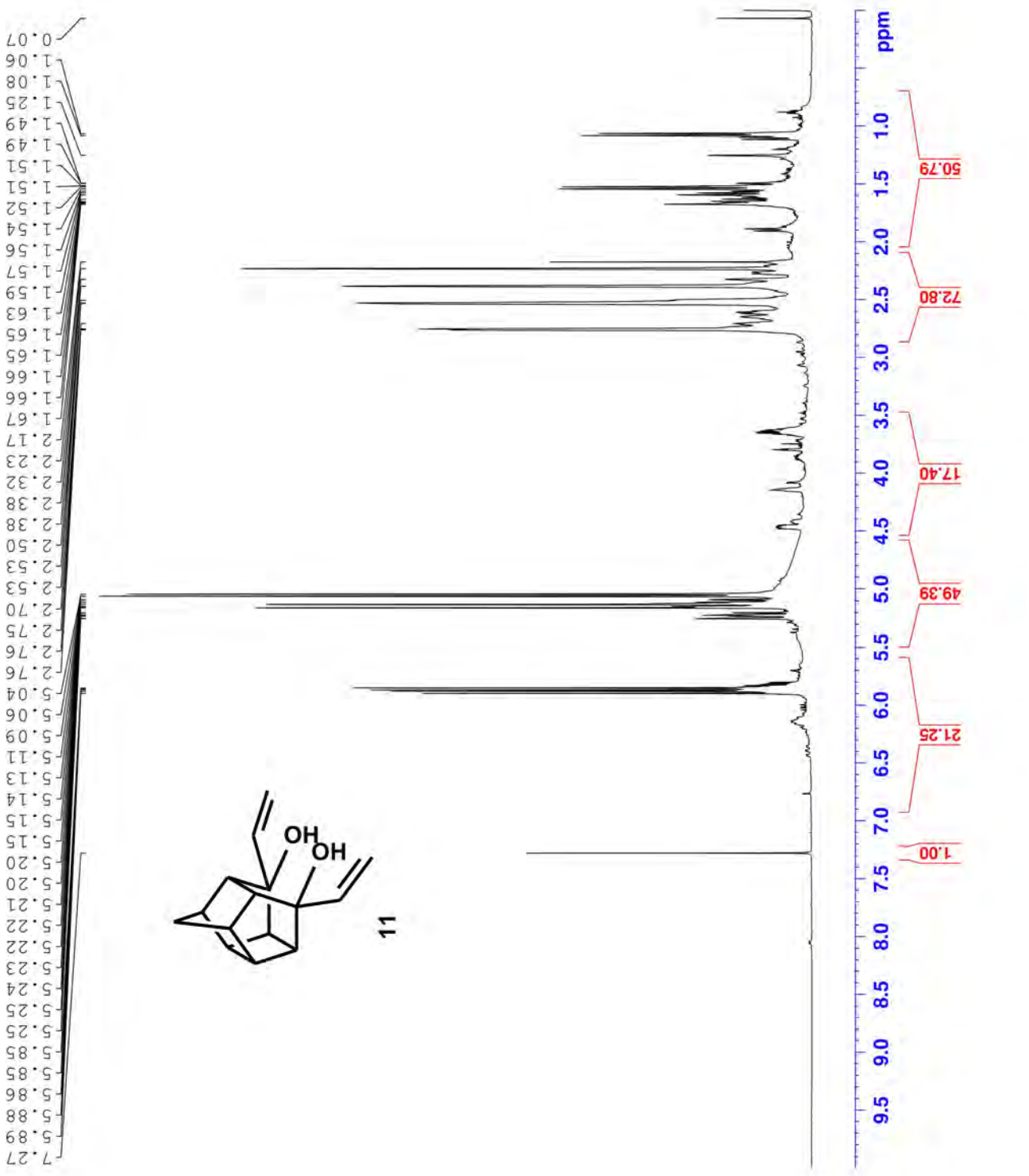

^{1}H NMR spectrum of **11**.

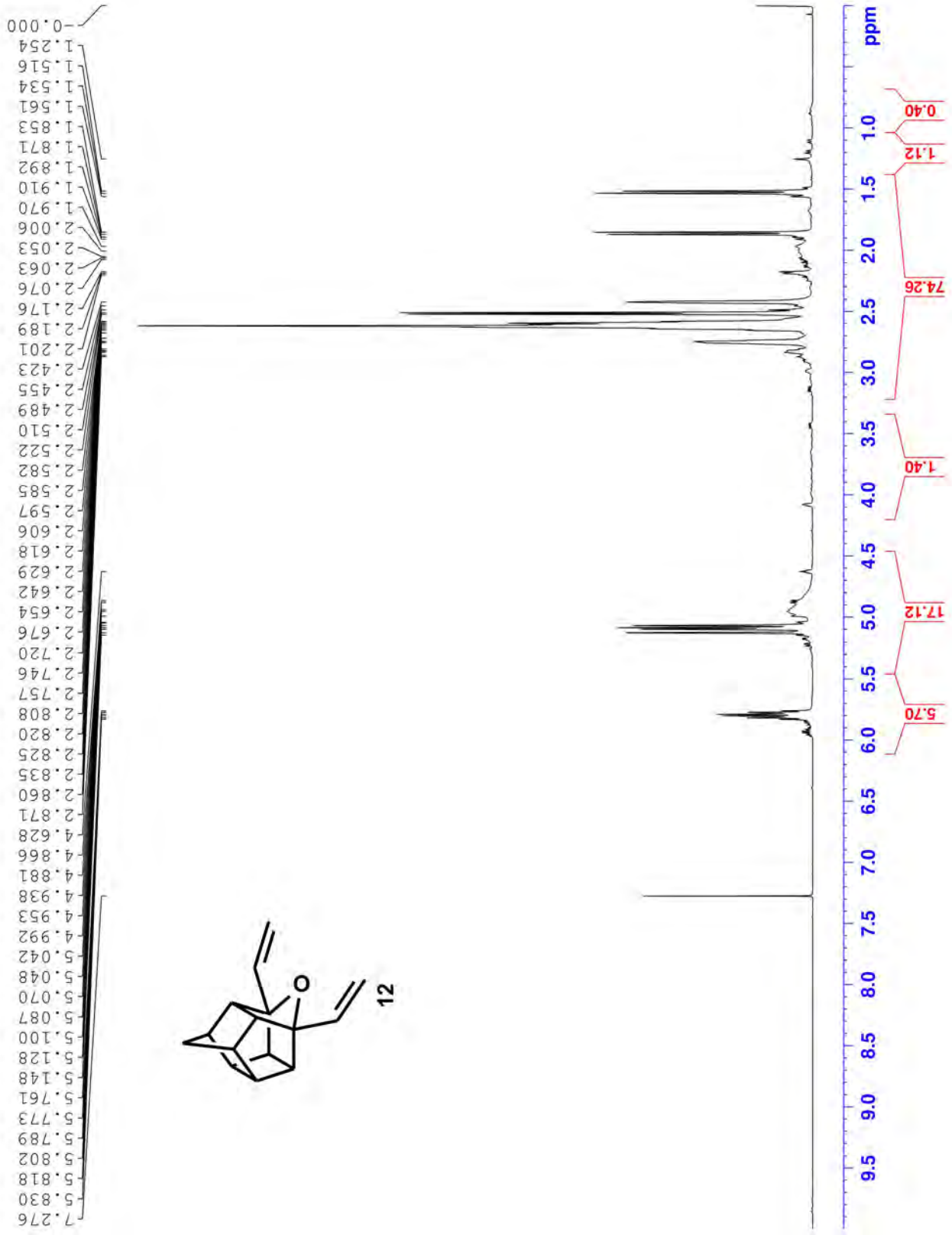

^{1}H NMR spectrum of **12**.

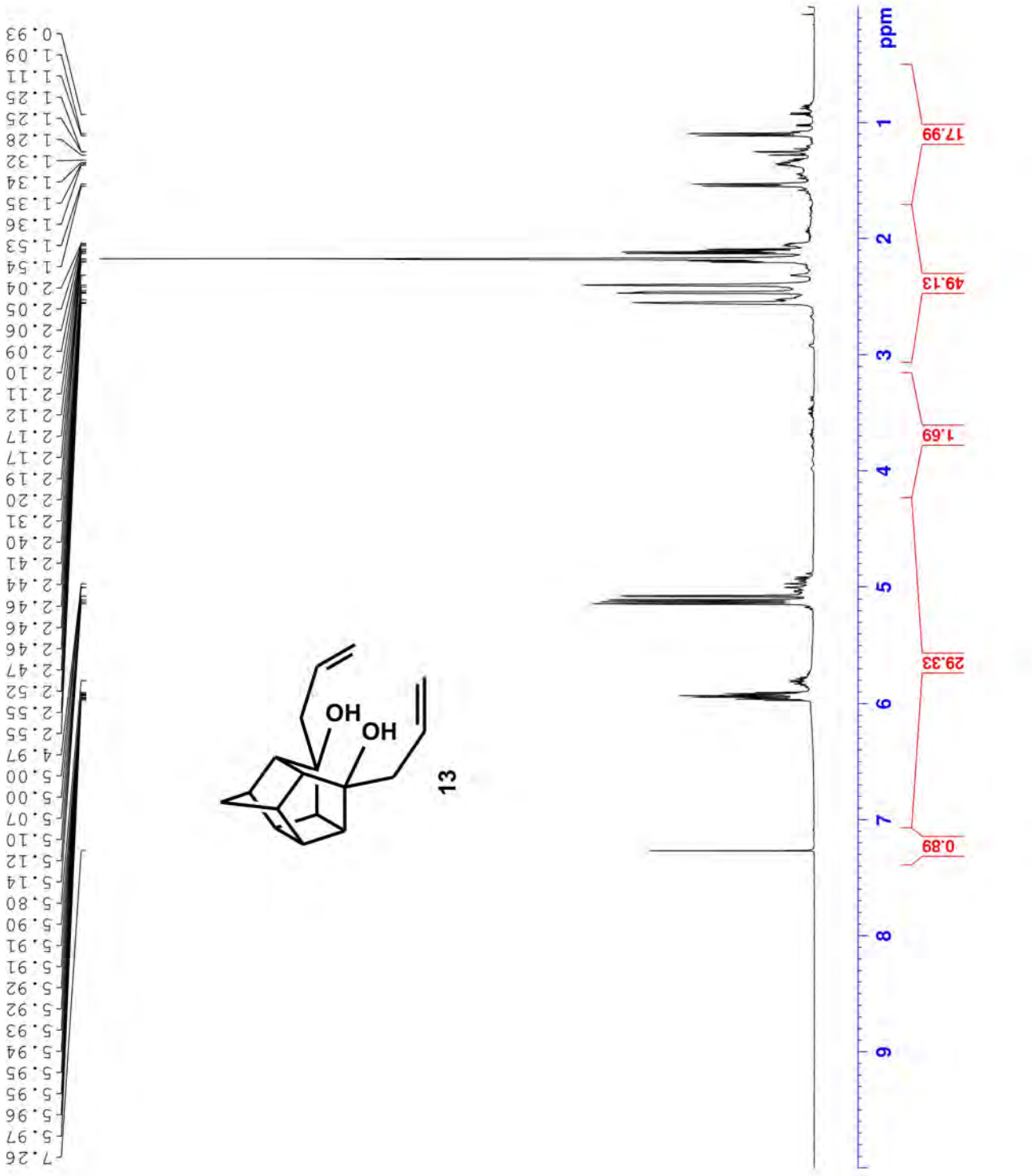

^{1}H NMR spectrum of **13**.

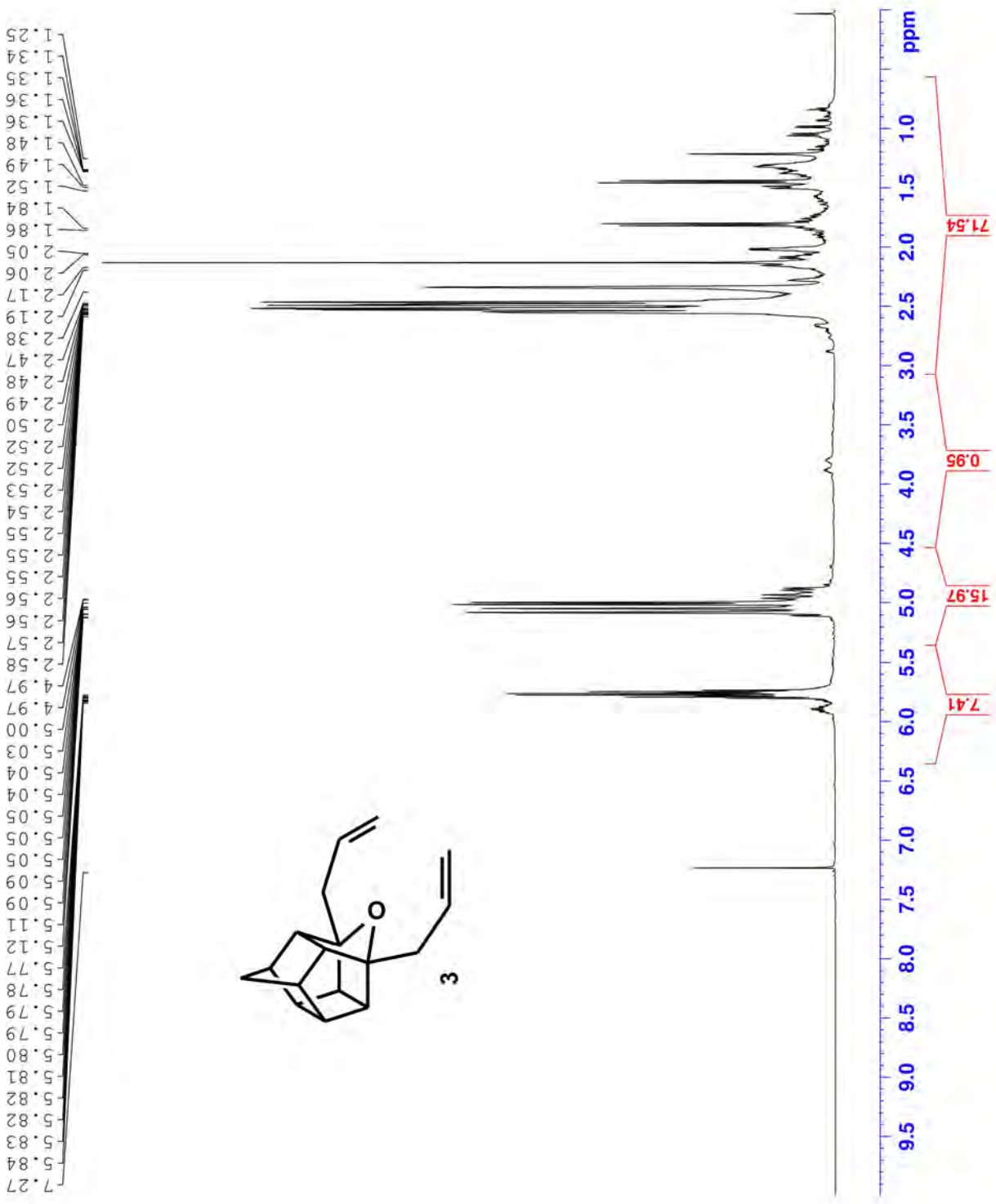

^{1}H NMR spectrum of **11**.

Appendix D: ^{13}C NMR spectra

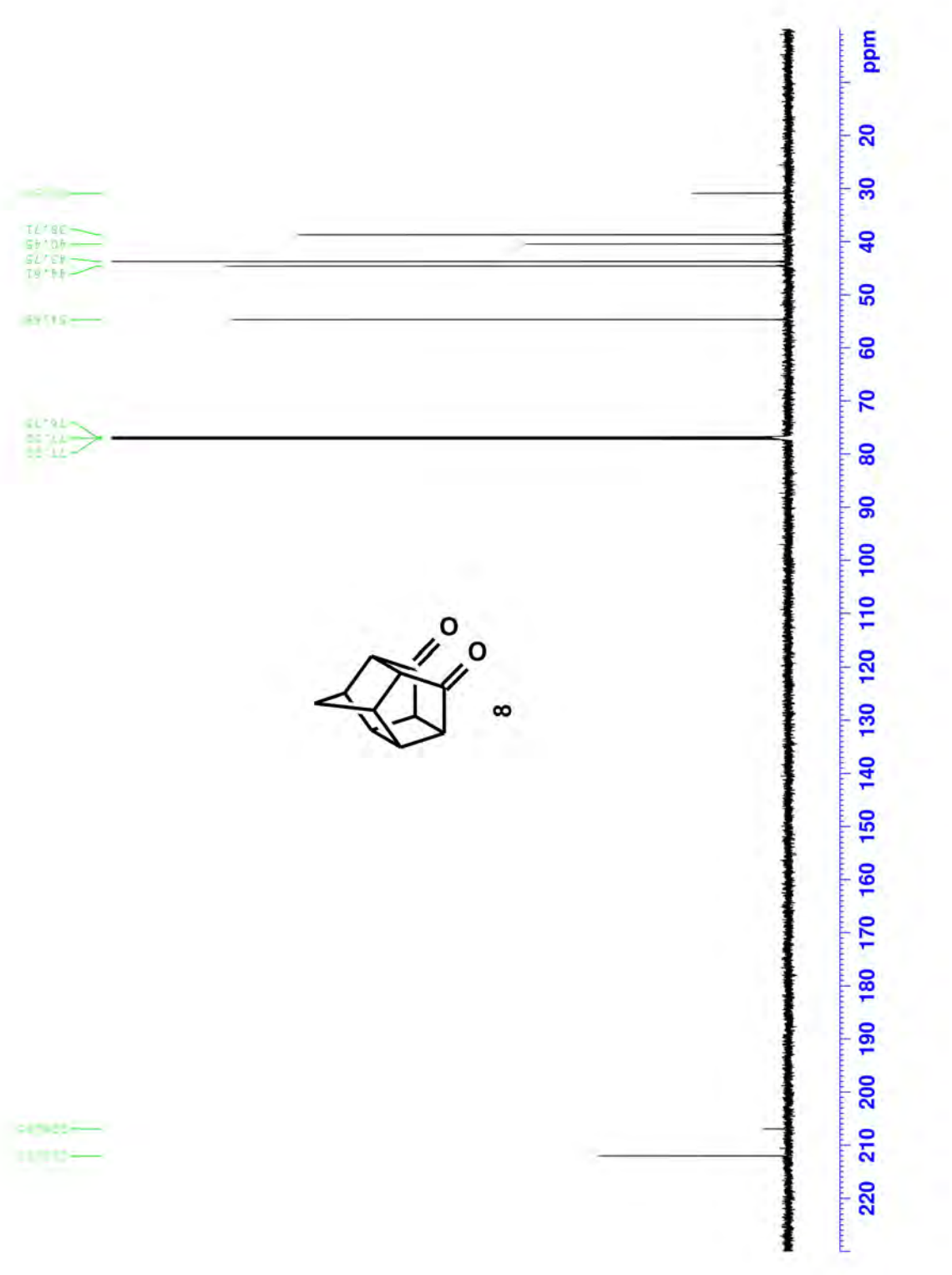

^{13}C NMR spectrum of **8**.

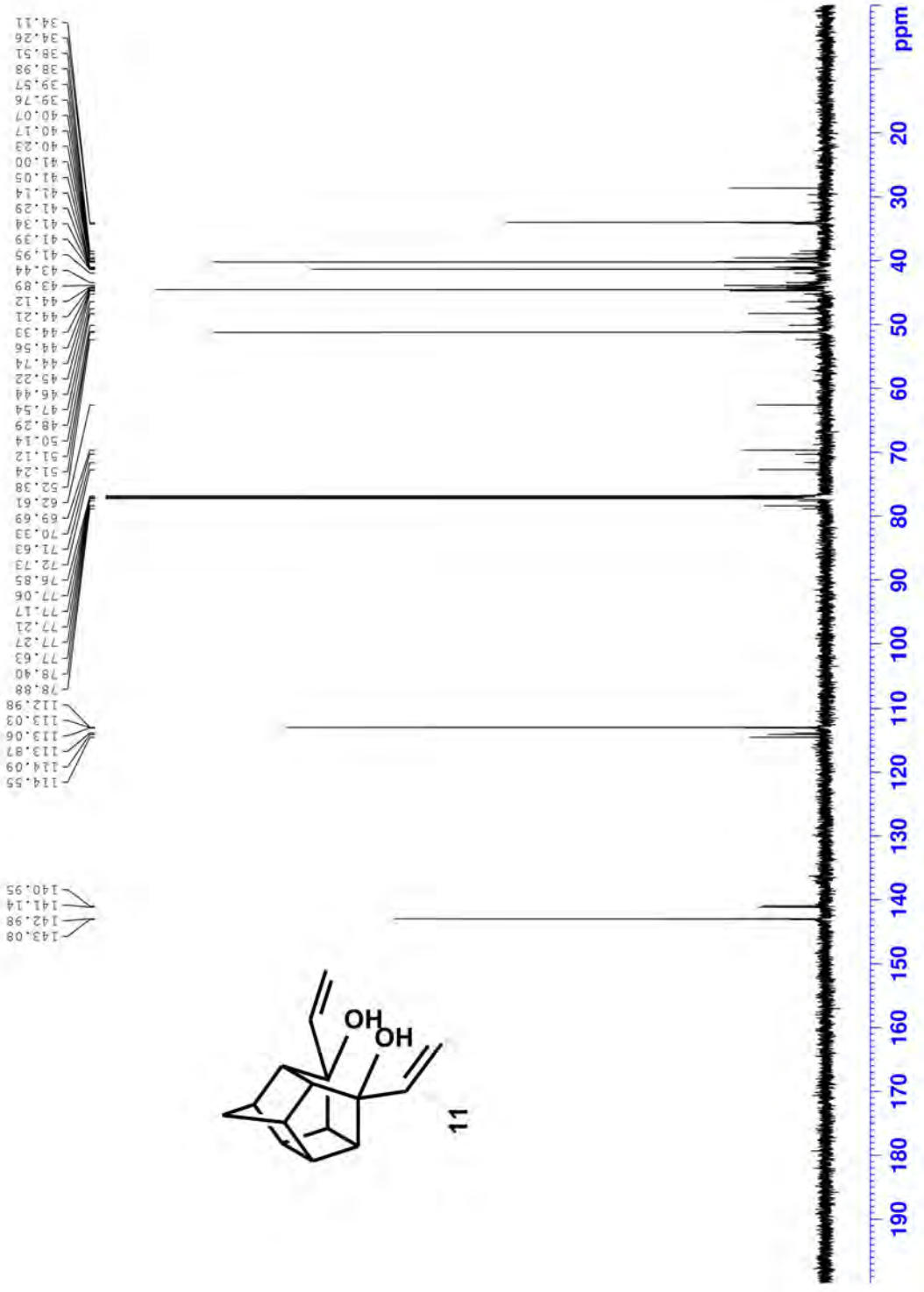

^{13}C NMR spectrum of **11**.

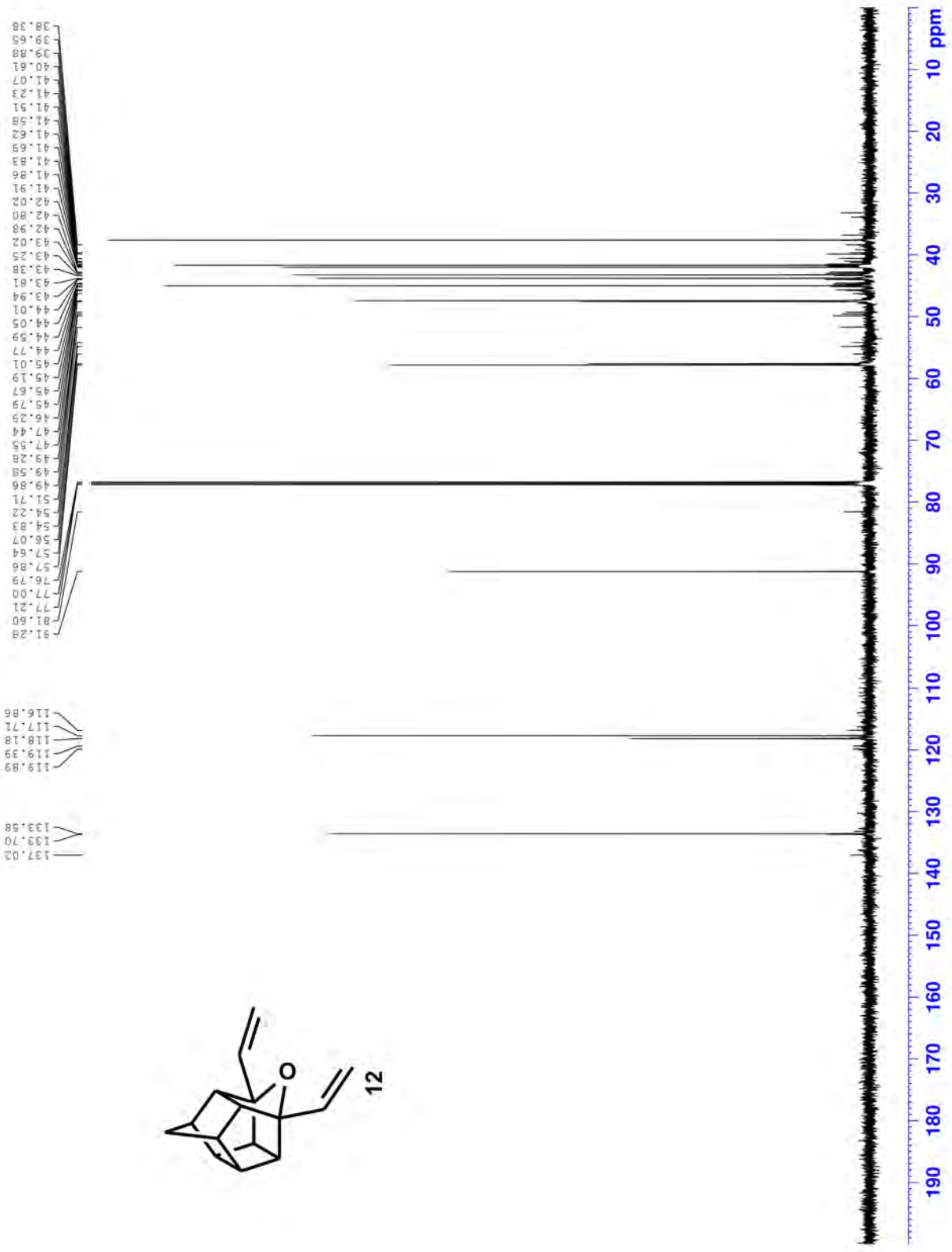

^{13}C NMR spectrum of **12**.

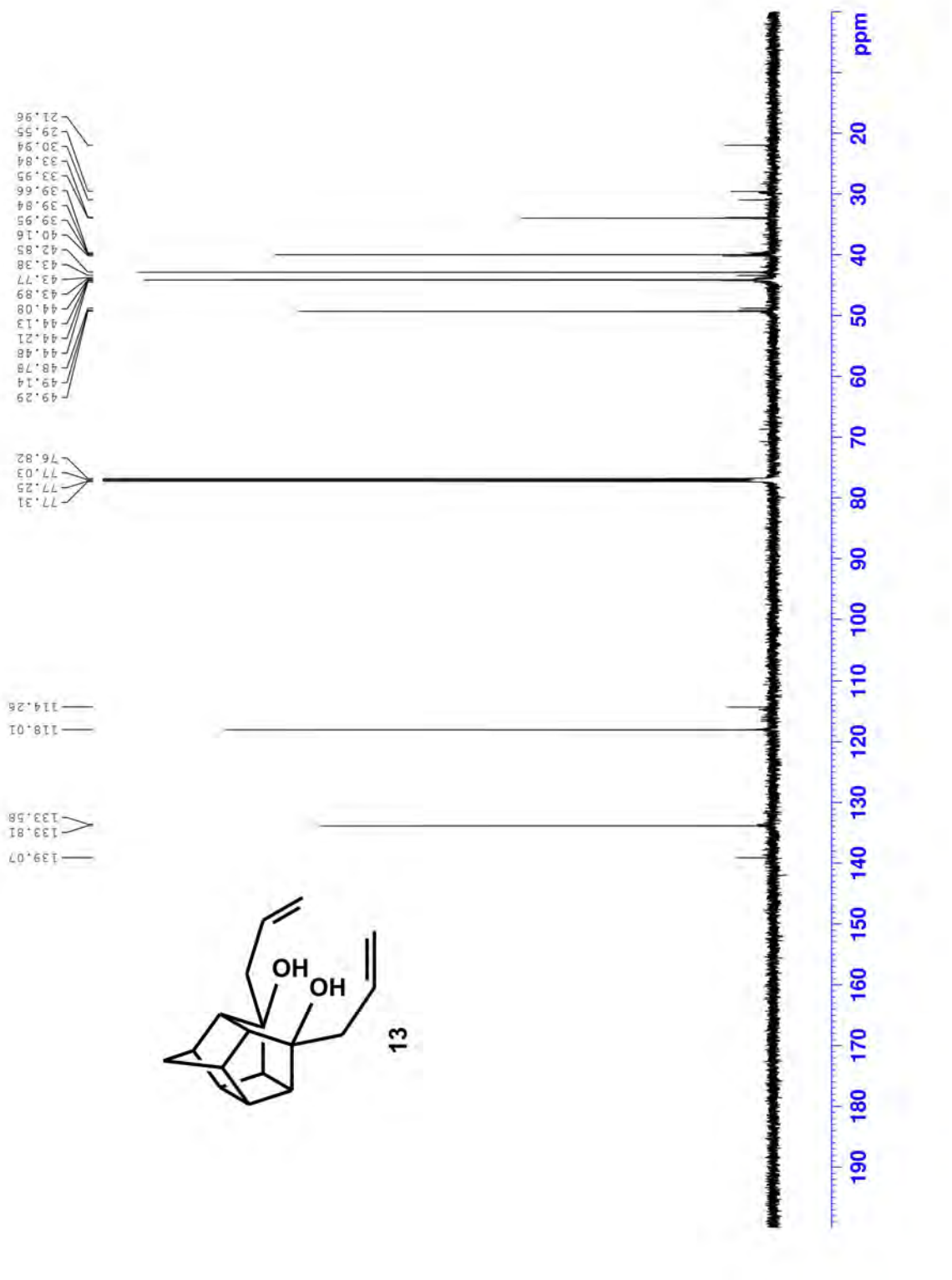

^{13}C NMR spectrum of **13**.

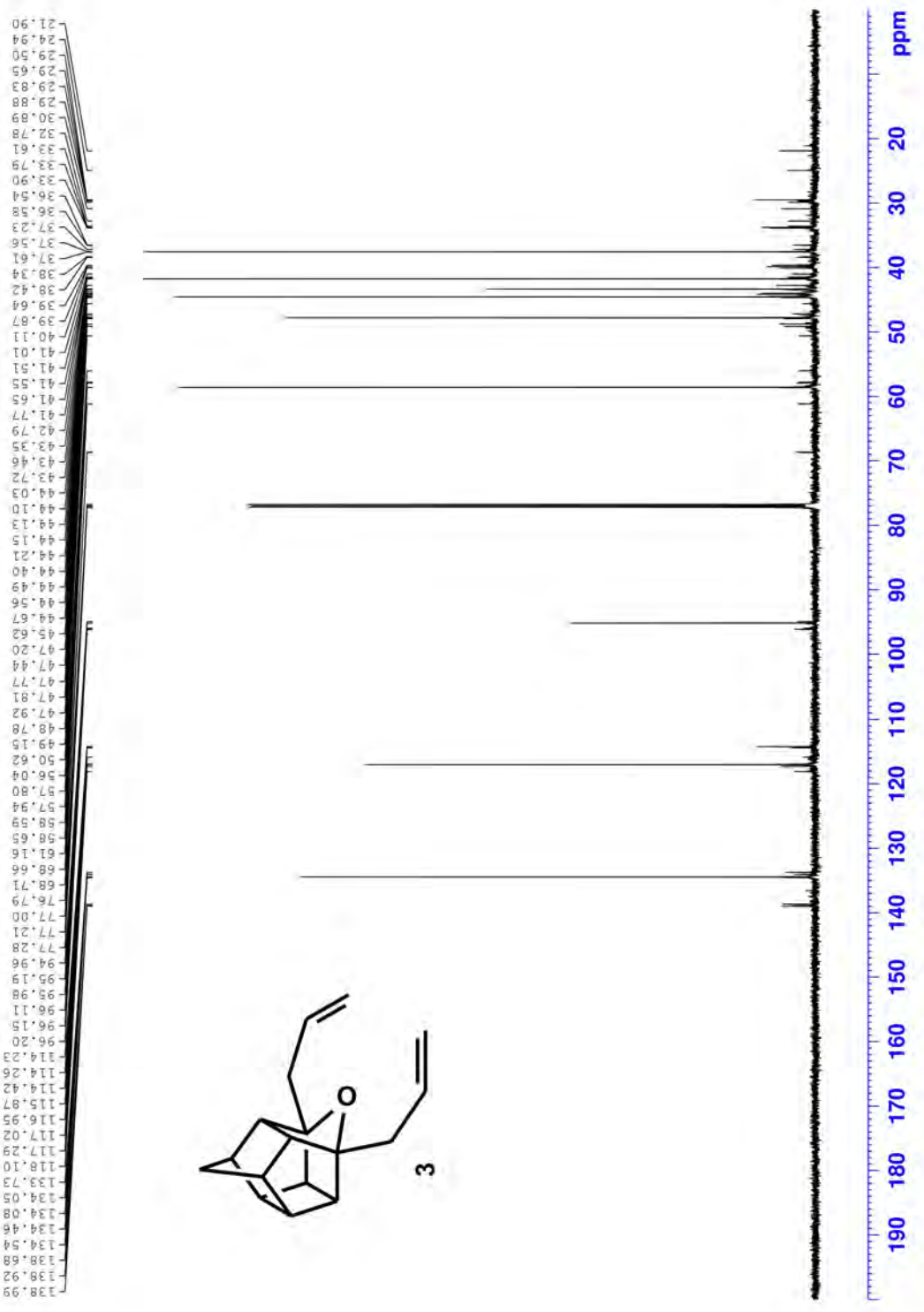

^{13}C NMR spectrum of **3**.